WL-TR-97-4091

WORK UNIT DIRECTION (WUD54) AMENDMENT - MATERIALS PROCESS DESIGN

Sponsored by:

Materials Directorate
Wright Laboratory
Air Force Materiel Command
Wright-Patterson AFB OH 45433 7734

DECEMBER 1996

FINAL REPORT FOR PERIOD OCTOBER 1995 - OCTOBER 1996

Approved for public release; distribution unlimited

MATERIALS DIRECTORATE
WRIGHT LABORATORY
AIR FORCE MATERIEL COMMAND
WRIGHT-PATTERSON AFB OH 45433-7734

NOTICE

When Government drawings, specifications, or other data are used for any purpose other than in connection with a definitely Government-related procurement, the United States Government incurs no responsibility or any obligation whatsoever. The fact that the Government may have formulated or in any way supplied the said drawings, specifications, or other data, is not to be regarded by implication, or otherwise in any manner construed, as licensing the holder, or any other person or corporation; or as conveying any rights or permission to manufacture, use, or sell any patented invention that may in any way be related thereto.

This report is releasable to the National Technical Information Service (NTIS). At NTIS, it will be available to the general public, including foreign nations.

This technical report has been reviewed and is approved for publication.

STEVEN R. LECLAIR, Chief
Materials Process Design
Integration & Operations Division
Materials Directorate

GEORGE F. SCHMITT, Chief
Integration & Operations Division
Materials Directorate

If your address has changed, if you wish to be removed from our mailing list, or if the addressee is no longer employed by your organization please notify WL/MLIM, Wright Patterson AFB, OH 45433 to help maintain a current mailing list.

Copies of this report should not be returned unless return is required by security considerations, contractual obligations, or notice on a specific document.

REPORT DOCUMENTATION PAGE

FORM APPROVED
OMB NO. 0704-0188

1. AGENCY USE ONLY *(Leave Blank)*	2. REPORT DATE	3. REPORT TYPE AND DATES COVERED
	December 1996	Final Report - Oct 95 - Oct 96

4. TITLE AND SUBTITLE

Work Unit Directive (WUD54) Amendment - Materials Process Design

5. FUNDING NUMBERS

PE: 61102F
PA: 2304
TA: DW
WU: OP

6. AUTHOR(S)

S.R. LeClair and A. Jackson

7. PERFORMING ORGANIZATION NAME(S) AND ADDRESS(ES)

Materials Directorate
Wright Laboratory
Air Force Materiel Command
Wright Patterson AFB OH 45433

8. PERFORMING ORGANIZATION REPORT NUMBER

9. SPONSORING MONITORING AGENCY NAME(S) AND ADDRESS(ES)

Materials Directorate
Wright Laboratory
Air Force Materiel Command
Wright-Patterson AFB OH 45433-7734
POC: Steven R. LeClair, WL/MLIM, 937-255-8787

10. SPONSORING/MONITORING AGENCY REP NUMBER

WL-TR-97-4091

11. SUPPLEMENTARY NOTES

12a. DISTRIBUTION/AVAILABILITY STATEMENT

Approved for public release; distribution unlimited.

12b. DISTRIBUTION CODE

13. ABSTRACT

The focus of materials process design research is to establish theories and scientific methods for *in situ* self-improvement of the design and control of material processing using self-directed computer aided systems. The specific objectives are to: 1) generate new methods and knowledge relative to the design process, 2) integrate, synthesize and generalize new knowledge in the form of axioms, and 3) automatically incorporate this new knowledge for use in improving materials research and process control metrics (i.e., quality, time and cost). Long term the objective is to develop a language, principled in theories, for the development of virtual material processing systems and integrated, intelligent manufacturing systems across a Materials and Processing Information Highway.

14. SUBJECT TERMS

material behavior models, optimization theory, fuzzy reasoning, cellular automata

15. NUMBER OF PAGES
133

16. PRICE CODE
N/A

17. SECURITY CLASSIFICATION OF REPORT	18. SECURITY CLASS OF THIS PAGE	19. SECURITY CLASS OF ABSTRACT	20. LIMITATION ABSTRACT
UNCLASSIFIED	UNCLASSIFIED	UNCLASSIFIED	SAR

TABLE OF CONTENTS

Resources & Mission

THE MISSION of the Materials Process Design research group is to research, develop and apply advanced computer technology to the design and control of materials processes. The research strategy involves the development of generic processing methods by advancing automated reasoning and computational techniques independent of any specific materials or processing research.

The research staff is led by government personnel, comprised of both military and civilians, together with visiting research scientists sponsored by the Air Force Office of Scientific Research. The team is complemented with research scientists and engineers from other 'in-house' research groups within the Materials Directorate, as well as contracted researchers (reference Tables 1-3).

Table 1. Universities/Research Institutes and Their Role

Eight (8) Government Personnel	**Position/Degree**
Dr LeClair	Branch Chief, & WUD Leader / PhD - Industrial Engineer
Mrs Lambert	Branch Secretary
Dr Malas	PhD - Systems Materials Engineer
Capt Busbee	BS - Aerospace Engineer
Capt Conrad	MS - Computer Engineer
Mr Ohrstedt	MS - Mechanical Engineer
Mr Fairchild	MS - Electrical Engineer
Mr Ruegsegger	Palace Knight - PhD Candidate - Electrical Engineer

Twelve (12) Contractor Staff	**Organization/Degree/Expertise**
Dr Jackson	TMCI - PhD - Physics
Dr Laube	TMCI - PhD - Electrical Engineering
Dr Mullins	TMCI - PhD - Materials Engineer
Dr Frazier	TMCI - PhD - Electrical Engineering
Mr Medeiros	TMCI - MS Candidate - Materials Engineer
Mr Adams	TMCI - MS - Computer Science
Mr Jones	UC - PhD Candidate - Electrical Engineering
Mr Cao	WSU - PhD Candidate - Computer Science
Mr Liptak (Soche Student)	WSU - BS Candidate - Computer Science
Mr Keener (Soche Student)	WSU - MS Candidate - Electrical Engineering
Mr Hamna	WSU - BS Candidate - Electrical Engineering
Mr Schueller	WSU - BS Candidate - Computer Engineering

RESEARCH CONTRACTS	**Organization/Position**
Dr Pao	CWRU -Prof. Electrical Engineering & Applied Physics Dept
Dr Anil Chaudary	UES, Inc - Mechanical Engineering
Dr Maguire	Southwest Research Institute - Analytical Chemist
Dr Igelnik	CWRU - Research Associate
Dr Chen	WSU (NRC) - Prof. Computer Engineering
Dr Trelease	Prof @ UCLA - Computer Science
Mr Chemaly	TechnoSoft, Inc., President
Mr Ress	NC State - PhD Candidate - Industrial Engineer
Dr Venapogal	India (NRC) - Metallurgy Researcher
Mr Medina	Austral Engineering Software - Systems Engineer

Table 2. Universities/Research Institutes and Their Role

Table 3. Companies and Their Role

Technosoft, Inc. Cincinnati, Ohio	Cooperative Research in (Integrated Material-Product-Process) Feature-based Design Research
AI Ware, Inc. Cleveland, Ohio	Associative Memory Research, Technology Transfer of Optimzation Research
ThinkAlong Software, Inc. Brownsville, California	Material and Process Discovery Research
UES, Inc. Dayton, Ohio	Automated Materials Research, Simulated Machining Research
Technolgy Transfer & Assessment, Inc., Annapolis, Maryland	Technology Development & Transfer of Molecular Beam Epitaxy Self-Directed Process Control Research
InfoScribe Technologies, Inc. Dayton, Ohio	Technology Development & Transfer of Self-Directed Process Control Research
Hohman Plating, Inc., Dayton, Ohio	Cooperative Research in Self-Directed Process Control
Youngstown Technology Development Corporation, Youngstown, Ohio	Cooperative Research in Aluminum Extrusions, Steel Forgings & Castings and Machining
Pratt & Whitney West Palm Beach, Florida	Cooperative Research in Shape Optimization of Turbine Disk Forging Processes

Case Western Reserve University, Cleveland, Ohio	Neural Networks for Memory-Driven Design & Self-Directed Control of Molecular Beam Epitaxy (MBE)
Ohio University Athens, Ohio	Thermomechanical Models for Deformation Processing
North Carolina State University Raleigh, NC	Qualitative Methods for Design of E-O Materials
University of Cincinnati Cincinnati, Ohio	Self-Directed Control for Pulsed Laser & Chemical Vapor Deposition
Wright State University Dayton, Ohio	Neural Networks for Process Design & Prediction
Baikov Institute of Metallurgy Moscow, Russia	Pattern Recognition Algorithms for Materials Discovery/Design of E-O Materials
The Ohio State University Columbus, Ohio	Neural Networks & Statistics for Modeling & Prediction
Imperial College, London University London, England	Nanoscale Materials Design
SouthWest Research Institute San Antonio, Texas	In situ Raman Spectroscopy
University of Kansas Lawrence, Kansas	Pattern Recognition Algorithms for Materials Discovery/Design of E-O Materials

Critical to the pursuit of Materials Process Design is the formation of alliances with other research, development and technology transfer companies such as:

R&D Alliances

Therein, a fundamental component of our research is the formation of alliances with other materials and processing research groups within the Materials Directorate and other organizations within the Department of Defense (reference Tables 4 and 5):

Table 4. Research Groups and Their Area of Collaboration

WUD 50 Surface Interactions Group, WL/MLBM (Dr Lampert)	Self-Directed Control of Semiconductor Wafer Processing via MBE
WUD 48 Electro-Optical Materials Group, WL/MLPO (Dr Hemenger)	Discovery of Non-linear Optical Materials & Self-Directed Control of PLD of Superconducting Films
WUD 51 Fluids, Lubs and Elastomer Group, WL/MLBT (Dr Zabinski)	Self-Directed Control of Thin-Film Tribological Coatings (Lubrication and Wear Protection)
WUD 49 Process Modeling Group, WL/MLLN (Dr Semiatin)	Feature-Based Process Modeling and Optimal Control of Forging Processes
WUD 40 Nondestructive Evaluation Group, WL/MLLP (Dr Crane)	Feature-Based Process Modeling and *In situ* Re-design for Eddy Current Inspection of Engine Components
WUD 26 Laser Hardened Materials Group, WL/MLPJ (Dr Pachter)	Protein Secondary Structure Prediction
WUD 53 High Temp. Composites Group, WL/MLLN (Dr Kerans)	Self-Directed Control of Oxidation Resistant Coatings for Ceramic Fiber
Flight Dynamics Directorate, WL/FIBG	Multidisplinary Design
Propulsion Directorate WL/POOX	Self-Directed Control of Pulsed Laser Deposition for Superconducting Materials

Table 5. Using Organizations and Area of Collaboration

U.S. Army Aviation & Troop Command, St Louis, MO	Feature-Based Process Modeling and *In situ* Re-design for Eddy Current Inspection of Engine Components
Oklahoma Air Logistic Center, Tinker AFB, TX	Self-Directed Control of Thin-Film Tribological Coatings (Lubrication and Wear Protection)
National Security Agency, University of Maryland, College Park, MD	Self-Directed Control of Semiconductor Wafer Processing via MBE
USAF Medical Centers (WPAFB, Brooks AFB, Travis AFB) Hyperbaric Medicine	Process Design & Automated Data Collection, Storage, Retrieval and Archiving
U.S. Marine Corps, Cherry Point, NC	Fatigue Monitoring Sensing using Thin Film Materials

Research Scope

The focus of materials process design research is to establish theories and scientific methods for *in situ* self-improvement of the design and control of material processing using self-directed computer aided systems. The specific objectives are to: 1) generate new methods and knowledge relative to the design process, 2) integrate, synthesize and generalize new knowledge in the form of axioms, and 3) automatically incorporate this new knowledge for use in improving materials research and process control metrics (i.e., quality, time and cost). Long term the objective is to develop a language, principled in theories, for the development of virtual material processing systems and integrated, intelligent manufacturing systems across a Materials and Processing Information Highway.

Fundamental to the research is the pursuit of advanced computer technology, i.e., concepts to extend the limits of conventional 'computer-aided' systems. These concepts involve **computational methods** to model materials (structure & property), geometry (shape & use) and processes (parameters and dynamics) involving:

material behavior models,

processing maps,

axiomatic design principles,

modern control theory,

optimization theory,

pattern recognition,

inferential (fuzzy) reasoning,

mathematical morphology,

qualitative physics,

genetic algorithms,

and ontology;

and advances in **computer science** (software and hardware):

object-oriented programming,

advanced numerical methods,

cellular automata,

associative memories,

neural networks, and

distributed parallel computing;

together with innovations in **materials processing** such as:

rapid prototyping processes,

deformable flow process/control modeling
multi-physics finite element analysis,
knowledge engineering systems, and
non-manifold geometry engines.

Central to our research endeavors are the pursuits of new levels of quality and affordability of aerospace components. The materials scope of our research encompasses

structural monolithic involving:

metals,
intermetallics,
ceramics, and
polymers

structural composites (fiber reinforced) involving:

metals,
ceramics, and
non-metal (organic),

and tribological, superconductor and semiconductor thin-films involving:

inorganics,
biologically-based and other organic, and
electro-optic materials.

Our goal is 'Virtual Materials Research' enabled through the use of advanced computing employing an integrated material-shape-process philosophy which when manifested in a material processing system enables on-line or *in-situ* generation of an evolving material process design and control cycle.

Toward
'Virtual' Materials Research

by Dr Sam J.P. Laube

It is generally acknowledged, physical processes yield materials, and resulting characteristics are determined by *in situ* process parameters. Moreover, data about physical processes and their evolution can yield new insights concerning specific material behaviors and/or subprocesses. In the area of thin-films, which may or may not exhibit bulk material properties, the opportunity to discover new phenomena becomes quite obvious, and therein, the need to sense and control a number of process parameters.

Also widely acknowledged is the use of the scientific method for materials research and its' dependence on measurement and the collection of data. Through computer control of process instrumentation, actuators and sensors, automation of the scientific method, and therein materials research, becomes plausible. Indeed, the relationships between a material, processing conditions and desired material properties can be derived via the 'intelligent' fitting of functions to empirical data.

Often, in a materials research environment, the objective is to develop or validate a model, or on occasion, reconsider the theoretical understanding of what is supposed to be occurring within a particular process. Measuring, storing, and retrieving information relative to monitored process parameters is fundamental to the research task as all science is based on the premise of measurement and the cognizant underlying suppositions about these measurements.

Process parameters are typically sensed and converted to electrical signals that can be displayed remotely. It is also becoming more common to digitize and store in a computer these electrical signals for later retrieval and analysis. There are many sensing techniques for utilizing basic principles to measure and/or infer phenomena of interest. Unfortunately, there are also many misconceptions about the information that is collected in the form of stored signals and how these represent reality, i.e., a specific physical state and/or event. It is the aim of this research to expand the current view of what measurement means.

This review will attempt to clarify the effects and errors in measurement, as well as explore the additional information that comes from multiple measurements.. Thus, the evolution of a process, i.e., its dynamical behavior, is via the conjunction of sensor and actuator signals that are combined to form an external conception of how the process is evolving.

Ambiguities in Virtual Measurement Space

Typically, a process parameter is inferred via some known physical effect that generates an electrical voltage or current. Suppose it is desired to measure the temperature of a fluid in a container such as a vat of liquid. A sensor could be inserted into the container and an electrical signal would be generated.

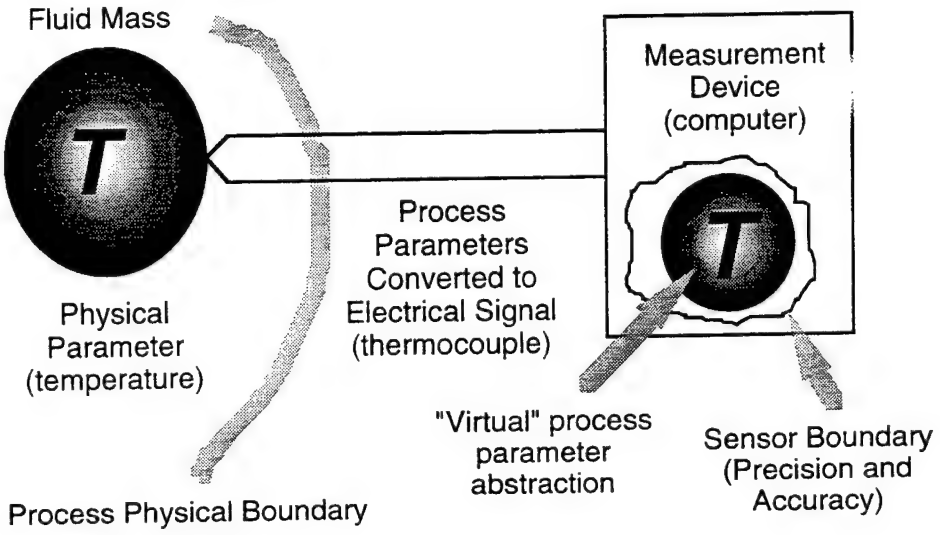

Figure 1. Measurement Of An Unambiguous Virtual Parameter

For this particular sensor, a bimetallic electrical effect, known as the Thermocouple effect, is used to generate a small voltage that can be filtered, amplified, digitized, and stored in an electronic computer. The process parameter of interest is the temperature measurement of a fluid mass. If properly designed, calibrated, and engineered, the signal from the thermocouple can faithfully represent the temperature of the mass. The signal can then be mapped into an abstract temperature domain; thus, a process parameter can virtually exist within a computer. This parameter can be analyzed, and used to control the fluid temperature or mixture. It is also possible to store the parameter for future reference.

Often, the sensor signals representing physical phenomena within the process are obscured by other phenomena that also are capable of generating electrical signals. Usually, these obscuring parameters do not become evident, until careful scrutiny of the sensor channel is performed by someone competent in this area. Often, the unknown parameter is due to some new, previously unknown process parameter that was previously not known to occur. The following (Figure 2) depicts this type of obfuscation.

As can be seen, there is ambiguity in the sensed data, which is contained in the electrical signals. There are two interfering temperature values that compete with one another, and they are both converted into an electrical signal. The measurement device is not capable of knowing the signals contain any ambiguity. Furthermore, the measurement device can not determine which parameter is significant, and which is superfluous. If the temperature is measured in a vat of fluid, or a curing composite, the unknown temperature can be due to exothermic reaction, convective flow, or even an unaccounted addition. The temperature sensor was designed to

measure a fluid of uniform temperature, but the uniformity criterion was compromised by some unknown effect. The abstract temperature parameter has been distorted and obscured. Some method of separating the physical parameters is needed.

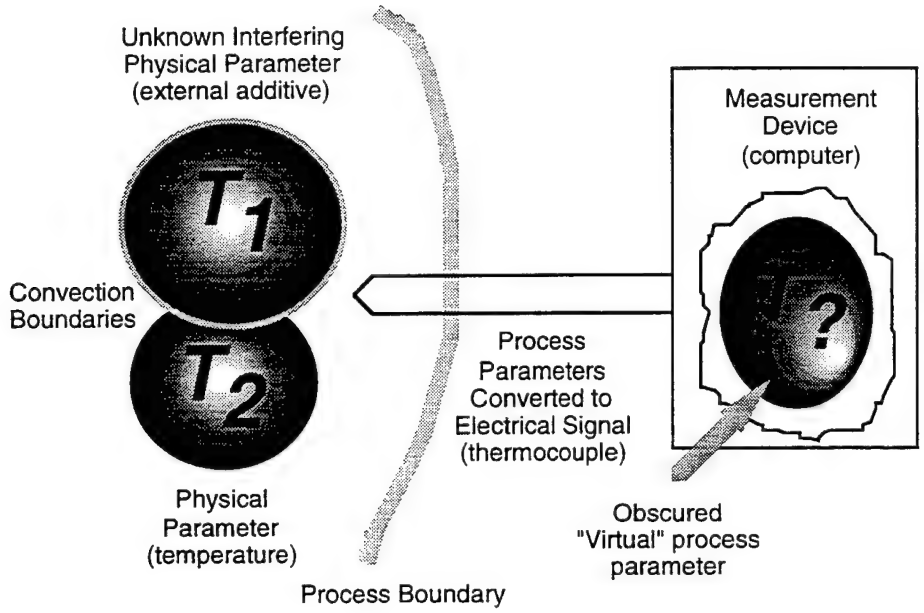

Figure 2. Measurement Ambiguity in Virtual Parameters

One method of separating the parameters is through multiple sensors. Another is based on separating the parameters in time or correlating with a previous model or data. In the case of multiple sensors, the means of measuring a process parameter is validated by providing corroborating information about certain parameters. This can be accomplished by placing an additional sensor in the fluid mass, preferably, one that operates on a different basic scientific principle. The next graphic (Figure 3) depicts this method.

A second sensor, while attempting to measure the newly discovered parameter, has also provided for parameter separation by being at a different location. The additional information provided by the extra sensor in the form of spatial interpolation increases the virtual process sensor space to include the unknown interfering physical parameter. It may not be possible to separate the parameters completely and measure the exact temperature, but at least the presence of the unknown interfering physical parameter can now be determined. This determination has increased the sensed dimension of the process, and may prove to be more valuable than the determination of the exact temperature.

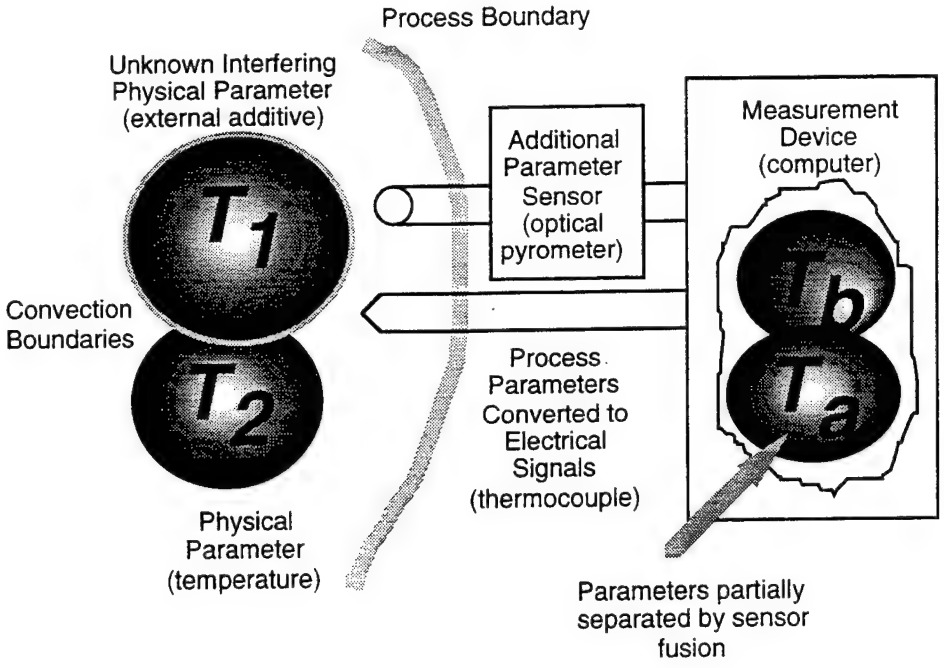

Figure 3. Parameter Separation by Fusion of Multiple Sensors

A similar separation can be performed by observing the time-series values of the temperature, and doing a separation based on frequency and/or time characteristics. A mathematical transform of the temperature data, such as a Fourier or wavelet, provides spectral characteristics to identify and separate the parameters. This is shown in the following Figure 4.

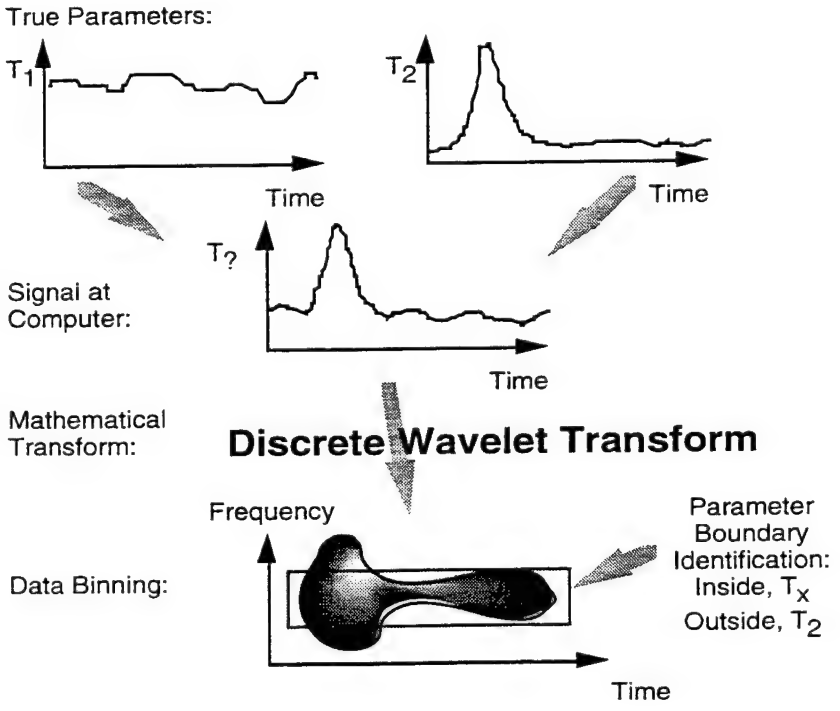

Figure 4. Parameter Separation Through Analysis

In this case, the determination of what is significant is based on *a priori* information. This *a priori* information may be predicted by physical models, generated by statistical methods, or generated by a few manual measurements. Based on this additional information, it now becomes possible to establish parameter boundaries in a transform space. These boundaries can be used to determine the presence of some unknown parameter event. In this way, the significance of the unknown parameter or event is determined by analysis of a transformed space.

Another alternative to adding an additional sensor to measure temperature is to add sensors for other process parameters. A correlation between changes in many sensors can indicate interactions, and provide a means of accounting for them, reference Figure 5:

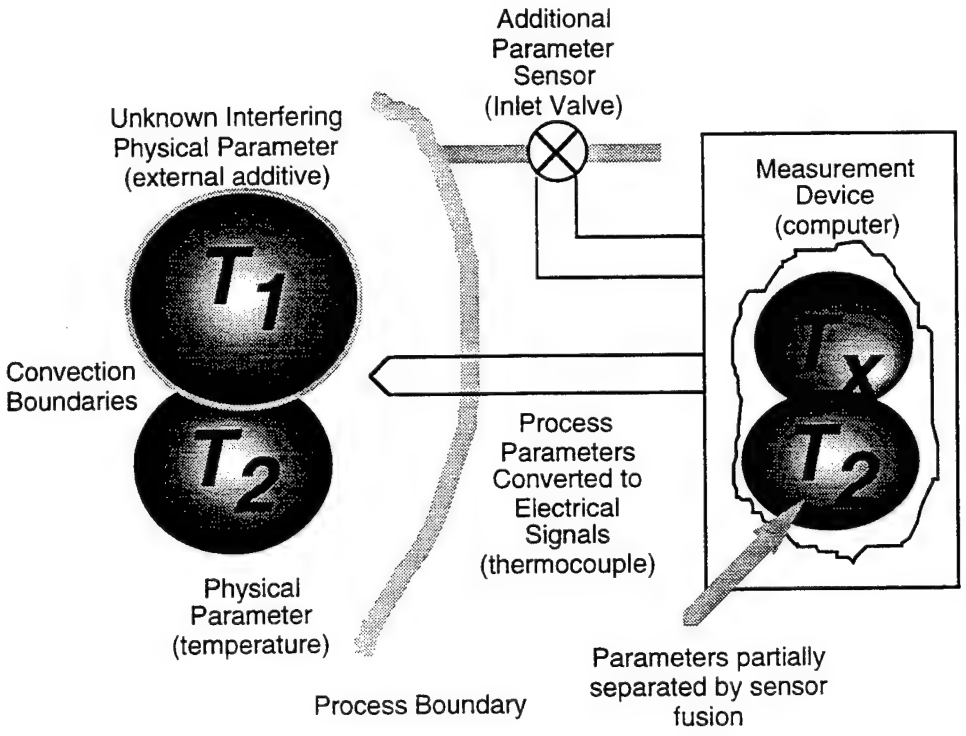

Figure 5. Parameter Separation Through Correlation

If a sensor is added to monitor an inlet flow signal, then this parameter can be used to determine temperature. The flow is plotted with respect to time, and a separation can be performed based on the temporal correlation between other parameters. Other process parameter effects can be separated from the actual process parameter, thus revealing the original parameter of interest, as depicted below in Figure 6. Separation is possible by examining the trends in the data, and the correlation coefficients. Correlation analysis can be carried out over time, or across several runs of a process. The interaction of several sensors and actuators can also be combined to ultimately form a dynamical model of known sensed process behavior. It becomes possible to determine the behavior of the process by the combination of several sensors.

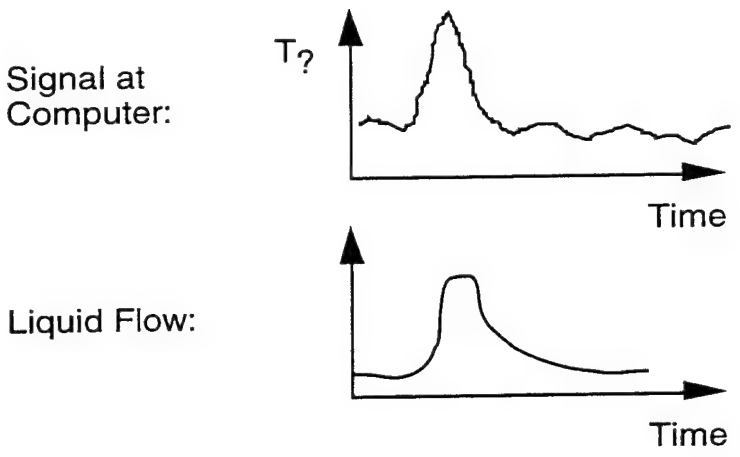

Figure 6. Event Correlation Observation

Virtual Measurement Space Usage

Once virtual process parameter interaction information is created within the computer, the process can be "virtually explored" without actually exercising the process. The virtual parameters can be used as parameters to test known theoretical models, or discover previously unknown phenomena. The unique sensor data path that indicates successful material product production is available as dynamical data that can also be compared with the current process run. A life-history of the process sensor parameters is stored and is made available to analyze, build models, understand process dynamics, and determine process repeatability and stability. This is shown in Figure 7.

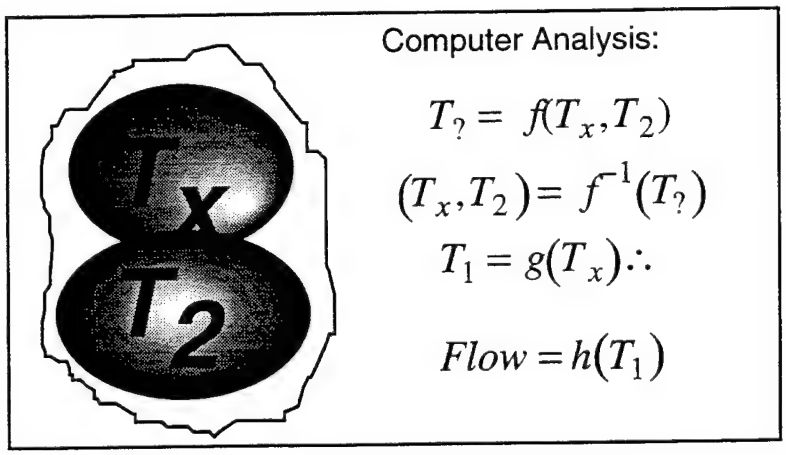

Figure 7. Virtual Parameter Modeling

In this manner, the process can be analyzed, explored and understood more completely within the computer. Furthermore, the computer virtual process can be made available as a subscription service to external users, with maintenance and improvement of the virtual sensor descriptions improved with each process run. It also becomes possible to simulate process behavior under feedback control without actually exercising the process.

Determining the connection between material characteristics, such as composition, morphology and stoichiometry, and the process parameters that determines the material characteristics is also possible with virtual process parameters. Currently, a material characteristic is desired. Candidate processes are considered, and then one is selected that can produce the desired material. Usually the selection is based on previous biases toward certain processes by what materials have previously been generated. Then, the selected process is used to attempt the generation of the desired material. A material is produced and then analyzed. Based on the results of the analysis, the material is found to be adequate, or some minor changes are performed on the process to improve the material. On occasion, a new material process is selected. Due to the time and number of process parameters, the parameters are seldom fully explored.

Theoretical models that determine materials characteristics can be tested by *ex situ* experiments combined with exercising the theoretical models on the virtual process. Perfecting the models to mimic the experimentally generated material structure based on sensor data provides a means of coupling the process parameters and generated material characteristics. The connection between *in situ* process dynamical models and resulting materials structures allow for virtual materials research, where a new film structure can be explored in preliminary fashion, prior to generation and analysis on the actual process. Multiple process verification runs can also be performed so that the virtual space does not stray from the actual process. Each type of processed material can be combined into a single data format, so that the combined process understanding stays with that process. Then a structural process mapping is refined with each run as in Figure 8.

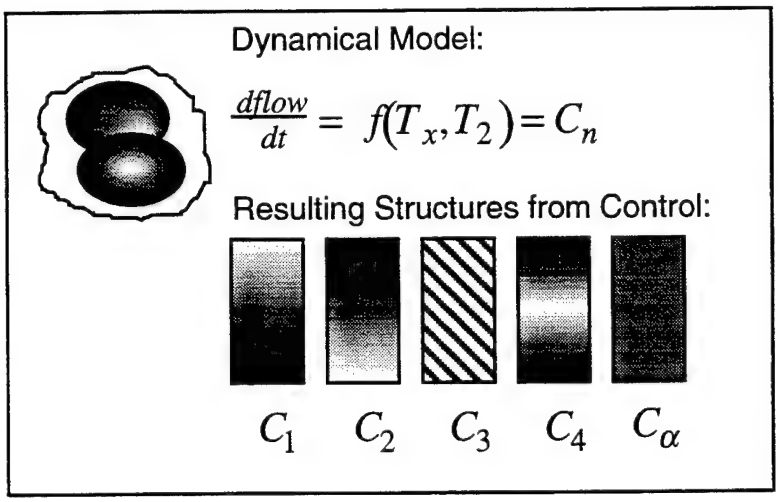

Figure 8. Virtual Materials Development

In Figure 8, the desired control law is found that generates a gradient in the fluid mass, that ultimately results in a gradient structure. A dynamical model is combined with a process mapping from process parameters that determine various structures. The dynamical mapping is explored to determine all possible structures, until the desired structure is found. Then the actual process can be controlled to generate this material. Each run of the process provides additional data to refine the virtual sensors. Each *ex situ* experiment also provides data that refines the possible structure types. This permits the exploration of materials by virtual means.

Virtual Materials Implementation

In order for the virtual materials concepts to be successful, processes must contain a full complement of necessary instruments so that automation via computer, combined with data acquisition and control can commence. It is from this complete sensor-actuator suite that a virtual materials processing environment can exist. Processes that do not incorporate sensors and actuators must also be modified to accommodate the sensing and control of process parameters. Furthermore, while additional instrumentation and process functionality is always desirous, the design and engineering solutions are different for each process. A unique solution will be required for each process. It also becomes important to carefully instrument each process, so that the information collected will be accurate, and, thus, can be disseminated and utilized with little error.

Undertaking the task of automated information dissemination and process control will require the conceptualization, design, engineering, testing and debugging of complex integrated hardware and software solutions. In this case, a most economical approach is through modularity. The need for modular solutions allows for multiple process reusability, such as a specific temperature control software module that can control temperatures from MOCVD reactors just as well as MBE Knudsen cell temperatures. A suite of modules will permit accomplishment of this task with a minimum of duplicative effort. Each process instrumentation suite can be approached by the addition and/or substitution of modular software and hardware components. The modules required must accommodate a diverse functionality, ultimately limited by the particular instrument restrictions that are imposed by the instrument hardware.

Automation of a process to achieve virtual material research requires that process parameters necessary to generate the desired material be known. This is seldom the case. There is usually a discrepancy as to what process parameters are important in altering the produced material and which are not. Also, if parameters are known to be significant, the parameter control ranges are seldom fully explored. Usually a fixed group of settings is all that is used to make a material. Instruments that can sense these disputed parameters thus require that a suite of sensors and actuators be specified that are capable of a wide range. It also is imperative that in specifying the sensors and actuators, full expert knowledge of how the process is to function is made available. A working synergy is necessary between the process experts and the specifications engineer. It is only then that a group of sensors and actuators can be determined that will fully utilize the physical principle of the process, reference Figure 9.

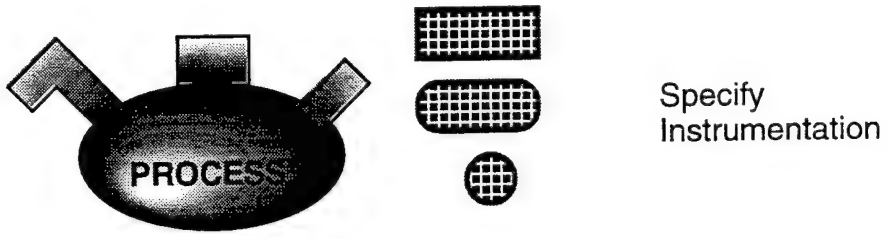

Figure 9. Instrumentation Specification

Once a suite of desired process parameters and subsequent methods to sense them are chosen, integration into the process is needed. This usually requires some physical modification of the process apparatus, requiring machinist skills along with engineering issue solutions. As a rule, it is desirable to modify the process without disturbing process operation, so that *in situ* sensing is available. In this way, process parameter measurement can occur without sacrificing the production of material as in Figure 10.

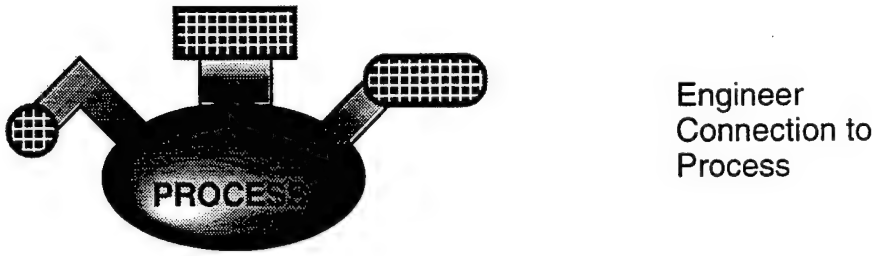

Figure 10. In-situ Sensor Process Integration

Upon the integration of sensors and actuators, it is then necessary to incorporate a computer to create the virtual material process space. Code modules are used for the chosen sensors to allow data collection and process control. This integration will be specific for each process, but utilizes several modules that are combined to achieve the specific functionality of the particular process. The process can be operated under control and the dynamical ranges can be explored. This is depicted in Figure 11.

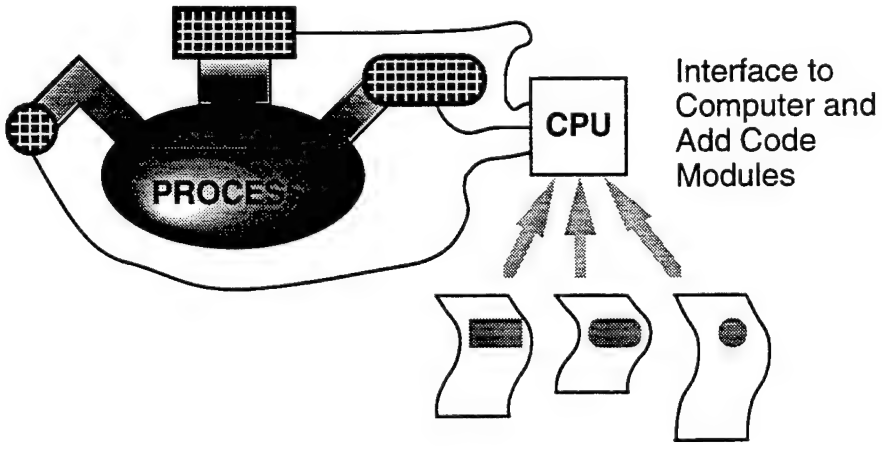

Figure 11. Code Module Installation and Integration

Once the process is engineered for functionality, a group of materials are generated and analyzed. Tests will be performed that pertain to the materials characteristics of interest, and are used to evaluate the functionality of modeling and control software modules. Material will be generated while the process is under instrumentation and control. The *ex situ* analysis of the produced materials will then be compared to *in situ* data to verify the validity of modeling and control modules. The models will then be modified and altered so that they correspond to the process more exactly as depicted in Figure 12..

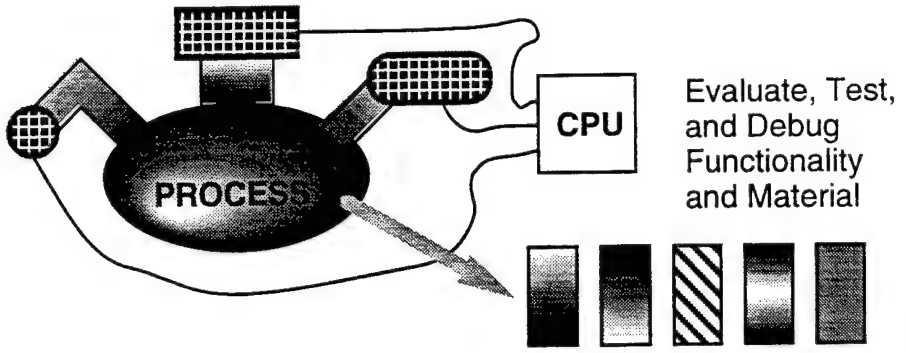

Figure 12. Virtual Process Integrity Verification

The collection of both *ex situ* and *in situ* data from several process runs can then be used to build a better understanding of the process operation as well as provide the foundation for virtual materials research. The research can then commence within the computer or over networks without requiring operation of the process.

Electronic Prototyping

To enable 'Virtual Materials Research' fundamental work in the are of learning a function from empirical data is needed, e.g., to support rapid response to customer needs for thin-film (oxidation resistance, thermal, wear, lubricious, superconductor, advanced semiconductor) materials. A near-term need is the development of methods for mapping or relating variables, and with regard to process data are also capable of distinguishing signal from noise. Such methods will enable a materials processing researcher to quickly surmise: 1) if the variables used to learn a mapping are sufficient, and 2) identify the amount of noise (unknown variable and/or gaussian-type instrument/process noise) present. Long term this research is targeting the development of autonomous process modeling methods, i.e., the capability to automate the modeling of a process directly from empirical data.

Research OBJECTIVES are

- to automate data driven computational methods for functional (n-dimensional) mapping to enable adaptive modeling (*in situ* remodeling) of materials processes, and
- to identify and distinguish signal vs noise incurred by instruments and/or process conditions.

Research FOCUS is

- extending neural network-based 'multi-variable' basis function selection, and
- apply selection algorithm to materials process discovery and processing.

Background

Traditional methods of function approximation or regression involve a linear combination of the product of single variable or fixed basis functions (e.g., polynomial, spline, and/or trigonometric expansions). From Barron [17], the problem with traditional methods is that there are exponentially many orthonormal functions but unless all of these orthonormal functions are used in the selection of the fixed basis, there will remain functions that are not well approximated. As a consequent, for fixed basis function approximation,

the order of the squared approximation error grows exponentially as $1/n^{(2/d)}$,

where n is the number of basis functions and d is the number of input variables. This problem is avoided by tuning or adapting the parameters of multi-variable basis functions, which are typically sigmoids or so-called squashing functions, to fit the target function as is true of neural networks, wherein the order of the squared approximation error is $1/n$, and independent of the number of input variables.

The biological origins of neural networks [18] as chronicled by Pao [19] established multi-variable sigmoidol functions as the basis for neural networks. Today the suite of multi-variable basis functions employed in neural networks is without bound, but the most commonly used are the sigmoid and radial basis functions. Radial basis function neural networks typically employ subset selection to identify a set of Gaussian basis functions. Broomhead and Lowe [4] have tried to choose such a subset randomly from the entire given set. In lieu of random selection, Rawlings [1] has proposed a systematic approach that employs forward selection to choose the subset that best explains the variation in the dependent variable incrementally. Based on this concept, Chen et al. presented an efficient implementation of forward selection using the orthogonal least square method (OLS) [8]. Subset selection can also be used to avoid overfitting by limiting the complexity of the network. From the literature, overfitting may be

avoided when combining subset selection with other methods such as regularization [2,3], and as contributed by Mark Orr, combining OLS and regularization [9].

We show that the traditional approach of subset selection is insufficient. We propose a new subset selection method as explained via the principle of regularization. Instead of picking the subset from the given functional basis, we select the subset from a combination of functional basis evolved from a set of heterogeneous basis functions. Using this approach, we fully utilize all the information provided in the given data set and propose a more efficient neural network architecture, the Orthogonal Functional Basis Neural Network (OFBNN). For generalization purposes, the well-known delete-1 [20] and generalized cross validation (GCV) [12] methods have been utilized in neural network training.

Research/Technical Achievements - 1996

The proposed method has been applied to four example problems. For benchmark purposes, each problem employs Regularization for RBF (RRBF) as proposed by Orr in [9]. These examples illustrate the improved accuracy of the proposed method over RRBF relative to generalization mean square error (MSE) defined as

$$\mathbf{MSE} = \frac{1}{N}\sum_{i=1}^{N}\left(y_i - \hat{y}_i\right)^2$$

where N denotes the number of testing patterns, y_i and $\hat{y}_i$ are the target and predicted target values, respectively. We have improved the speed and the accuracy of developing a functional mapping model to enable dynamic *in-situ* re-modeling of material processes. The method and algorithm are detailed below and followed by illustration using one of the four example problems.

Algorithm Orthogonal Functional Basis Functional Mapping (OFBFM)

Input:: The training patterns $\left\{\mathbf{x}_t,\ y_t\right\}_{t=1}^{P}$.

Output: The connection weights, **g**, the orthogonal basis set, **H**, the subset, $\mathbf{H}_{\mathbf{subset}}$, the linear weight, **w**, connected from the nodes in **Y** layer to the output nodes, and the mapping.

Step 1. *Construct a* ***Heterogeneous*** *Regressor Set:*, $\mathbf{F}=\left\{\mathbf{f}_i\right\}_{i=1}^{N}$:

Build the regressor matrix **F** of size $P * M$, where P is the number of training patterns. Each column of the **F** matrix is a basis. As opposed to the traditional approach, e.g., RBF or FLN, in which either Gaussian or sigmoid basis are used, we use a combination of heterogeneous functions. In our implementation we pick functional basis randomly from a set of heterogeneous basis functions. The functions that we use are Gaussian Function, Sigmoid Function, Cauthy Function, Multi-quadratic Function, and Inverse multi-quadratic Function.

Step 2*: Build orthogonal basis matrix* **H** *according to orthogonal transformation.*

Step 3: *Initialization:*

Let $\mathbf{H}_{\mathbf{subset}} = \boxed{\phi}$, where ϕ is an empty set and let $k = 1$.

Step 4. *Subset selection, regularization, and generalized cross validation*: (GCV):

The original mapping problem is transformed to the following form:

$$\mathbf{y} = \mathbf{H}\mathbf{g} + \mathbf{e} \tag{4.0}$$

With zero-order regularization employed, the objective function is

$$E = \mathbf{e}^{\mathbf{T}}\mathbf{e} + \lambda\, \mathbf{g}^{\mathbf{T}}\mathbf{g} \tag{4.1}$$

We can use similar approach to find the most efficacious subset of $\mathbf{H}$ [9]. The GCV is used as the stopping criterion.

Find $\mathbf{h}_i$ such that:

$$\max_i \left\{ \frac{(\mathbf{y}^{\mathbf{T}}\mathbf{h}_i)^2}{\lambda + \left(\mathbf{h}_i\right)^{\mathbf{T}}\mathbf{h}_i} \right\} \tag{4.2}$$

Include $\mathbf{h}_i$ as an element of the $\mathbf{H}_{\text{subset}}$, i.e., $\mathbf{H}_{\text{subset}} = \mathbf{H}_{\text{subset}} \cup \mathbf{h}_i$.

Because all the columns in $\mathbf{H}$ are orthogonal to each other, in implementation of selecting $\mathbf{H}_{\text{subset}}$ we can set the corresponding selected column to 0, and the next $\mathbf{h}_i$ that satisfies Eq. (4.2) can be selected easily. Compared with the computational cost of order $\mathbf{O}\left(P^2\right)$--$\mathbf{O}\left(P^3\right)$ for $\mathbf{h}_i$ shown in [9] where:

$$\mathbf{H} = \mathbf{H} - \frac{\mathbf{h}_t\mathbf{h}_t^{\mathbf{T}}\mathbf{H}}{\mathbf{h}_t^{\mathbf{T}}\mathbf{h}_t} \tag{4.3}$$

$\mathbf{h}_t$ is the selected orthogonal basis from Eq. (42), our process is much more efficient. In general, the computational complexity to generate the $\mathbf{H}$ matrix using our OFT method described above is of the order of $\boxed{\mathbf{O}(k * N)}$, where k is the rank of $\mathbf{F}$ and N is the number of the given regressors. In functional mapping, where $P >> N$, our approach takes advantage of replacing the complicated process of updating orthogonal basis with a pre-selection process.

For regularization, we modify λ based upon the GCV derivation as described by [9]. Denote $\mathbf{Z}$ as $\mathbf{I}_P - \sum_{\mathbf{h}_i \in \mathbf{H}\text{subset}} \left\{ \frac{\mathbf{h}_i\mathbf{h}_i^{\mathbf{T}}}{1 + \mathbf{h}_i^{\mathbf{T}}\mathbf{h}_i} \right\}$, λ is modified with the following equation:

$$\lambda = \frac{\left[\partial\, trace(\mathbf{Z}) / \partial\lambda\right]\mathbf{y}^{\mathbf{T}}\mathbf{Z}^2\,\mathbf{y}}{trace(\mathbf{Z})\mathbf{h}_t^{\mathbf{T}}\left(\mathbf{H}^{\mathbf{T}}\mathbf{H} + \lambda\,\mathbf{I}_k\right)^{-1}\mathbf{h}_t} \tag{4.4}$$

In each step, r is calculated per reference [9]

$$\rho = \frac{1}{P}\frac{\|\mathbf{Z}\mathbf{y}\|^2}{\left[(1/P)\, trace\ (\mathbf{Z})\right]^2} \tag{4.5}$$

Stop if r reaches its minimum point; otherwise $k = k+1$, repeat this step.

End of OFBFM learning algorithm.

The OFBFM finds the $\mathbf{H}_{subset}$ with d basis, and the orthogonal weights $\mathbf{g} = [\mathbf{g}_1 \quad , \mathbb{L} \, , \quad \mathbf{g}_d]$. Since $\mathbf{H} = \mathbf{Y} * \mathbf{G}$ and $\mathbf{H}_{subset}$ is the subset of the $\mathbf{H}$, we have $\mathbf{H}_{subset} = \mathbf{Y} * \mathbf{G}_{subset}$. Finally, the system equation is:

$$\hat{\mathbf{y}} = \mathbf{H}_{subset} * \mathbf{g} = \mathbf{Y} * \mathbf{G}_{subset} * \mathbf{g} = \mathbf{Y} * \mathbf{w}$$

where $\mathbf{w} = \mathbf{G}_{subset} * \boxed{\mathbf{g}}$ is the equivalent final weight from the original basis nodes to the output nodes. The final network structure is a single layer net as shown below (Figure 1), where $\mathbf{w} = \mathbf{G}_{subset} * \boxed{\mathbf{g}}$.

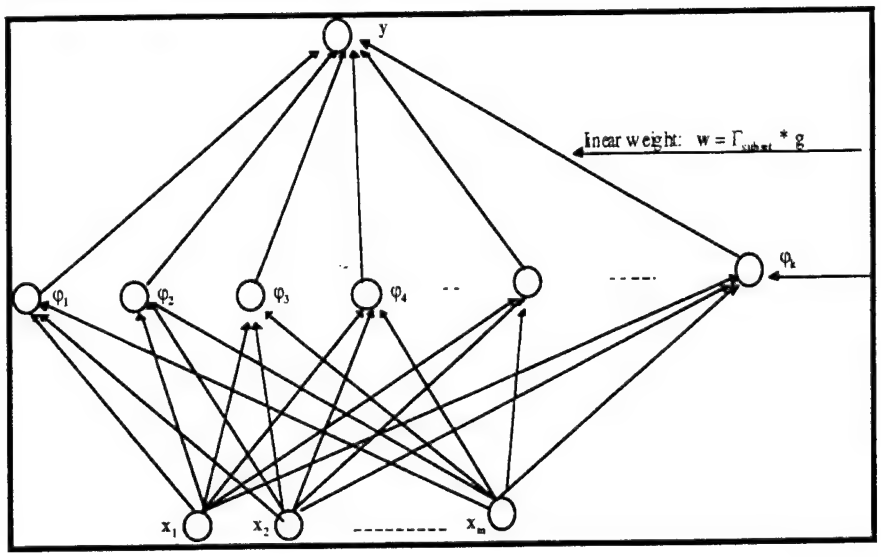

Figure 1. The Orthogonal Functional Basis Neural Network (OFBNN).

The following example demonstrates the performance of the proposed algorithm and network structure.

Example : A 3-dimensional sine wave is considered as follows:

$$f(x,y) = (1-y^2) * \sin(\pi x)$$

A set of 225 (15 * 15) training patterns, with random Gaussian noise, are generated uniformly from the interval [-1,1]. The noise added to each pattern is with zero mean and standard deviation 0.2. Initially, 225 Gaussian basis nodes (width ρ=1.0) and 225 heterogeneous functions with random parameters are used as basis candidates for RRBF and OFBNN, respectively. The final RRBF neural network has 33 basis functions using RRBF approach, while the OFBNN requires only 19 basis functions. The generalization MSE for RRBF is 0.0086 and the generalization MSE for OFBNN is 0.0022. Another set of 900 (30 * 30) testing data, shown in Figure 13, is also generated in the interval between [-1,1] to test the final networks. In this case, the generalization MSE is 0.0068 for OFBNN, while the MSE result for RRBF is 0.0114. Furthermore, we use Gaussian-only function for our OFBNN and use heterogeneous functions for RRBF for more testings. The testing result is shown in Table 1. The comparison again illustrates that the proposed new method yields a more efficient and accurate functional approximation of the signal.

Table 1. Comparison of RRBF and OFBNN

	Gaussian function MSE		Heterogeneous Functions MSE	
	Training(15*15)	Testing (30*30)	Training (15*15)	Testing (30*30)
RRBF	0.0086	0.0114	0.0035	0.0095
OFBNN	0.0031	0.0075	0.0022	0.0068

The above are comparisons of functional approximation methods - specifically regularization and the traditional view of subset selection. We have identified inherent problems with these methods when attempting to learn an efficient and accurate functional approximation. We have explained a new method, referred to as the Orthogonal Functional Transformation (OFT), and a new neural network architecture, Orthogonal Functional Basis Neural Network (OFBNN) to address these problems. We have shown that using the proposed method better convergence speed in the regularization process can be achieved. Also the computational complexity is less than that proposed by Orr regarding "regularization in the selection of RBF centers" [9]. The OFT method we have proposed here not only uses fewer basis functions in the final neural network structure, but also achieves more accurate generalization results.

Several examples are used for testing our method, and from which, simulation results have demonstrated the reduced architecture, and therein, improved computational intractability, and most important an improvement in approximation accuracy relative to functional mapping of input to output.

Future Work - 1997

An important trend in materials research is to predict properties for a new material that has similar property values with known compounds. Often the prediction involves several important materials property features. The selection of the property features becomes very crucial for the prediction.
The future work will focus on using a neural network computing approach to address such an important issue. Our initial objective is to identify and distinguish property features that are significant for purposes of prediction. The primary task of the future work is to use the OFBNN for feature discovery. We will also apply the proposed OFBNN to the problem of real-time process control of physical vapor deposition of thin films for Rugate filters (refer to project description).

The comparison of the OFBNN and traditional neural net approach will be carried out. We believe that the OFBNN can filter out noisy data created by sensors in acquisition stage. In identifying important features for materials process, we hope that we are able to model and remodel materials process in-situ. This will provide us effective and efficient design of materials. In addition, we hope that we can discover a method for new materials discovery. Our focus is feature extraction from the given variables and/or feature discovery.

References

1. Rawlings, J. O., 1988, *Applied Regression Analysis.*, Wadsworth & Brooks/Cole, Pacific Grove, CA.
2. Barron, A. R., and Xiao, X., 1991, Discussion of "Multivariable adaptive regression splines" by J. H. Friedman. *Ann. Stat.* 19, pp. 67-82
3. Breiman, L., 1992, *Stacked Regression.*, Tech. Rep. TR-367, Department of Statistics, University of California, Berkeley
4. Broomhead, D. S., and Lowe, D., 1988, *Multivariable functional interpolation and adaptive methods.* Complex Syst. 2, pp. 321-355
5. Park, J., and Sandberg, I. W., 1991, "Universal approximation using and radial-basis-function networks," *Neural Computation*, Vol. 3, No.2, pp. 246-257.
6. Igelnik, Boris and Pao, Yoh-Han, 1995, "Stochastic Choices of Basis Functions in Adaptive Approximation and the Functional-Link Net", *IEEE Trans. on Neural Networks*, Vol. 6, No.6, pp. 1320-1328.
7. Funahashi, K., 1989, "On the approximate realization of continuous mappings by neural networks," *Neural Networks*, vol.2, pp.183-192.
8. Chen, S., Cowan, C. F. N. and Grant, P. M., 1991, "Orthogonal least squares learning algorithm for radial function networks," *IEEE Trans. on Neural Networks*, Vol.2, No.2, pp.302-309.
9. Orr, M. J. L., 1995, "Regularization in the Selection of Radial Basis Function Centers", *Neural Computation.*, 7, pp. 606-623.
10. Tikhonov, A. N. and Arsenin, V. Y., 1977, *Solutions of Ill-Posed Problems.*, Winston, Washington.
11. Press, W. H., Teukolsky, S. A., Vetterling, W. T.,and Flannery, B. P., 1992, *Numerical Recipes in C*, 2nd ed. Cambridge University Press, Cambridge, UK.
12. Golub, G.H., Heath, M., and Wahba, G., 1979, "Generalized cross-validation as a method for choosing a good ridge parameter," *Technometrics* 21 (2), pp. 215-223.
13. Mackay, D. J. C., 1992. Bayesian interpolation. *Neural Computation* 4 (3), pp. 415-447.
14. AllebmD, N., 1974, "The relationship between variable selection and data augmentation and a method for prediction," *Technometrics* 16 (1), pp. 125-127
15. Berliner, L. M., 1987, "Bayesian control in Mixture Models", *Technometrics*, November 1987,Vol.29, No.,4 pp 455-460
16. Chen, S., Chng, E.S., and Alkadhimi, K., 1995. "Regularized orthogonal least squares algorithm for constructing radial basis function networks," *International Journal of Control*, submitted.
17. Barron, A. R. 1993, "Universal Approximation bounds for superpositions of a sigmoidal function", *IEEE Transactions on Information Theory*, 39(3), pp. 930-945.
18. McCulloch, W.S. and Pitts, W., 1943. "A logical calculus of the ideas immanent in nervous activity", Bulletin of Mathematical Biophysics, 5, pp. 115-133.
19. Pao, Y.H., 1996. "Memory based computational intelligence for materials processing and design", Wright Laboratory Technical Report WL-TR-96-4062, Wright-Patterson AFB, OH, pp. 1-14.
20. Allen, D. M., 1974, "The relationship between variable selection and data augmentation and a method for prediction," Technometrics, Vol. 16, No. 1, pp. 125-127.

Papers and Presentations

In Preparation

S. B. Fairchild, Y, Cao, C. L. Philip Chen, and S. R. LeClair, **Control and Monitoring of Rugate Filter Fabrication Using Orthogonal Functional Basis Neural Network,** Submitted to *IEEE Transaction on Systems, Man, and Cybernetics*, 1997.

C. L. P. Chen, Y. Cao, and S. R. LeClair, **Material Structure-Property Prediction using Orthogonal Functional Basis Neural Network,** Proceeding of ***Australasia Pacific Forum on Intelligent Processing and Manufacturing of Materials (IPMM)***, July 14-17, 1997.

C. L. P. Chen, Y. Cao, and S. R. LeClair, **Orthogonal Functional Neural Network,** Proceeding of *IEEE Int'l Conference on Neural Networks*, Houston, TX, June 9-12, 1997.

Published

C. L. P. Chen, S. R. LeClair, and Y-H. Pao, **A Rapid Supervised Learning Neural Network for Function Approximation and Time-Series Prediction**, To appear in *Journal of Mathematical Modeling and Scientific Computing*, Principia Scientia, 1996.

C. L. P. Chen and Y. Lu, **FUZZ: A Fuzzy-Based Concept Formation System that Integrates Human Categorization and Numerical Clustering**, To appear in *IEEE Trans. on Systems, Man and Cybernetics*, Vol. 27, No. 1, 1997.

C. L. P. Chen, **A Rapid Supervised Learning Neural Network for Function Interpolation and Approximation**, *IEEE Trans. on Neural Networks*, Vol. 7, No. 5, pp. 1220-1230, 1996.

H. N. Kamhawi, C. L. P. Chen, and S. R. LeClair, **Feature Sequencing in the Rapid Design System Using a Genetic Algorithm**, *Journal of Intelligence Manufacturing*, Vol. 7, No. 1, pp. 55-67, 1996.

C. L. P. Chen and S. Xie, **A Freedhand Drawing System using Fuzzy Concepts**, *Computer Aided Design*, Volume 28, Number 2, pp. 77-89, 1996.

S. Ye and C. L. P. Chen, **Periodic Time-Series Analysis Using Neural Networks**, Proceeding of *Artificial Neural Networks in Engineering*, pp. 719-724, 1996; and *Adaptive Distributed Parallel Computing Symposium,* Aug, 1996.

C. L. P. Chen and Y. Lu, **A Fuzzy-Based Concept Formation System for Categorization and Numerical Clustering**, *Artificial Neural Networks in Engineering*, pp. 185-190, 1996.

C. L. P. Chen and S. R. LeClair, **A Real-time Stepwise Supervised Learning Algorithm for Time-Series Prediction and System Identification**, <I> Proceeding of *IEEE Int'l Conference on Neural Networks*, pp. 2009-2014, Washington, DC, June 3-6, 1996.

Patents

S. R. LeClair, Pao, Y.H., Westhoven, T.E., Kamhawi, H. N., Chen, C. L. P., Jackson, A. G., and Chemaly, A. C., **Inductive-Deductive Process Design for Machined Parts**, AF Invention #21134, Patent #5,485,390, 16 Jan. 96.

Y. Cao, S. R. LeClair, and C. L. P. Chen, **Orthogonal Functional Basis Method for Function Approximation**, AF Invention #1981x, Patent Applied, Dec, 1996.

Research Leaders: Dr Steven R. LeClair & Dr James C. Malas, **Team:** Dr C. L. Philip Chen (NRC), Y. Cao (Ph.D. Student), Dr Y.H. Pao (V/S), Dr B. Igelnik (V/S)

'Atomic-Scale' Materials Process Design

The atomic-scale materials process design effort is driven by near-term and pervasive (aircraft, spacecraft and missle) needs for improved threat/detection materials and their attendant wear, anti-reflection, etc. coatings. Long term there is need for nanoscale or crystal lattice level methods to design 3D variations in physical, compositional, and morphological features of thin-films for: 1) 'in-flight' performance sensors - smart materials - which are embedded and/or deposited onto bulk materials (monolithic or composite), and 2) for 'in situ' sensing to monitor and control thin-film processing (e.g., design of a Rugate notch filter to recover Stokes and anti-Stokes peaks in a Raman spectrum).

Research OBJECTIVES are

- to generate new methods for nanoscale materials-process design,
- to develop methods for discovering patterns in materials-process data, and
- to automate the exploration and mapping of physical materials structure-property-process-use data.

Research FOCUS is

- developing methods for visualizing resultant crystal structures and the causal processing conditions and phenomena suitable for simulating thin-film materials process design,
- investigating the use of rules/constraints for thin-film modeling of the formation and growth using a qualitative (linear) reasoning approach,
- developing 'transitional' cellular automata-like methods to improve the accuracy and speed of simulating micron to millimeter thick depostions over irregular surfaces,
- applying novel classification methods (e.g., Pyramidal Networks) to discover and/or predict new material compounds having desirable structure and property.

Background

An atomic-scale design environment for new materials must contain methods for selecting candidate materials, simulating their behavior under defined conditions, and displaying the behavior in easily interpretable form by a user. Efforts to achieve such an environment have focused on designing the algorithms for simulating thin-film formation and growth. The initial step requires constructing the substrate from any type of crystal desired. Commercially available software could accomplish part of this task, but all are focused on creating structures, not substrates. Hence, algorithms were written and translated to code that allows a user to create any crystal structure in a display window and add to that window an independently controllable crystal structure. This allows the user to orient one structure with respect to the other easily in order to visually determine the optimum orientation of a film on a substrate or the expected orientation on the substrate. In addition, single atoms may be moved to any position, and their attributes changed (color, size, transparency). New atoms can be added as desired to any position via drag and drop action. Multiple unit cells can be created via menu function, thereby allowing creation of substrates of arbitrary thickness and extent. Single layer films can also be created and manipulated with respect to the substrate. Defects and doping can be accomplished simply.

Cellular-Automata Modeling of Thin-Films

Modeling thin-film growth is typically performed via quantitative models [1], but the penalty is often computational intractability. Although these models perform well for limited cases, performance degrades with increased complexity, e.g., quantum wells, organic films, those with various defects and grain boundaries [2] - hence the interest in seeking more computationally efficient alternatives. One such alternative are cellular automata (CA) or CA-like methods to not only improve tractability but also to integrate multiple modeling paradigms (physical, thermodynamic, and chemical) and scales (from 'first principle' type interactions, i.e., interatomic collisions, @ 10^{-13} seconds to process temperature changes @ 10^{-3} seconds) into one framework [3].

There are many advantages to the CA approach. The time steps for first principle type calculations are orders of magnitude too small for practical consideration [5]. Monte Carlo methods work well, but they too become intractable when process times are on the order of seconds [4]. Large numbers of atoms 10^{23} [5] require large, often parallelized, computational machines to accomplish these calculations in a reasonable time e.g., five (5) minutes or adustable between 2-10 times faster than real-time. Since such a large number of atoms cannot be handled in such a short time, new ways of viewing the problem are required.

CAs are also designed to improve tractability via parallelization in software, and sometimes, but not necessarily hardware. CA's are defined as parallel implementations of a finite state machine (computer processor) in software. In addition, CA's offer a second advantage, one which distinguishes them from parallel computing machines. CAs operate on linearized models or sets of rules formulated in IF-THEN statements that include not only symbolic but mathematical expressions, allowing for the combination of multiple models and/or extensive but simple adaptation of the models. Structures that contain sub-rules can be easily formulated. The major effort involved in such an approach is the formulation of the rules from physical, thermodynamic and chemical principles.

CA rules for atomic-scale materials process simulation must capture physical-chemical behavior known or expected to be important for film formation, e.g., local interaction with the substrate is fundamental. We have chosen to use random motion of many atoms to simulate the case of

- **a vapor approaching the substrate from a source**, and
- **a gas with random motion of the atoms in the lattice.**

These two modes of physical simulation represent the principle physical-chemical behaviors associated with thin-film deposition methods of immediate interest (pulsed laser deposition, molecular beam epitaxy, and chemical vapor deposition).

The depositions can involve several species, which require simple binary interactions to be considered first. Bonding and related rules of behavior must incorporate the chemical interactions appropriate for the elements considered. These rules include the concepts of bond type, electronic structure of the element, geometric factors such as radius and type, charge state, and electronegativity difference. These attributes are sufficient for a simple bonding concept to be represented through a set of rules. Table 1, created from basic rules of chemistry [6], shows the possible bonds that result from various combinations of atom states. The bond may change when electronegativity is added as a decision rule. For example, Na and Cl are neutral atoms which when brought together form a covalent bond. But the electronegativity difference is large enough to drive electrons to produce an asymmetric charge cloud, resulting in an ionic bond of Na^+ and Cl^-.

To accommodate the differences in physical-chemical behaviors among the elements, data structures must be formed which include the essential variables that characterize the atom. A first attempt at such a data set is as follows:

- atom {shell, charge, radius, atomic number, atomic weight}
- shell {open, closed}
- charge {positive, negative}
- positive {1, 2, 3, 4, 5, 6}
- negative {1, 2, 3, 4, 5, 6}
- radius {atomic, covalent, ionic, metallic}

With regard to process modeling of physical-chemical behaviors, it is noteworthy that atomic number and atomic weight are numeric data, while atomic radius, covalent radius, ionic radius, and metallic radius have two values: a symbolic value that indicates type and a numeric value.

Table 1. Possible combinations of two elements.

Element			Element			
period	group	orbital	period	group	orbital	bond
1	1	open	1	1	open	covalent
1	1	open	2-7	1	open	covalent
1	1	open	2	2	closed	covalent
1	1	open	2	13-17	open	covalent
1	1	open	1-7	18	closed	covalent
1	1	open	3-7	3-11	open	covalent
1	1	open	3-7	12	closed	covalent
1	1	open	3-7	13	open	covalent
2	2	closed	1	1	open	covalent
2	13-17	open	1	1	open	covalent
2	13-17	open	2-7	1	open	covalent
3-7	13	open	1	1	open	covalent
3-7	3-11	open	1	1	open	covalent
3-7	12	closed	1	1	open	covalent
2-7	14-17	open	1	1	open	covalent
2	2	closed	2	13-17	open	ionic
2	13-17	open	2	2	closed	ionic
2	13-17	open	2	13-17	open	ionic
2	13-17	open	1-7	18	closed	ionic
2	13-17	open	3-7	12	closed	ionic
2	13-17	open	3-7	13	open	ionic
3-7	13	open	2	13-17	open	ionic
3-7	3-11	open	2	13-17	open	ionic
3-7	12	closed	2	13-17	open	ionic
2-7	14-17	open	2-7	1	open	ionic
2-7	14-17	open	2	2	closed	ionic
2-7	14-17	open	2	13-17	open	ionic
2-7	14-17	open	3-7	3-11	open	ionic
2-7	14-17	open	3-7	12	closed	ionic
2-7	14-17	open	3-7	13	open	ionic
2	2	closed	2-7	1	open	metallic
2	2	closed	2	2	closed	metallic
2	2	closed	3-7	3-11	open	metallic
2	2	closed	3-7	12	closed	metallic

2	2	closed	3-7	13	open	metallic
3-7	13	open	2-7	1	open	metallic
3-7	13	open	2	2	closed	metallic
3-7	13	open	3-7	3-11	open	metallic
3-7	13	open	3-7	12	closed	metallic
3-7	13	open	3-7	13	open	metallic
3-7	3-11	open	2-7	1	open	metallic
3-7	3-11	open	2	2	closed	metallic
3-7	3-11	open	3-7	3-11	open	metallic
3-7	3-11	open	3-7	12	closed	metallic
3-7	3-11	open	3-7	13	open	metallic
3-7	12	closed	2-7	1	open	metallic
3-7	12	closed	2	2	closed	metallic
3-7	12	closed	3-7	3-11	open	metallic
3-7	12	closed	3-7	12	closed	metallic
3-7	12	closed	3-7	13	open	metallic
2	2	closed	1-7	18	closed	none
2	13-17	open	3-7	3-11	open	none
3-7	13	open	1-7	18	closed	none
1-7	18	closed	1	1	open	none
1-7	18	closed	2-7	1	open	none
1-7	18	closed	2	2	closed	none
1-7	18	closed	2	13-17	open	none
1-7	18	closed	3-7	3-11	open	none
1-7	18	closed	3-7	12	closed	none
1-7	18	closed	3-7	13	open	none
3-7	3-11	open	1-7	18	closed	none
3-7	12	closed	1-7	18	closed	none
2-7	14-17	open	1-7	18	closed	none
1-7	18	closed	1-7	18	closed	vanderWaals

Types of Ions possible

Cation

period	group	ion config	ion charge	sign
1-7	1-2, 13	noble gas or pseudo noble gas [(n-1)d^10]	grp 1: 1	pos
1-7	1-2, 13	noble gas or pseudo noble gas [(n-1)d^10]	grp 2: 2	pos
1-7	1-2, 13	noble gas or pseudo noble gas [(n-1)d^10]	grp 13: 3	pos
1-7	13-15	ns^2	grp 13: 1	pos
1-7	13-15	ns^2	grp 14: 2	pos
1-7	13-15	ns^2	grp 15: 3	pos

Anion

period	group	ion config	ion charge	sign
1-7	15-17	noble gas or pseudo noble gas	grp 15: -3	neg
1-7	15-17	noble gas or pseudo noble gas	grp 16: -2	neg

1-7	15-17	noble gas or pseudo noble gas	grp 17: -1	neg

Sources:

D. D. Ebbing & M. S. Wrighton, *General Chemistry*, Houghton Mifflin Co., Boston, 1987;

J. E. Huheey, E. A. Keiter, and R. L. Keiter, *Inorganic Chemistry*, HarperCollins College Pubs., New York, 1993.

The interactions are assumed to take place in a binary mode, i.e., only two-atom interactions initially to form dimers. The electronegativity difference is used to determine the expected bond state.

In order to accommodate the rules for a CA that involve nearest neighbors, multi-atom interactions must be considered. There are several ways to do this. One could have a two step process in the rule: part one considers the binary interaction most likely to occur among the nearest neighbors. Part 2 then considers the effects of the nearest neighbors on the dimer formed.

Case 1. Atom A approaches a surface containing atoms A and B. The A-B Bond probability is very high and A-A bond very low. For a square cell arrangement, the first step is to allow A-B bond to occur with one of the B atoms. The second step is to consider that if another B atom is near the dimer, then the dimer rotates and locates the A atom between the two B atoms. The effect of A atoms is negligible. Definition of nearness is within two B-atomic diameters. If A-A bonds have a 'negative' probability (repulsive effects), then the influence of A must be considered as well. For the case shown in the figure, the location of an A atom from the vapor will be as shown, assuming that the A repulsion is exactly opposite the B attraction.

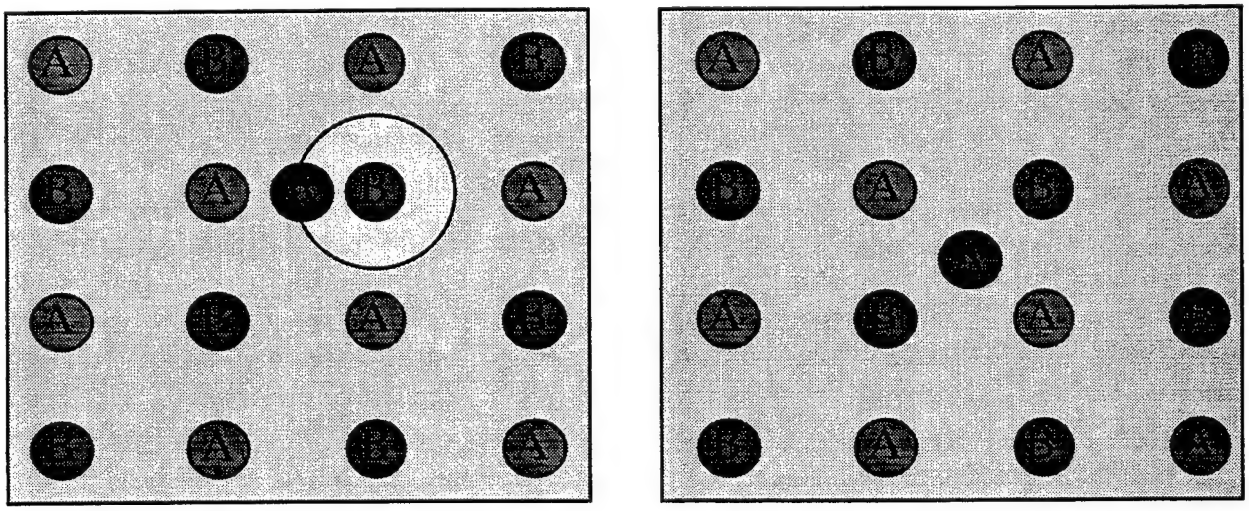

Figure 1. Atom A on substrate of AB atoms.
Two step process for bonding. (a) initial contact (left); and
(b) adjustment of position (right) to accommodate the attractive potential of the A-B bond.

Case 2. Given the surface is comprised of atoms B and C, and the vapor atom A: (a) the A-B bond is favored, the A-C bond is not favored, which is similar to Case 1, (b) A-C bond is favored, and the A-B bond is not, which is again similar to Case 1, (c) the A-B and A-C bonds are equally favored. The result is the same as Case 1, (d) the A-B bond is stronger than A-C. The equilibrium position of A in this case is closer to B than to C, which for the square array is similar to Case 1. If the structure is

not square then the equilibrium position lies along the line connecting the strongest bond atoms, in this case the B-B line.

Case 3. The surface contains A,B atoms, the vapor A,C atoms.
(a) A-B bonds and C-B bonds favored.
(b) A-B and C-A favored
(c) A-C favored only.
(d) A-B favored only.
(c) C-B favored only.

Alternatively, one could use the table of possible bonds and the electronegativitiy differences to determine the initial dimer and then consider what atoms are near the dimer. Adjustments to the dimer orientation and position then follow from Table 1. This approach is the simpler of many alternate routes, because it is easier to generalize in an algorithm.

Rules

The above cases have assumed the CA lattice to be square (2D) or cubic (3D). More complex, irregular (voronoi-like) lattices will yield different bonding results, but these have not been explored as fully [7]. To date, depositions involving single atom species have been demonstrated, and an experimental multiple species case has been attempted. Temperature effects have not been explicitly included except throught varying the probabilities of bonds at various sites as a weak interaction. Finally, the substrates have been flat and with steps. The basic 2D rule is derived from a square lattice in which an atom is surrounded by 8 neighbors: 4 nearest and 4 next-nearest neighbors.

Rule 1: An atom bonds to the substrate when the atom is next to three sites that are occupied. The structures produced were tree-like and rather long relative to the substrate.

Rule 2: Variable probabilities of bonding are assigned to the substrate positions relative to the atom. As shown in the figure, nearest neighbors were given highest probability. Thickening of the trees occurred.

Rule 3: Variable percentages are assigned to all surrounding sites and there must be at least 2 atoms in those sites in order for bonding to occur. Thickening of trees occurred.

Rule 4: Similar to Rule 3 but 3 atoms must be present. Rather dense growth was noted.

Rule 5: Similar to Rule 3 but more than 3 atoms must be present. Dense growth noted, and some gas atoms were occluded, that is, were trapped inside the growth of bound atoms.

The substrate atoms do not move. Any atom that is within a nearest neighbor distance or next nearest neighbor distance is bonded and no longer is able to move.

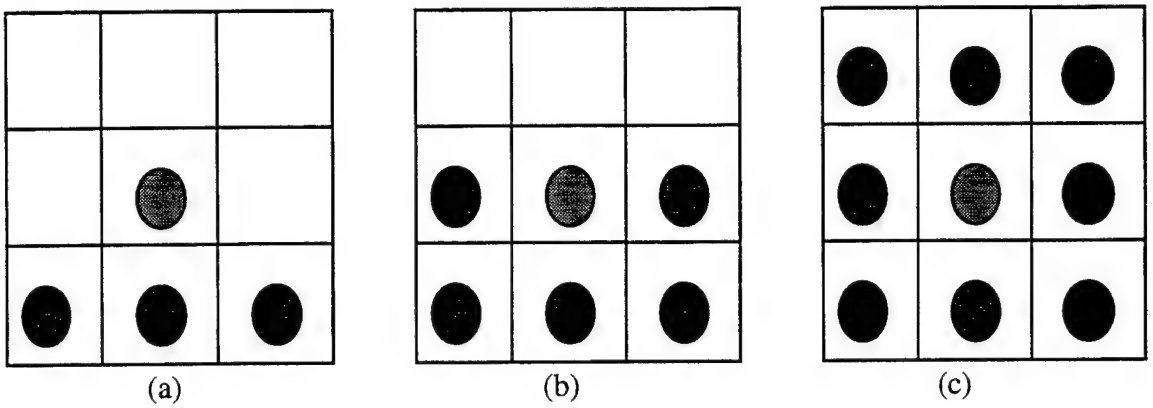

Figure x. 2D Rules: (a) Rule 1 geometry; (b) Rule 2 geometry; variable probabilities applied to each red atom; (c) Rules 3, 4, and 5; various coordinations required for each rule.

The starting atoms are lined up parallel to the substrate. Initially the atoms were chosen starting at the left and moving to the right. This produced what visually appeared to be a random dispersion of atoms as the system cycled through its states. On reaching the substrate the atoms stick and other atoms then stick to them, producing a tree. The broad appearance of the final state is very similar to the ballistic model images presented in Machlin's book [2].

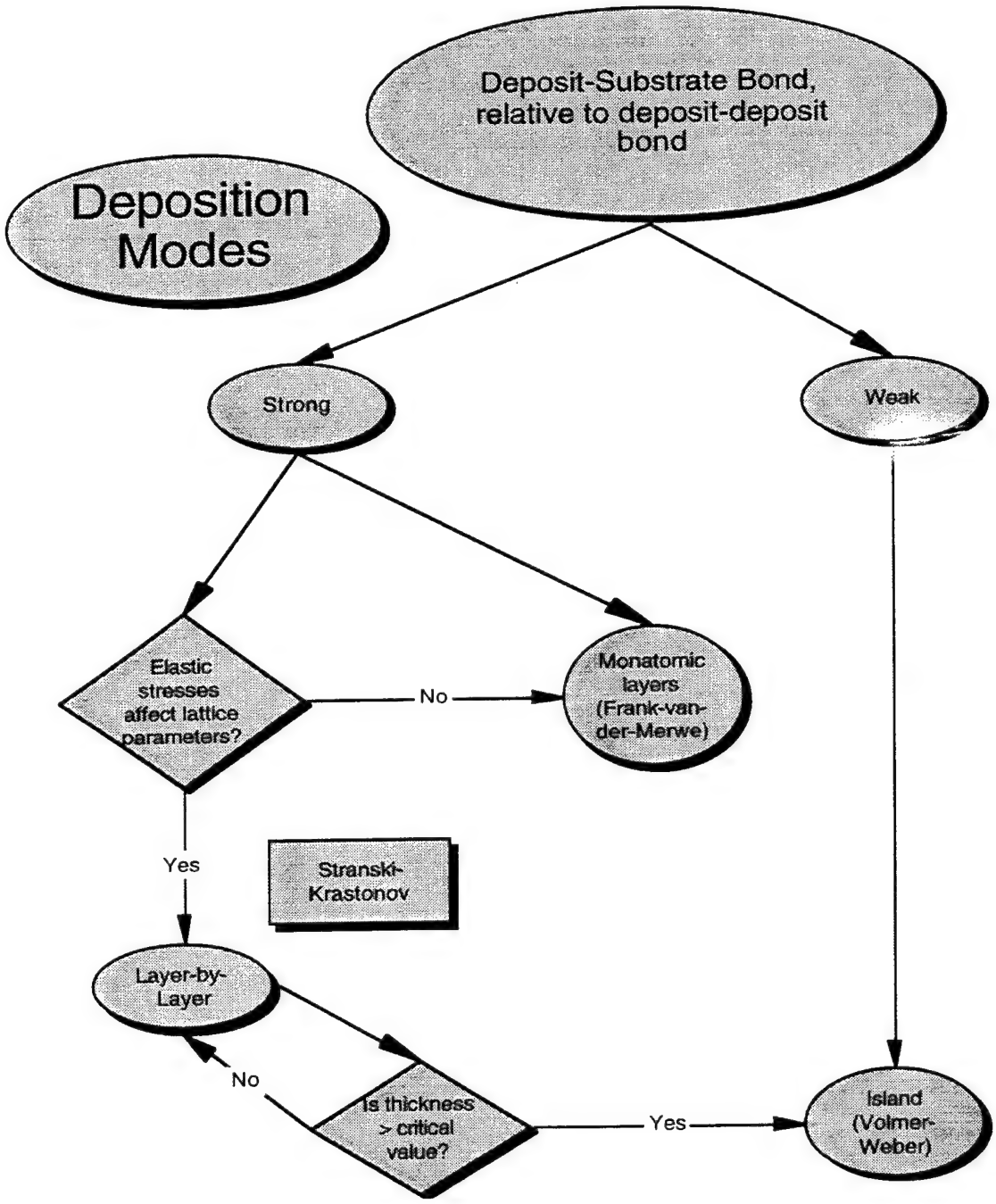

Figure 2. Deposition modes flow diagram in terms of weak and strong bonding models.

3D Cases

For 3D experiments, variants of Rule 5 were applied to allow for the 3D nature of the possible neighbors. Hills of atoms were observed that are reminiscent of grains, but the microstructure is not clear yet. Expitaxial growth occurs in every case, that is, the growth patterns duplicate the structure of the substrate, even though the overall structure appears to be rather rough.

Generic Rules

The first step in using a CA-like model as a method for simulating deposition processes is to extract rules for thin-film growth and lattice formation. Machlin [2] provides a number of points that are translatable to qualitative rules and semi-quantitative rules that include behavior statements and simple formulas involving the parameters. A simple flow diagram, shown in Figure 2 above, illustrates the possible format for decisions about the film growth and formation process in terms of parameters and behavior. The flow diagram represents a starting set of rules for initial CA-like film modeling. Development of a more detailed flow diagram to improve the versatility and accuracy is being pursued by examining the literature and discussing the process with local experts. Although a CA-like approach to molecular modeling requires a knowledge acquisition step similar to that used to create an expert system, the future benefit enabled by a rule-based representation is the autonomous refinement of the rule-set.

References

1. A.-L. Barabasi and H. E. Stanley, *Fractal Concepts in Surface Growth*, Cambridge University Press, New York, NY, 1995.
2. E. S. Machlin, *Materials Science in Microelectronics*, GIRO Press, Croton-on-Hudson, NY, 1995.
3. T. Toffoli and N. Margolus, *Cellular Automata Machines*, The MIT Press, Cambridge, MA, 1988.
4. D. Dorsey, Private Communication, 1996.
5. *Physics Today*, September, 1996.
6. James E. Huheey, Ellen A. Keiter, and Richard L. Keiter, Inorganic Chemistry, Harper Collins College Publishers, 1993.
7. Adamatzky, A., Voronoi-like partition of lattice in cellular automata. *Mathematical and Computer Modeling*, 1996, 23, 51-66.

Research/Technical Achievements - 1996

In reference to the research focus of *investigating the use of rules/constraints for thin-film modeling of the formation and growth using a qualitative (linear) reasoning approach and developing methods for visualizing resultant crystal structures* and *the causal processing conditions and phenomena suitable for simulating thin-film materials process design:*

Up through October 1996:

- An architecture for CA-like thin-film modeling has been developed using the latest three dimensional display software available for Macintosh and PC platforms (Quickdraw 3D). This nanomodeler architecture consists of a substrate generator, a cellular automaton based simulator, and a graphical visualizer.
- A data visualization module was created for viewing three dimensional data sets and which allows real time on-screen rotation of the data set.
- Simple rule sets were abstracted from the literature on thin-films. Metal, semiconductor, and other types of films behave in specific ways each of which has associated qualitative modes of behavior. Descriptions of thin film growth based on this classification were used to organize the statements into rules of behavior, mostly in simple if-then formats. Multiple nested if-then rules are typical for thin films.

In reference to the research focus of *applying novel classification methods (e.g., Pyramidal Networks) to discover and/or predict new material compounds having desirable structure and property:*

• A number of small data sets were created for use by the pyramidal net program. The data was drawn from the KnowBe database application and from handbooks of data, particularly optical data. These data sets proved very useful for testing the CONFOR program and eliciting errors in formating and nomenclature that would otherwise not have been obtainable. The CONFOR program proved to be awkward and difficult to use because of manual entry requirements, limitations on the size of the database used, obscure error calls, and extreme fragility in format tolerance. As a result a new interface shell was designed.

• Developed an interface to the CONFOR pyramidal net software, referred to as CONSHELL, to accommodate external data input from an EXCEL-created text file. CONSHELL accepts a text file created in Excel and converts it to a format acceptable to the CONFOR program. The shell then runs CONFOR and collects results into an output text file. Multiple experiments using the same data can be run automatically, allowing comparison of predicted properties against actual values in a test set. Because properties cannot depend on the order of the data, the training data set is shuffled randomly for n trials. The results of each trial are tabulated against a test set and the combined results of the n trials are collected into a results file. This approach avoids the manual entry now required using the CONFOR software.

• A pyramidal nets program based on the concepts of Gladun et al. was created by F. Brown, University of Kansas, using a LISP environment. The program reproduces the nets observed with the CONFOR program, and prediction capabilities have been added. However, the class bins are limited to positive and negative. A class range of up to 10 classes is required in order to allow suitable prediction of materials properties.

Future Work - 1997

In reference to the research focus of *developing 'transitional' cellular automata-like methods to improve the accuracy and speed of simulating micron to millimeter thick depostions over irregular surfaces:*

Diamond and diamond-like films are of considerable importance to component life-extension efforts, e.g., such films and coatings offer protection against erosion and corrosion of components in adverse environments, e.g., rain impinging on optical windows at supersonic speeds. Hence, examining the process of formation via a modeling system provides an efficient means for uncovering aspects of the processing that would be difficult to obtain by direct experiments. To address this area, development of the CA-like modeler will consider methods and application-specific problems associated with the deposition of diamond and diamond-like films. Candidate issues to be explored include: identification of multilayer film formation processes, influence of layered materials on IR absorbance, materials parameters related to hardness, and the effects of defects and irregular substrate surfaces.

Further development of rule statements based on general physical and chemical principles is planned. The structure of these rule sets must be explored to determine useful approaches, because there are hundreds of variables associated with elements and compounds/alloys. The potential complexity of such rules is high, and hence careful consideration of the structure of the relationships must be accomplished to avoid a large network that is not interpretable. Taxonomies and multiple hierarchies must therefore be constructed.

Experiments using the CONSHELL program are planned in order to establish the utility of the CONFOR program and pyramidal nets for prediction of materials properties. Results in 1996

were not encouraging. However, the great difficulty in conducting a large number of experiments precluded a satisfactory set of outputs. Having the CONSHELL program available is expected to reduce the difficulty in conducting the experiments and to lead to a sound assessment of pyramidal nets for prediction of properties.

Papers and Presentations

Several articles were prepared, two of which were published this year. The remainder will appear in the next year. Several more papers and presentations are in preparation.

In Preparation

LeClair, S.R., Jackson, A. G., Benedict, M.D., Conrad, D.M., and Cao, Y., **Electronic prototyping: toward future applications of sensors in materials processing**, TMS Symposium on *Advanced Sensors in Materials Processing*, Orlando, FL, February, 1997.(ASC-96-2910)

Jackson, A. G., Laube, S. J. P., and Jones, J. , **Spectroscopic methods for control of thin film growth**, TMS Symposium on *Advanced Sensors in Materials Processing*, Orlando, FL, February, 1997.(ASC-96-2788)

Busbee, J. D., Lubbers, D. P., Jackson, A. G., Biggers, R. R., Liptak, D. C., and Iman Maartense, **Raman spectroscopy for determining YBCO thin-film paramters in situ**, TMS Symposium on *Advanced Sensors in Materials Processing*, Orlando, FL, February, 1997.(ASC-96-2991)

Jackson, A.G., Ohmer, M., and LeClair, S.R., **Relationship of the second order nonlinear optical coefficient to bandgap in inorganic non-centrosymmetric crystals**, submitted to *Infrared Physics and Technology*. (ASC-95-1193)

Published

Jackson, A.G., Laube, S.J.P., and Busbee, J.D., **Sensors, methods and physical properties**, *JOM*, The Minerals, Metals & Materials Society, Warrendale, PA, September 1996. ASC-96-1769

Jackson, A.G., LeClair, S.R., Ohmer, M.C., Ziarko, W., and Al-Kamhawi, H., **Rough sets applied to materials data,** accepted by *Acta Materialia*, ASC-95-0483, ASC-95-2492

Brown, F. M., Peterson, N., Jacobs, G., Jackson, A.G., & LeClair, S.R., **A description and analysis of Gladun's pyramidal net classification theory**, Proceedings of the Adaptive Distributed Parallel Computing Symposium, Dayton, OH, 8-9 August 1996. ASC-96-1903

Jackson, A.G., **Analysis of semiconductor compounds using discovery methods**, Proceedings of the International Conference "Information Theories and Applications" Troyan and Sofia, Bulgaria, 12-22 May 1996. ASC-96-0931

Jackson, A.G., and Kiselyova, N.N., **Finding compound propery patterns in empirical data sets using discovery methods**, Proceedings of the International Union of Crystallography XVII Congress and General Assembly, Seattle, WA, 8-17 Aug 1996. ASC-96-0177

Patent

LeClair, S.R., Pao, Y.H., Westhoven, T.E., Kamhawi, H.N., Chen, C.L.P., Jackson, A.G., Chemaly, A.C., **Inductive-Deductive Process Design for Machined Parts**, AF Invention #21134, Patent Applied For, #08/159,968, 24 Jul 95, Patent #5,485,390, 16 Jan 96.

International Conferences Attended

International Conference "Information Theories and Applications" Troyan and Sofia, Bulgaria, 12-22 May 1996.
International Union of Crystallography XVII Congress and General Assembly, Seattle, WA, 8-17 Aug 1996.
15th International meeting of CODATA, Tsukuba, Japan, September 27-Oct 4, 1996.

Research Leader: Dr Al Jackson, **Team**: Dr Steve LeClair, Mr Mark Benedict, Mr David Ress (V/S) Students: Mr David Hanna, Mr Jesse Anderson

Biologically-based Materials: Protein Secondary Structure Prediction

The protein secondary and tertiary structure prediction effort is driven by the need to develop analysis and prediction tools that will aid the biomaterials design process. Biomaterials have demonstrated considerable potential for nonlinear optical and laser hardening for various threat/detection applications. The ability to successfully predict the three dimensional structure of a protein will be a significant contribution toward the development of biomaterials with tailored optical properties.

Research OBJECTIVES are to

- evaluate the use of neurocomputing and statistical pattern recognition techniques for predicting secondary structures in proteins
- develop a reliable database classification of protein secondary and tertiary structures for designing nonlinear optical materials

Research FOCUS is

- developing a two stage model for secondary structure prediction using a Mahalanobis distance classifier and a probabilistic neural network (PNN).

Background

It has been demonstrated that given a contiguous length of 5 or more amino acids in the chain of a protein, the folding type (helix, sheet, or coil) can be predicted to a high degree of accuracy. More recently Chou and Zhang demonstrated that a Mahalanobis distance classifier can be used to predict the folding type of 'all-a' and 'all-b' proteins to 100% accuracy, 'a/b' to 89.7%, and 'a+b' to 88.9%. This technique takes into account the correlative effect among different amino acid components, making it significantly more successful than classification methods that simply use geometric distances. The knowledge of the folding type of the protein can help in the prediction of the local secondary structure confirmations.

Research/Technical Achievements - 1996

In reference to the work of Chou and Zhang, a successful classifier for protein folding types involving a two stage model (Figure 1) for secondary structure prediction has been designed. The first stage is the Mahalanobis classifier which will assign an unknown protein to a 'fold' class. The second stage is a probabilistic neural network (PNN), with separate training sets developed for each fold class. This method differs from other successful neural network secondary structure prediction models, such as that by Rost and Sander. They include proteins from multiple families in the training set and encode information about the family of a protein in the amino acid sequence representation that is presented to the neural network.

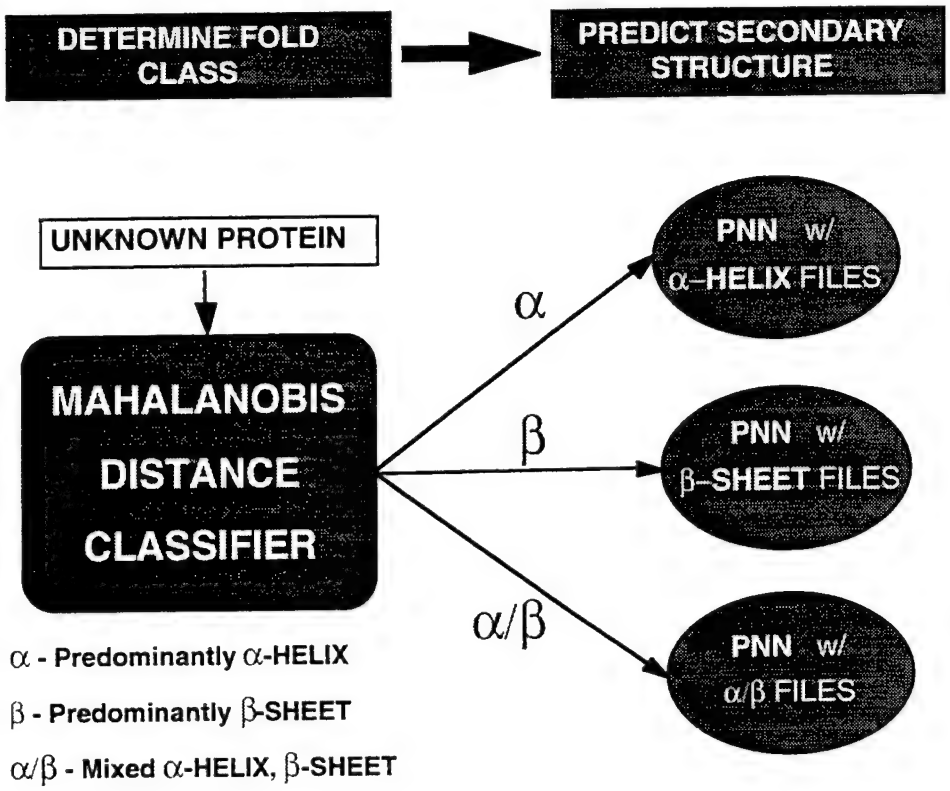

Figure 1. Two Stage Model.

The protein secondary structure prediction is *a priori* defined for three fold classes. Proteins are categorized into a fold class based on the contents of secondary structures:

- 'all-a' - having predominantly alpha helical secondary structure;
- 'all-b' - having predominantly beta sheet secondary; and
- 'a/b' - having approximately equal distributions of alpha helices and beta sheets.

The 'a+b' fold class was not attempted for this preliminary study. The database used consisted of 71 proteins from the Brookhaven Protein Data Bank. Secondary structure assignments for each residue were obtained using Kabsh and Sander's DSSP program. These files were taken from the 105 files used by Kneller et al., updated where appropriate. Separate training sets for each fold class are developed, and the encoding scheme for the amino acids in the training set is fold class dependent.

So far the results of this approach are quite encouraging, reference Tables 1-8. For predicting alpha helices in the 'all-a' fold class, the success rate is 75.8%. For predicting beta sheets in the 'all-b' fold class, the success rate is 72.1%. The prediction success rate for alpha helices in the 'a/b' fold class is 69.4%, and for beta sheets it is 84%. The average overall prediction success for alpha helices in the 'all-a' proteins is 75.8%, and the average value for C is 0.457. The average overall prediction success for beta sheets in the 'all-b' proteins is 72.1%, and the average value for C is 0.438. The average overall prediction success for alpha helices in the 'a/b' proteins is 69.4%, and the average value for C is 0.314. The average overall prediction success for beta sheets in the 'a/b' proteins is 84.0%, and the average value for C is 0.397.

Future Work - 1997

Effort will focus on expanding the data set, i.e., more proteins will be incorporated into the training set. Only a small number of proteins have been tested to this point, which limits generalization ability. The probabilistic neural network algorithm currently being used is from a commercial package, and there are limitations. A new PNN architecture (Figure 2) will be developed which should improve prediction accuracy for the 'all-b' and 'a/b' fold classes.

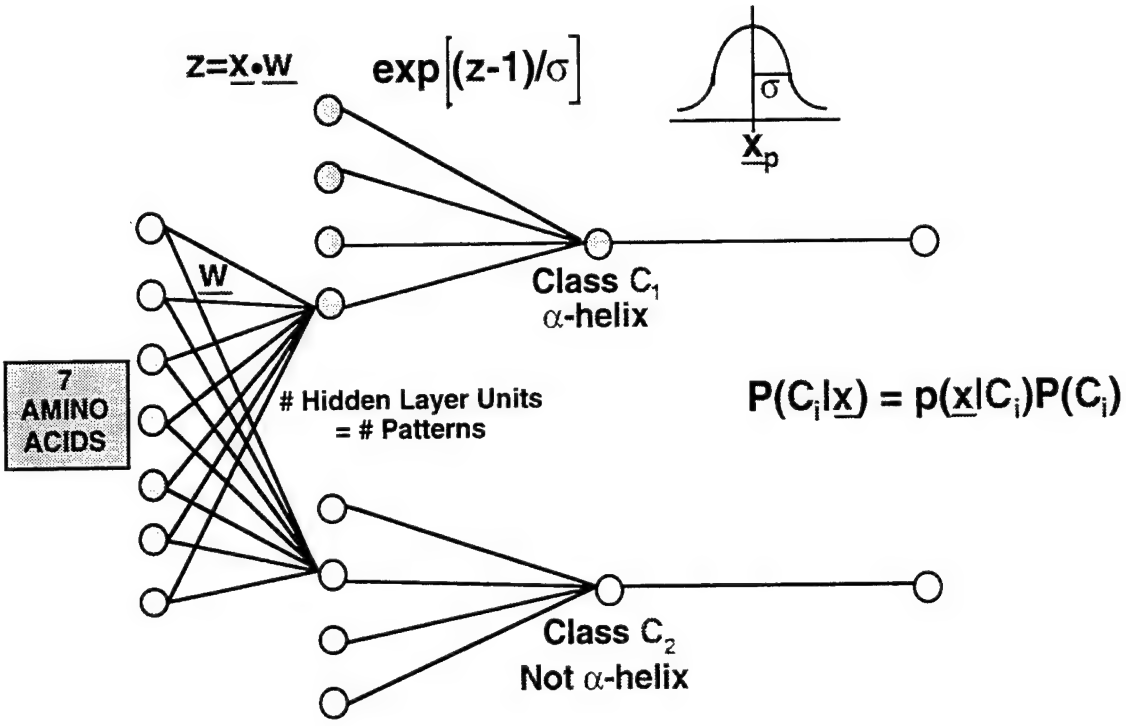

Figure 2. New Probabilistic Neural Network Architecture.

Papers and Presentations

In Preparation

Pachter, R., Fairchild, S., Lupo, J., Adams, W., *"Biomolecular Structure Prediction at a Low Resolution Using a Neural Network and the Double Iterated Kalman Filter Technique", accepted to Biopolymers*

Fairchild, S., Meng, Z., Pachter, R. *"A Two Stage Model for Protein Secondary Structures Prediction"*

Published

Fairchild, S., *"Protein Secondary Structures Prediction using a Mahalanobis Distance Classifier and a Probabilistic Neural Network,"* Proceedings of the Adaptive Distributed Parallel Computing Symposium, Dayton, OH, 8-9 August 1996.

Fairchild, S., Pachter, R., Perrin, R., *"Protein Structure Analysis and Prediction,"* The Mathematica Journal, volume 4, issue 5, pp. 64-69

Pachter, R., Fairchild, S., Lupo, J., Perrin, R., Sennet, B., Crane, R., Adams, W. (1995) In:"Parallel Computing in Computational Chemistry" (Mattson, T.J., ed.) 592, 202-210.

Pachter, R., Wang, Z., Lupo, J., Fairchild, S., Sennet, B. (1996) In:"Global Minimization of Complex Energy Functions: Molecular Confirmation and Protein Folding" (Pardalos, P., Shalloway, D., Xue, G., eds.) volume 23, pp. 169-180.

Lupo, J., Pachter, R., Fairchild, S., Perrin, Adams, W. (1994) In:"Biomolecular Materials by Design" (Alper, M., Bayley, H., Kaplan, D., Navia, M. eds.) 330, 71-75.

Table 1. The Mahalanobis distances calculated for 26 proteins in the 'all-a' fold class. Rate of correct prediction = 26/26 = 100%.

PDB Code	$D^2(x,m_a)$	$D^2(x,m_b)$	$D^2(x,m_a/b)$	Predicted Fold Class
1bp2	0.0035	0.0479	0.7490	a
1mbs	0.0056	0.0485	2.2065	a
2ccy_A	0.0018	0.0311	0.4182	a
5cpv	0.0045	0.0532	0.3113	a
4p2p	0.0046	0.0201	0.0606	a
1cc5	0.0007	0.0495	0.0980	a
1ccr	0.0006	0.0199	0.1366	a
1cyc	0.0090	0.0723	0.1931	a
1ecd	0.0053	0.0488	0.2645	a
1fdh_A	0.0021	0.0441	0.9117	a
1fdh_G	0.0039	0.0474	1.3278	a
1hds_A	0.0030	0.0574	0.3912	a

PDB Code	$D^2(x,m_a)$	$D^2(x,m_b)$	$D^2(x,m_a/b)$	Predicted Fold Class
1hds_B	0.0088	0.0772	0.0940	a
1mbd	0.0030	0.0138	0.1341	a
2c2c	0.0012	0.0515	0.3274	a
2cyp	0.0017	0.0266	0.2848	a
2dhb_A	0.0058	0.0131	0.4786	a
2dhb_B	0.0037	0.0086	1.2618	a
2hmq_A	0.0019	0.0169	0.3970	a
2lh1	0.0047	0.0201	0.0972	a
2lhb	0.0007	0.0495	0.0980	a
2lzm	0.0012	0.0220	0.0523	a
3hhb_A	0.0215	0.0252	0.3902	a
3hhb_B	0.0010	0.0259	0.6013	a
3icb	0.0046	0.0426	0.5818	a
4cts_A	0.0069	0.0385	0.2467	a

Table 2. The Mahalanobis distances calculated for 25 proteins in the 'all-b' fold class.
Rate of correct prediction = 25/25 = 100%.

PDB Code	$D^2(x,m_a)$	$D^2(x,m_b)$	$D^2(x,m_a/b)$	Predicted Fold Class
1acx	0.0594	0.0096	2.6235	b
1est	0.0638	0.0020	0.8975	b
1fc2_D	0.1804	0.0044	0.7437	b
1pfc	0.0059	0.0028	0.1599	b
1rei_A	0.0115	0.0073	0.2977	b
1tgs_Z	0.0203	0.0013	0.4346	b
2alp	0.1745	0.0031	0.1340	b
2apr	0.0179	0.0051	0.6280	b
2gch	0.1813	0.0036	0.1663	b
2ig2_L	0.1689	0.0017	0.0332	b
2kai_A	0.0465	0.0012	0.0635	b
2mcp_H	0.0348	0.0031	1.6310	b
2mcp_L	0.1031	0.0022	0.8026	b
2pab_A	0.0197	0.0006	0.1268	b
2rhe	0.0153	0.0056	0.1699	b
2sga	0.0883	0.0009	0.9458	b
2sod_O	0.0103	0.0031	1.0713	b
2tbv_A	0.0176	0.0010	0.0967	b
3app	0.1381	0.0055	0.3247	b
3cna	0.0224	0.0066	0.4286	b
3pcy	0.2068	0.0086	0.1973	b
3rp2_A	0.0160	0.0070	0.2735	b
3sgb_E	0.0634	0.0034	1.1926	b
4ape	0.0878	0.0038	0.4178	b
4gcr	0.1823	0.0078	1.0213	b

Table 3. The Mahalanobis distances calculated for 20 proteins in the 'a/b' fold class.

Rate of correct prediction = 17/20 = 85%.

PDB Code	$D^2(x,m_a)$	$D^2(x,m_b)$	$D^2(x,m_{a/b})$	Predicted Fold Class
1bp2	0.1004	0.2295	0.0158	a/b
1mbs	0.6062	0.2269	0.1043	a/b
2ccy_A	0.1748	0.0557	0.0533	a/b
5cpv	0.1292	0.0469	0.0192	a/b
4p2p	0.0952	0.0776	0.0159	a/b
1cc5	0.0812	0.0313	0.0177	a/b
1ccr	0.7850	0.2069	0.1067	a/b
1cyc	0.2942	0.1135	0.0537	a/b
1ecd	0.5914	0.0971	0.0621	a/b
1fdh_A	0.0940	0.1069	0.0221	a/b
1fdh_G	0.1902	0.0748	0.0045	a/b
1hds_A	0.0347	0.0982	0.0152	a/b
1hds_B	0.1102	0.0996	0.0218	a/b
1mbd	0.0650	0.0939	0.0476	a/b
2c2c	0.1121	0.2970	0.1692	a
2cyp	0.0523	0.0688	0.0097	a/b
2dhb_A	0.2568	0.1392	0.0490	a/b
2dhb_B	0.2354	0.0363	0.0396	b
2hmq_A	0.1075	0.0631	0.0214	a/b
2lh1	0.0771	0.0354	0.0386	b

Table 4. Amino acid probability representation for the 'all-a', 'all-b', and 'a/b' training sets.

Amino Acid	all-a Training Set	all-b Training Set	a/b Training Set (a)	a/b Training Set (b)
Glutamate	239/306 = **0.781**	58/159 = **0.365**	159/338 = **0.470**	32/338 = **0.095**
Methionine	67/96 = **0.698**	32/47 = **0.681**	54/121 = **0.446**	27/121 = **0.223**
Alanine	468/610 = **0.767**	147/371 = **0.396**	226/491 = **0.460**	57/491 = **0.116**
Leucine	392/545 = **0.719**	190/338 = **0.562**	202/495 = **0.408**	112/495 = **0.226**
Lysine	310/520 = **0.596**	69/191 = **0.361**	163/411 = **0.397**	55/411 = **0.134**
Phenylalanine	162/259 = **0.625**	119/186 = **0.640**	73/210 = **0.348**	44/210 = **0.210**
Glutamine	114/166 = **0.687**	92/196 = **0.469**	73/169 = **0.432**	9/169 = **0.053**
Tryptophan	46/75 = **0.613**	44/76 = **0.579**	39/82 = **0.476**	14/82 = **0.171**
Isoleucine	126/182 = **0.692**	134/229 = **0.585**	114/345 = **0.330**	137/345 = **0.397**
Valine	262/373 = **0.702**	254/388 = **0.655**	145/509 = **0.285**	173/509 = **0.340**
Aspartate	168/332 = **0.506**	58/246 = **0.236**	112/356 = **0.315**	23/356 = **0.065**
Histidine	120/215 = **0.558**	33/78 = **0.423**	44/123 = **0.358**	15/123 = **0.122**
Arginine	98/148 = **0.662**	68/150 = **0.453**	86/208 = **0.413**	26/208 = **0.125**
Theronine	151/288 = **0.524**	205/425 = **0.482**	101/327 = **0.309**	49/327 = **0.150**
Serine	158/317 = **0.498**	192/544 = **0.353**	104/409 = **0.254**	50/409 = **0.122**
Cysteine	53/89 = **0.596**	55/107 = **0.514**	20/80 = **0.250**	19/80 = **0.237**
Tyrosine	83/150 = **0.553**	115/197 = **0.584**	64/175 = **0.366**	37/175 = **0.211**
Asparagine	128/255 = **0.502**	61/236 = **0.258**	70/238 = **0.294**	16/238 = **0.067**
Proline	92/226 = **0.407**	37/231 = **0.160**	48/250 = **0.192**	21/250 = **0.084**
Glycine	180/426 = **0.426**	151/513 = **0.294**	98/510 = **0.192**	52/510 = **0.102**

Table 5. Prediction Results for the alpha helices in the proteins in the 'all-a' fold class.

PDB code	Q	C
1bp2	0.8291	0.6580
1mbs	0.7415	0.3014
2ccy_A	0.8430	0.5282
5cpv	0.6863	0.3433
4p2p	0.7542	0.5292
1cc5	0.7143	0.4300
1ccr	0.7333	0.4508
1ecd	0.7154	0.2833
1fdh_A	0.8370	0.5763
1cyc	0.6495	0.3449
1fdh_G	0.7786	0.4775
1hds_A	0.7407	0.4653
1hds_B	0.7050	0.3859
1mbd	0.7891	0.3438
2c2c	0.7642	0.5668
2cyp	0.6551	0.3098
2dhb_A	0.7556	0.4963
2dhb_B	0.8214	0.5720
2hmq_A	0.7315	0.4676
2lh1	0.8095	0.3991
2lhb	0.8042	0.5062
2lzm	0.6835	0.3123
3hhb_A	0.8148	0.5272
3hhb_B	0.8000	0.5110
3icb	0.8406	0.6856
4cts_A	0.7077	0.4116

Table 6. Prediction Results for the beta sheets in 10 proteins in the 'all-b' fold class.

PDB code	Q	C
1acx	0.7129	0.4303
1est	0.6838	0.4165
1fc2_D	0.7900	0.5766
1pfc	0.7714	0.4953
1rei_A	0.7030	0.4050
1tgs_Z	0.6986	0.3742
2alp	0.7188	0.4552
2apr	0.6740	0.3448
2gch	0.6853	0.3611
2ig2_L	0.7667	0.5192

Table 7. Prediction Results for alpha helices in 10 proteins in the 'a/b' fold class.

PDB code	Q	C
1abe	0.6823	0.3644
1fx1	0.6879	0.3259
1gp1_B	0.6180	0.1562
1rhd	0.7038	0.4050
1tim_A	0.7012	0.3991
2ldx	0.6769	0.3058
2sbt	0.7222	0.1508
2taa	0.7267	0.3143
3adk	0.6862	0.3807
3gpd_R	0.7324	0.3421

Table 8. Prediction Results for beta sheets in 10 proteins in the 'a/b' fold class.

PDB code	Q	C
1abe	0.8796	0.6027
1fx1	0.6838	0.4165
1gp1_B	0.8596	0.3668
1rhd	0.9164	0.4760
1tim_A	0.8755	0.5161
2ldx	0.7969	0.2779
2sbt	0.8623	0.3254
2taa	0.8623	0.3254
3adk	0.8670	0.3066
3gpd_R	0.7998	0.3546

Research Leader: Mr. Steve Fairchild, **Team**: Dr.Ruth Pachter, Dr. Steve LeClair, & Prof Yoh-Han Pao (Visiting Scientist), Zhuo Meng (Graduate Student, CWRU)

Design/Control of Forging Microstructure

Design and control of bulk deformation processes is of strategic importance to the performance and life of future Air Force systems involving:

- producibility and affordability of wrought TiAl alloys are critical to achieving the required performance of future Air Force systems, namely the F119 growth turbine engine for the F22 System. Other important forging applications for TiAl alloys include: large scale blings (24" diameter and 3" thick) for the Integrated High Performance Turbine Engine Technology (IHPTET) initiative and 6th stage blades for the CEASAR program.
- solving urgent metal processing problems that affect the required performance of existing Air Force systems. For certain structural components, the F22 System is presently experiencing serious metal forming problems, namely strain-induced porosity in Ti-6Al-4V and other titanium alloys which produces unacceptable properties.
- lead times and responsiveness of part suppliers are essential for mission readiness and cost reduction via lean manufacturing practices. Costly and long lead time material processes such as the forging of turbine engine disks offer significant potential for improvements in productivity.

Research OBJECTIVES are

- to develop rigorous process design and control optimization strategies
- to automate the mapping of physical materials structure-property-process
- to demonstrate methods for efficiently forging TiAl into near net shape components with specified microstructures and mechanical properties.

Research FOCUS is

- improve workability, end-product microstructure and mechanical properties of certain titanium aluminide alloys via optimization of material deformation trajectories;
- improve forging process model capabilities for effective tracking and achieving of optimal material behavior trajectories throughout critical regions of workpieces;
- improve metal flow patterns by optimizing initial workpiece geometry, die configuration and number of processing steps;
- reduce sensitivity of forging process parameters with respect to variations in the material, die system, and equipment responses;
- transition and transfer of new controller design techniques to various hot metal forging and extrusion processes.

Background

The design/control of forging microstructure research focuses on materials, processing and equipment as a complete system, i.e., emphasizing the importance of processing parameters as well as the effective utilization of equipment as critical to fabrication of defect-free aerospace components. More specifically,

- Design Focus: Processing parameter selection is performed by combining modern control and optimization theory with simulation techniques for material processing. This involves developing state-space models and a Hamiltonian from material constitutive relationships and

process models. The time evolution of the state and co-state variables is then solved using methods of variational calculus.

- Control Focus: The equipment servo-hydraulic system is evaluated with respect to its ability to deliver the dynamic response of process parameters and optimal settings are determined for the servo-mechanisms such that the deviations from the desired process parameters are minimized. This servo-valve tuning procedure is deemed necessary due to the newly evolving specialized requirements for TiAl processing which were typically not considered during the original fabrication of the equipment.

The overall method may be illustrated in three basic stages as shown in Figure 1.

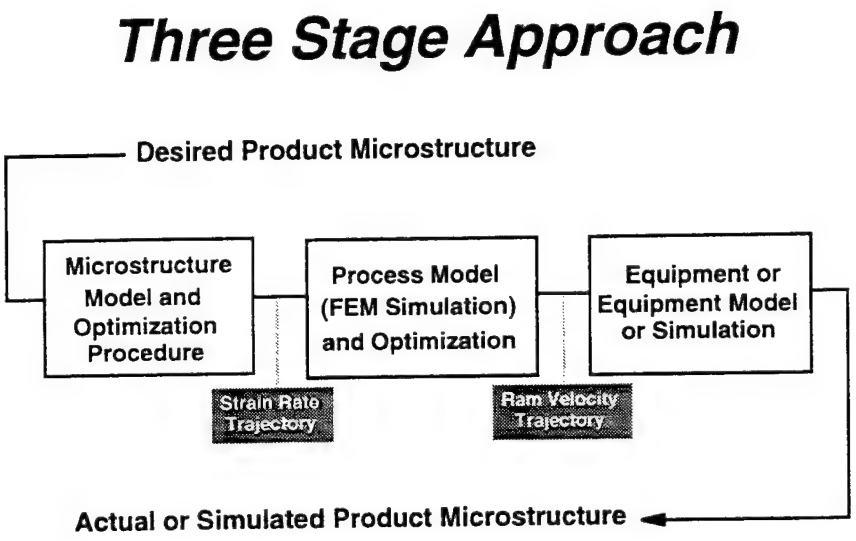

Figure 1. Three Stage Approach to Forming Process Control

First stage, the kinetics of certain dynamic microstructural behavior and intrinsic hot workability of the alloy system are used, together with an appropriately chosen optimality criterion, to calculate ideal strain, strain-rate, and temperature trajectories. Then, the objective in the next two stages is to ensure that the material follows this ideal trajectory as closely as possible during the forging/extrusion/rolling process.

Second stage , the particular process of interest is numerically simulated to aid in the development of a process model for optimal control trajectory. This process trajectory model will be utilized to calculate process parameters such as ram velocities and billet temperatures which closely achieve the ideal strain, strain-rate, and temperature material trajectories calculated in the first stage. Next, these process control parameters are verified and fine tuned by applying closed-loop control and optimization techniques in conjunction with a finite element simulation of the deformation process.

Third stage, the press equipment capability is compared with demands of the optimized process trajectory model using an equipment model which is based on the operation of hydraulic servo-valves, fluid principles, and the actual load versus stroke characteristics of the press. This model is then utilized to reverse engineer the actual press settings needed to most closely match the material-process needs.

Research/Technical Achievements - 1996

Methodology Validation

Method for Optimization of Microstructural Development During Hot Deformation

A major milestone in FY96 has been the experimental verification of a new process design and control method for microstructural optimization during deformation processing. In-house research personnel performed extrusion experiments on the 700 ton Lombard horizontal extrusion press located in the experimental materials processing laboratory (EMPL) located in building 655.

Experiments involving extrusion of plain carbon steel were performed to validate new state-variable based trajectory optimization techniques for precise control of final microstructure. The research objectives were to evaluate: (a) a new type model for describing dynamic recrystallization behavior using a state-space system representation and (b) new applications for existing trajectory-based optimization techniques. The approach involved computing the optimized strain and strain-rate profiles for achieving a DRX grain size of 26 microns with minimal heat generation. The throat geometry of a round-to-round converging extrusion die was calculated from the optimized strain and strain-rate profiles using reasonable assumptions about homogeneous deformation. 1030 steel billets were partially and fully extruded through the "optimized" die geometry and the extruded microstructures were characterized using optical microscopy. The dynamically recrystallized grain size was 26 μm and the post extrusion grain size was 35 μm due to grain growth. The results of the characterization showed the final grain size matched the grain size predicted thus verifying the new state-space methodology for calculating optimized material parameters for producing a desired microstructure. This is shown in Figure 2.

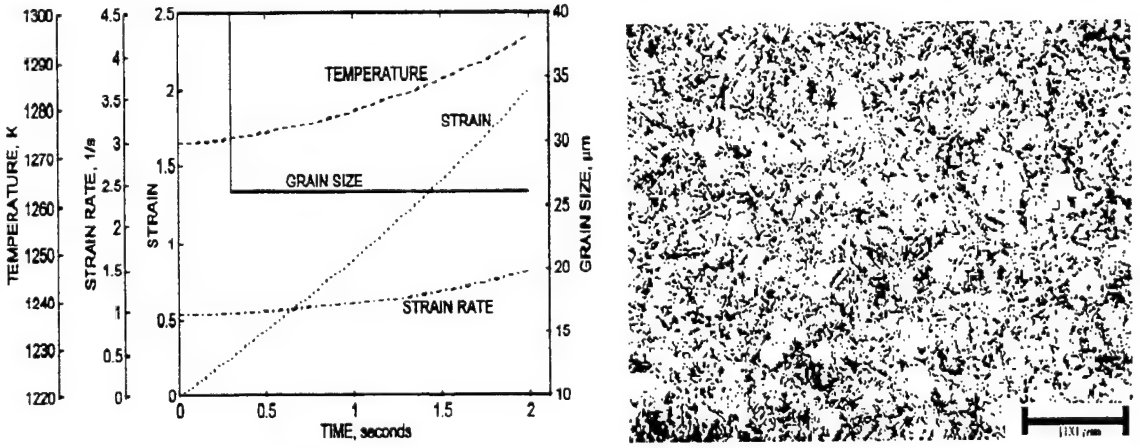

Figure 2. Extruded 1030 steel microstructure (a) predicted and (b) actual.

Material Processing Map for Gamma-Titanium Aluminide Alloy

A processing map for TiAl (Alloy 7) in the cast + hip'd condition was generated for the determination of the optimal processing conditions for the forging of a subscale bladed ring (bling) component. The flow stress behavior and microstructural evolution during deformation were

characterized using the hot compression test method in the temperature range 1025-1225°C and strain rates varying from 0.0001 up to 0.1 s^{-1}. The salient results are:

(1) flow stress decreases with increase in temperature,

(2) as the strain rate increases, the flow stress increases,

(3) at the strain rate of 0.0001 s^{-1}, the flow stress corresponding to test temperatures below 1200°C exhibit maxima indicative of flow softening. This flow softening is the result of non uniform deformation of the specimens during testing,

(4) for temperatures above 1200°C, steady state flow is attained at very low levels of plastic strain, without any peaks in the flow curves, and

(5) The flow curves corresponding to temperatures below 1100°C exhibit a greater degree of flow softening than flow curves corresponding to the intermediate temperatures.

The apparent activation energy values have been calculated using the flow curve data. The DMM stability maps have also been generated. Extensive microstructural studies have been carried out on the deformed samples. As shown in Figure 3, the workability of g-TiAl material has been optimized based on the activation energy, DMM stability analysis and microstructural examination.

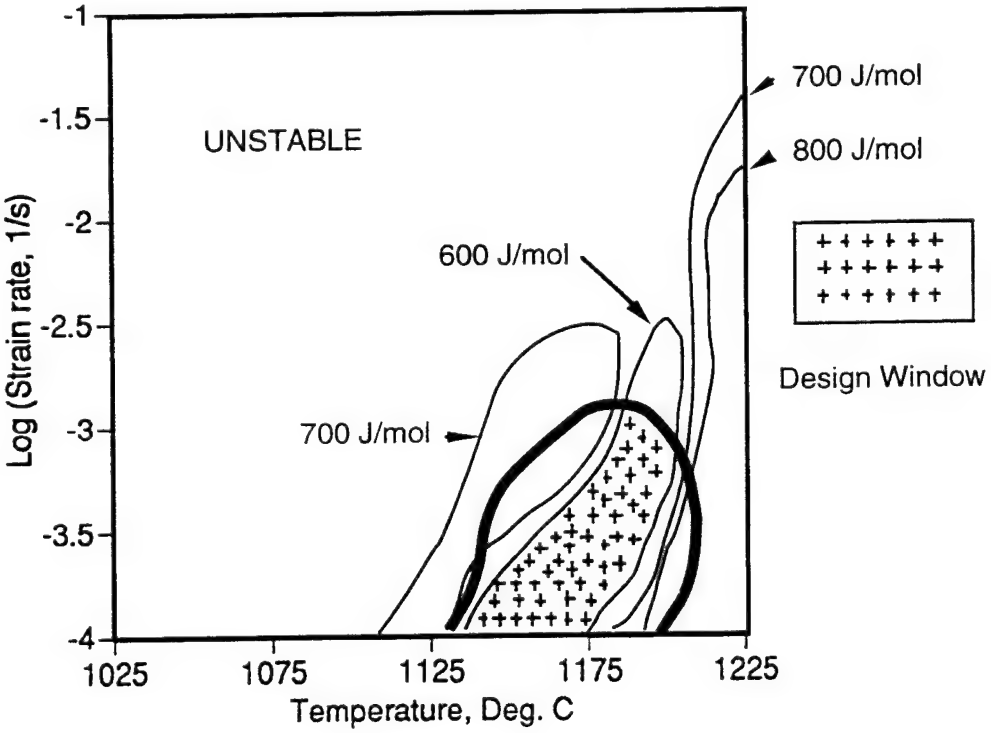

Figure 3. Processing map for Alloy 7

Microstructure Optimization Algorithm

Significant enhancements to existing microstructure evolution optimization software were accomplished. The first enhancement was the addition of the capability for achieving multiple final

microstructure states and other objectives explicitly, rather than implicitly through weighting schemes. For example, the user can specify multiple design objectives, such as:

a) 1200°C < final temperature < 1300°C
b) 30 micron < final grain size < 50 micron
c) 95 % < dynamic recrystalization < 100 %

while simultaneously achieving certain workability constraints, such as maintaining the strain-rate below a specified level throughout the process.

Figures 4 a-d illustrate the case for a material undergoing dynamic recrystallization. The constraints on the final state of the material are a) final temperature < 1315°C, b) final average grain size < 30 micron, c) precent recrystallized > 90 %.

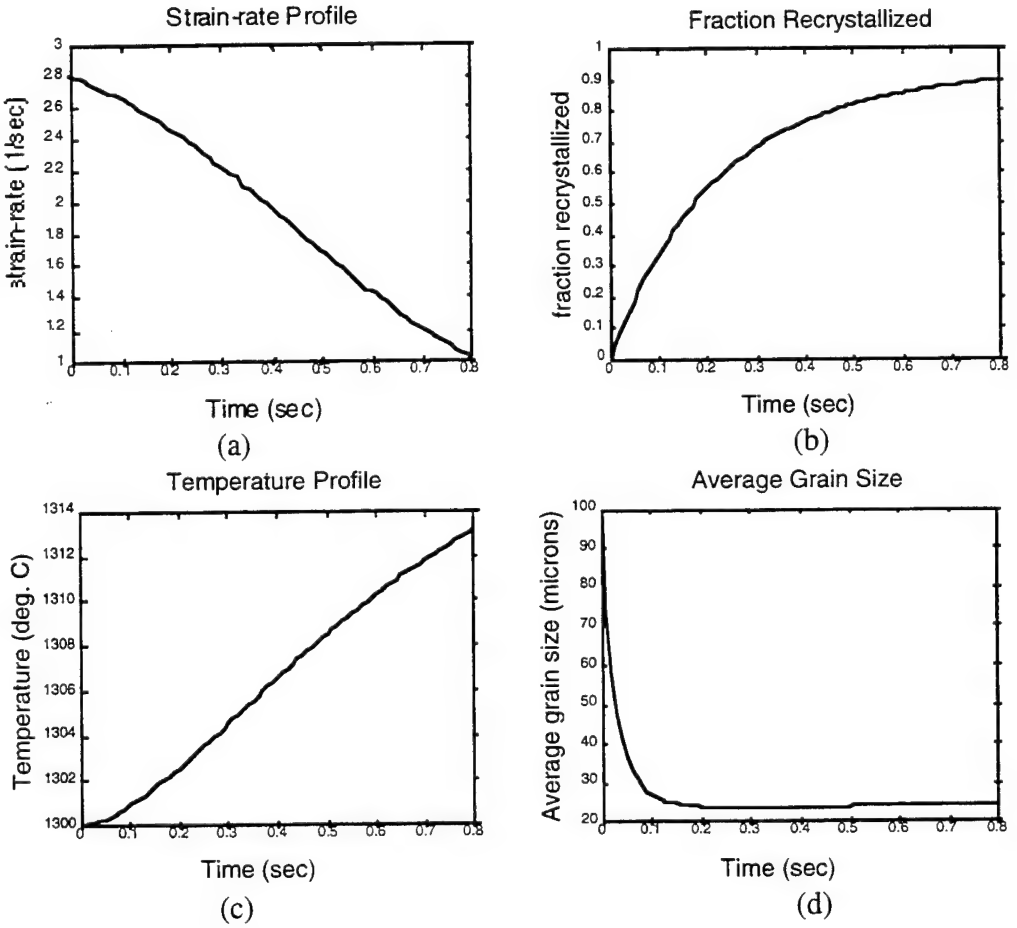

Figure 4. (a) strain rate, (b) % recrystallized, (c) temperature, and (d) grain size as functions of time

The second enhancement was the addition of a graphical user interface to the software. This interface facilitates the specification of the microstructural model, the constraints, and the objectives. It also provides real-time data plotting capability to aid the user in understanding the optimization procedure and results.

Shape Optimization and Geometric Mapping for Deformation Process Design

Research toward the development of a novel, computer-based technique for designing optimal metalforming processes was initiated. The technique promises to yield an approach to

metalforming problem solving that is oriented toward design rather than analysis and should afford a good accuracy vs. computational requirement trade-off. The technique is founded in principles of geometric mapping and optimization in function space using finite-dimensional bases other than finite-elements. The problems that are anticipated to be solved include, *the ideal forming problem* (the best way to form a part assuming fully articulated tooling), the optimal initial billet aspect ratio problem, and the optimal blocker die design problem. Initially, all research has been focused on two-dimensional forging problems.

Microstructure Evolution Modeling and Stability Analyses

Kinetic, micro-mechanical based state models have been developed for the deformation of simple metals. Similarly-based constitutive equations have also been derived. These models have been used to predict the stress-strain and creep behavior with good success, as can be seen in Figure 5. These models have already been incorporated into detailed forge-press simulations. Classical kinetic stability criteria have been applied to the model to explain a variety of physical phenomena with some success. The application of bulk, non-equilibrium thermodynamic stability criteria to metal deformation behavior in the literature is fairly controversial. The relationships between kinetic stability criteria and thermodynamic criteria will be investigated and the links between the two further clarified. Since the behavior of metals, particularly undergoing internal relaxation reactions (recrystallization for example) is known to be stochastic in nature, companion effort in the development of stochastic-state system stability criteria will initiated. This effort will seek to develop kinetic stability criteria for the stochastic system, and link these criteria to bulk non-equilibrium thermodynamic approaches to stability.

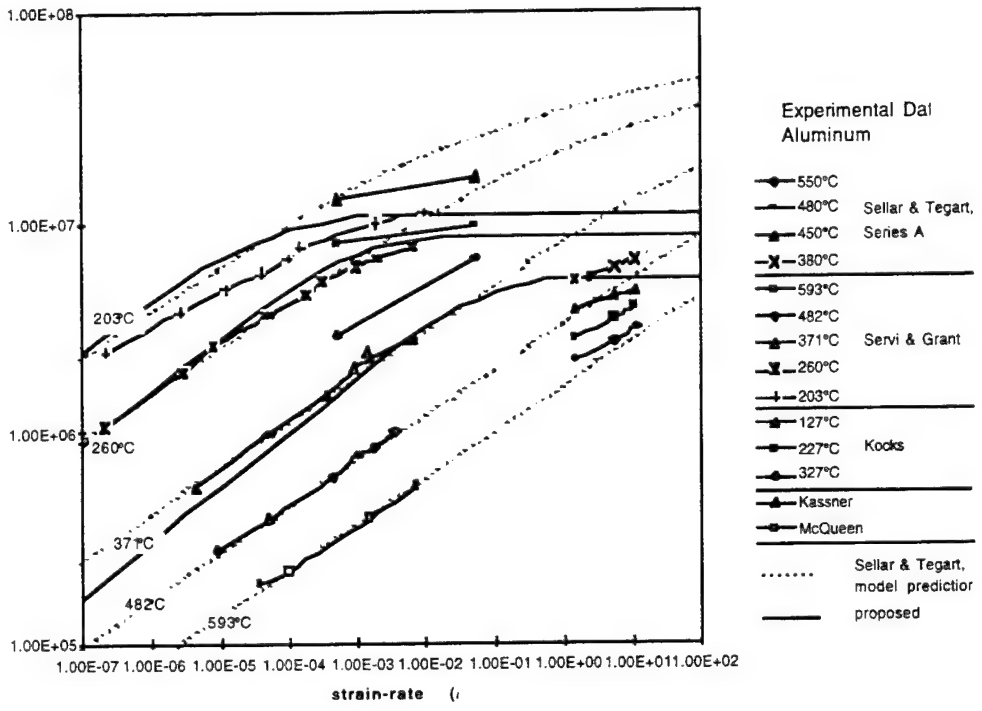

Figure 5. Steady state flow stress vs. stress for polycrystalline high-purity aluminum at various temperatures taken from Sellars and Tegart, and the references therein.

Note: The dotted lines are the empirical model proposed by Sellars and Tegart. The solid lines are the low temperature models proposed here for 203, 260 and 371°C.

Computer Simulation of Metalforming Equipment

The integration of analytical models for microstructure development were integrated directly into an existing computer-based simulation model for the 1000 ton Erie Forge Press located in the High Bay, Building 655. The inclusion of these models into the simulation provide for accurate simulation of forging loads for simple forgings of various materials. These models have also provided for the study of the effects of forging equipment dynamics on experimental behavior. One study performed by our research team has shown that the variation of a single, common press control system parameter can produce misleading results in flow stress data. Another study has shown the viability of feedback control of workpiece field quantities such as stress and strain-rate assuming the existance of appropriate sensors. This result should provide motivation for researchers in sensor technology to develop sensors suitable for measure these quantities. An example showing feedback control of stress during a simulated forging process is shown in Figure 6 below.

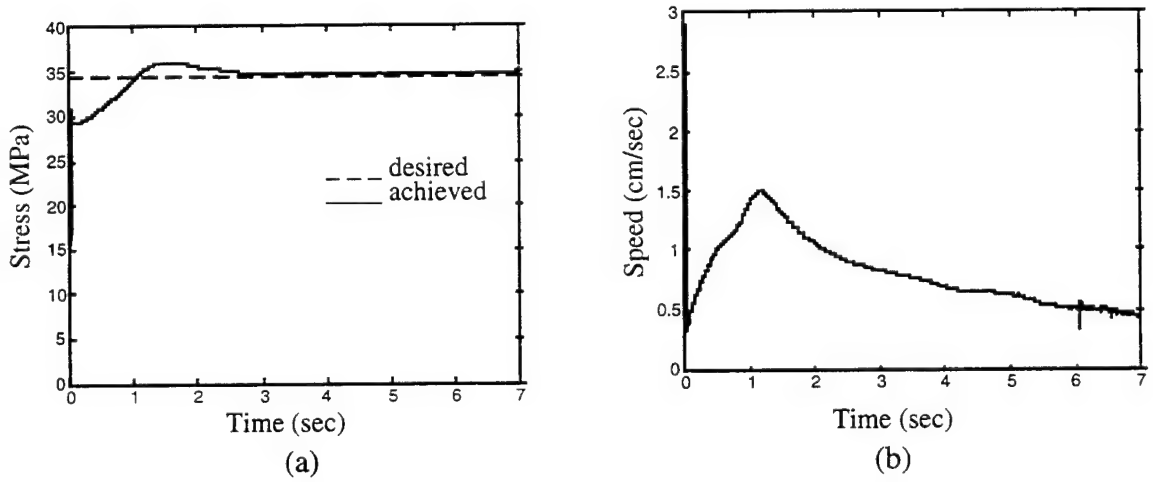

Figure 6. (a) Simulated flow stress under feedback control and (b) Ram velocity for flow stress control

Optimization of Workability in Stainless Steels

Activation energy maps for Stainless steels type AISI 304L, 304, 304 (as-cast) and 316L have been developed to optimize the workability. Microstructural investigations at TEM (transmission electron microscopy) level have been carried out to characterize the above maps. Attempts have also been made to validate these maps using industrial forming operations such as rolling and forging. Investigations towards the development of state-space-models for stainless steels are in progress. Experiments have been planned to assess the influence of 'inter-pass' conditions on the overall workability of stainless steels during multi-step thermomechanical processing. It has also been planned to apply the Axiomatic Design approach to design hot working processes for this material.

Processing Sensor Research

Physical models for acoustic emission (AE) were introduced and expressions were derived to predict AE activity from such parameters as applied stress, strain and strain-rate. These models

were then incorporated into a visco-plastic finite-element simulation program, and the acoustic emission event rate generated during metal forming operations were predicted. Simulations were then performed for upsetting operations on a typical C-Mn type steel for various friction and die geometry conditions. The AE model predictions compared well with the limited available experimental results reported in the literature, as can be seen in Figure 7, which demonstrates that AE signatures can be reliably simulated. The signatures predicted for metal forging were observed to be fairly insensitive to processing parameter changes. This suggests that AE event rate monitoring may not be well suited to process monitoring for forging. However, the amplitude and shape of the AE response are conjectured to be as or more representative as the frequency content of the AE signals. Thus, since current simulations include only the ability to predict the number of events for a set of processing conditions, future work is required to simulate the duration and magnitude of acoustic events.

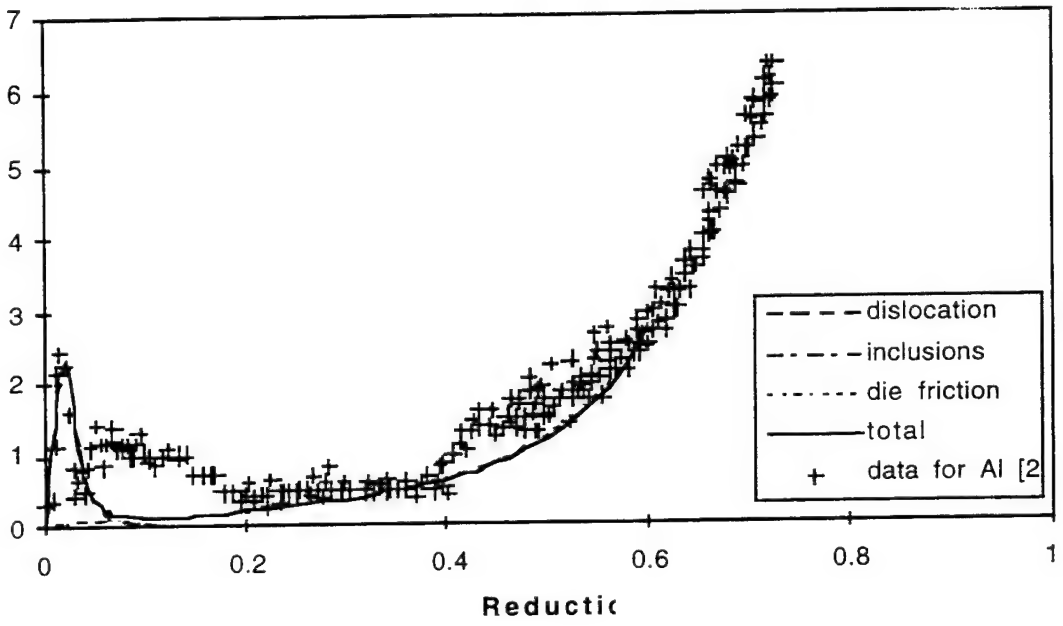

Figure 7. Calculated and experimental AE for simple upsetting

Discrete Event Dynamical System Optimization of Rotor Manufacturing Process

Despite the dearth of suitable deformation processing models for application to this optimization technique, significant progress has been made on the rotor forging problem. The first theoretical breakthrough is the identification of convergence conditions for the various Metropolis-type (generalized hill climb or GHC) optimization techniques. These convergence conditions reduce the need for novel neighborhood designs in the configuration space of the problem, but do not appear to point out methods to speed convergence. A preliminary cost model has been constructed for the rotor forging problem that includes known details on the costs of individual processing operations and Taguchi-type functions for microstructural requirements. The predictions of this cost model have been demonstrated to compare favorably with observed cost breakdowns on known parts. Initial calculations have been carried out using this cost function. The results have demonstrated the capability of the method to converge on a good solution in 10^4 iterations from a search space of $\sim 10^{23}$ with computation times of the order of 20 minutes. In addition, the feasibility of determining the sensitivity of final cost on final part geometry has been demonstrated through simple finite-

difference techniques --- even when the optimal processing sequence changes significantly due to variations in shape.

Finally, to account for uncertainties in the cost function and errors in the individual processing operation models, noise trend analysis and ordination have been applied. Significant approximation errors have been observed in the 'zero-th' order processing models as compared to finite-element results. By the evaluation of 6 to 20 significantly different candidate designs, systematic errors in the ordinal cost ranking of the designs can be estimated and used to correct the zero-th order results. This allows zero-th order processing models and "noisy" cost models to be used for preliminary design problems.

Because of the potential value of the ordination method in reducing the effects of uncertainties in the optimization calculations, future work will seek to exploit this. Ordination will be applied to the GHC techniques to create ordinal hill-climb (OHC) methods. Selection rules for the problem need to be developed and, finally, convergence conditions need to be determined for the OHC. In addition, the development of stochastic cost models for all of the likely processing techniques available for rotor manufacturing need to be developed. For this, strong teaming is expected with an engine manufacturer so that data on operation costs and the effects of manufacturing lead-time and mid-stream engineering changes can be adequately determined. Lastly, the use of zero-th order models for deformation processing models has limited the implementation of the optimization technique to reasonable (but not altogether challenging) geometries. For this reason, the development of first order models based on metal flow-pattern analysis, simultaneous with the investigation of feature-based workpiece description methods will be investigated.

Technology Transition

Failure Analysis of Missile Casting

This technology transition effort focused on determining the reason why mechanical properties of missile component castings were below the specifications called for in AMS 4241A. This effort supported the Joint Direct Attack Munitions Program managed at Eglin Air Force Base. Various methods of non-destructive testing such as radiography and computed tomography were unsuccessful in attempts to quantify reasons for the low properties. Sectioning of the component for microstructure examination revealed macroscopic porosity throughout the casting which can be seen in Figure 8.

Optical microscopy revealed the porosity to not be interdendritic in nature. Scanning electron microscopy of the pores shows the pore morphology to be elongated which leads to the conclusion the porosity was due to turbulent flow during the filling of the mold. These results were incorporated into the casting simulation software PROCAST, and a redesign of the riser and gating system was performed. Castings with the required mechanical properties are now being supplied to the Air Force. The customers have been impressed with both the responsiveness of the Air Force and the effectiveness of their solutions.

Figure 8. Missile component cross-section revealing macroscopic porosity

Electroupset Process for Gamma Valve

The electroupset process was considered as a possible candidate for forging gamma titanium automotive valves due to its *in-situ* temperature control adaptability. The electroupset press is equipped with temperature feedback mechanisms and a relatively rapid control to counteract the loss of temperature is available due to the electrical heating. The press would hold a 6.25mm diameter gamma rod between gripper and anvil dies which have a dual function as electrodes. The resistive heating brings the gamma material to forge temperature within a local region. The forge region looses heat to atmosphere which would be compensated by the resistive heat.

A preliminary evaluation of this process shows significant technical options, but the cost of processing is anticipated to be higher due to the need for the stock material of a smaller diameter and a smooth enough surface finish to permit good electrical contact. An initial test of the process was performed at Pioneer Forge in Pioneer, OH and compared with conventional isothermal forging. The latter was deemed to be a better process for three reasons, namely: the stock size diameter of 19 mm, relaxed surface finish requirements, and the extensive process experience involving aerospace alloys and led to the subsequent effort for valve forging focused on designing an optimal isothermal forge process.

Strain Induced Porosity

An on-going concern with plate-forged Ti-6-4 is the formation of cavities or cracks at the prior-beta grain boundaries. This porosity is observed prior to the final forging and requires the material to be either HIP'ed to close the porosity or scrapped. Preliminary investigations have determined that the open-die plate-forging procedure employed by the material vendor to condition the initial ingot material is poorly designed and subjects the material to excessive tensile deformation. The fundamental cause of the cracking phenomenon has not been determined. Three initial candidates have been identified: critical strain cavitation; grain-boundary fracture at a critical stress and; transient phase plasticity. Mechanical testing has determined that the former is unlikely leaving the latter two phenomena to be investigated. Each of these candidates lead to similar criteria for the formation of porosity (see Figure 9) which have been recommended as boundaries for the processing window. More experimental work is planned to verify the deformation stability criterion and determine the mechanism responsible.

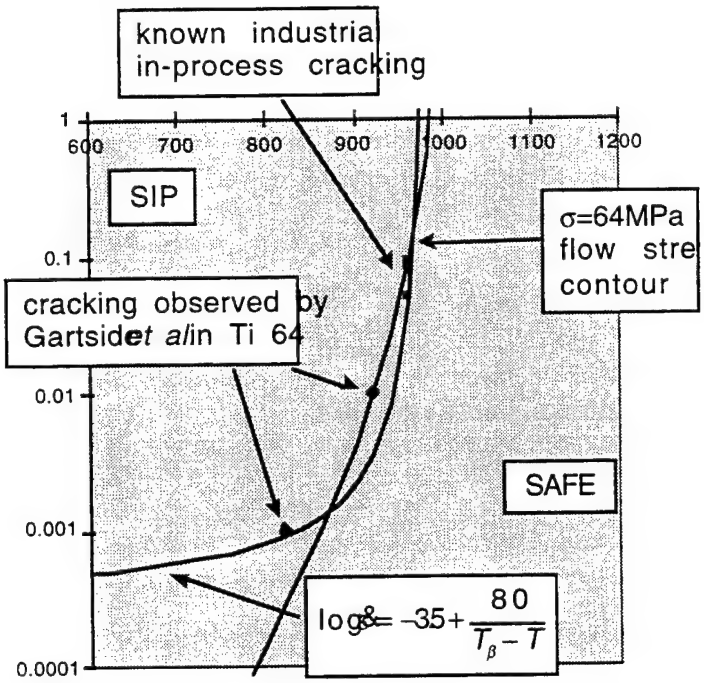

Figure 9. Strain rate vs. temperature behavior criteria for Ti-6Al-4V.

Advancment in Copper Extrusion Technology

Problems such as poor tool life, surface quality, eccentricity and uneven wall thickness were encountered during the hot-tube extrusion of deoxidized high-phosphorus copper after increasing the extrusion ratio. In collaboration with the HeatCraft Company of Bossier City, LA, a systematic study was initiated to solve the above problems with a view toward increasing productivity. The task involved studying the hot deformation characteristics of deoxidized high-phosphorus copper in detail through an extensive experimental investigation to develop the optimum design window for the extrusion using suitable material modeling techniques. Improved tooling design was also developed for the hot-tube extrusion of deoxidized high-phosphorus copper. A stability map was generated in temperature-strain rate space as follows:

(1) at temperatures below 775°C the material exhibits flow localization,

(2) above 875°C and strain rates of 0.1 s^{-1} or less the material exhibits grain growth, and

(3) at 700°C and 10 s^{-1} the material exhibits adiabatic shear deformation.

The activation energy was calculated and then superimposed on the stability map to optimize the workability of this material. The optimal design range appears to be at a strain rate of 10 s^{-1} and temperatures between 700°C and 975°C. The microstructures of the deformed specimens were then quantified in terms of average grain size using the linear intercept method. It should be noted that as the test temperature is increased, the average grain size increases. The results from this study indicate that a 'safe' processing window for copper alloy CU12200 is fairly large and that present processing conditions, i.e., temperature and ram speed, are within the process window. It was determined that the problems associated with the hot copper tube extrusion were due to excessive lateral loading on the mandrel as a result of increasing the extrusion ratio. To reduce the loading of the mandrel, which will cause less wear on the mandrel and increase productivity. A novel die design using a flow control plate was suggested, as shown in Figure 10, and implemented with satisfactory results.

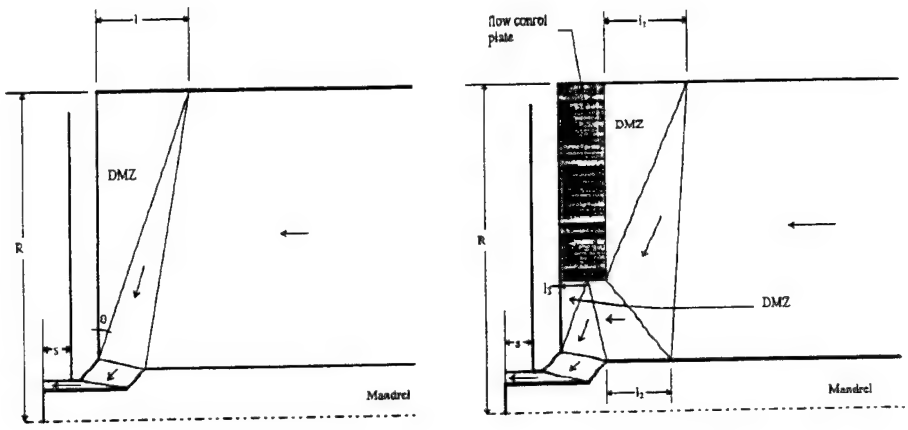

(a) (b)

Figure 10. Extrusion schematic (a) initial set-up and (b) with the addition of flow control plate

GM-Delphi Casting Porosity

GM-Delphi was experiencing an unacceptable frequency of faulty parts which were causing leaks in their main product, automotive air-conditioner compressors. These leaks were identified as resulting from porosity in the die-cast aluminum casing components that were exposed during machining operations, as seen in Figure 11. Metallographic analysis of defective parts showed the presence of shrinkage porosity in the isolated, thick sections of the parts. This is classically attributed to poor die design or uncontrolled cooling of the part. A simple method of rapidly demonstrating the cause and quickly evaluating design alternatives was desired.

This effort was brought to the Materials Directorate by the Wright Connection Summer Faculty Program. The use of a finite-element or boundary-element technique was discarded as a means to design a solution due to the short time and rather uncomplicated requirements. It was demonstrated that the solidification calculation could be roughly approximated by a simple linear heat-transfer model that could be solved in 2D by the use of a Green's Function technique. Further, the convolutions required are identical to the convolutions performed by many image analysis packages. This allowed the analysis to be performed by simply digitizing the sample cross-section using an optical scanner, filtering the image to represent the initial temperature distribution and "blurring" the image with the appropriate Green's Function. Trial-and-error redesign of both the part and the die cooling characteristics could be easily accomplished with a "paint" program. The results compared favorably with a detailed 3D finite element analysis of the solution.

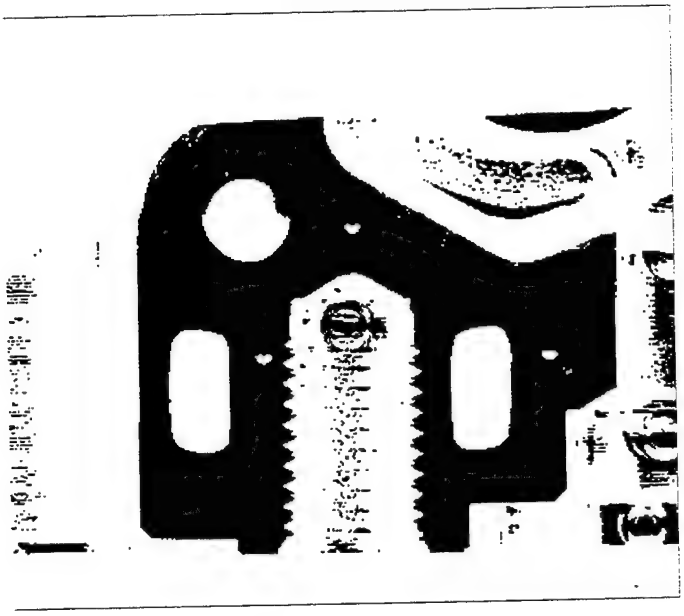

Figure 11. Casing cross-section revealing porosity

Future Work - 1997

Methodology Validation

Shape Optimization

The algorithms developed for general forging shape optimization will be validated by solving a sequence of problems, each increasing in difficulty as follows, find:

1) the shape trajectory from a given starting shape to a given final shape that minimizes the variance in the final strain distribution in the part,
2) the best aspect ratio for the starting billet in a single step forging process,
3) the optimum shape for the blocker die in a two-step forging process, and
4) common billet diameters and blocker dies suitable for multiple finish forge shapes as shown in Figure 12.

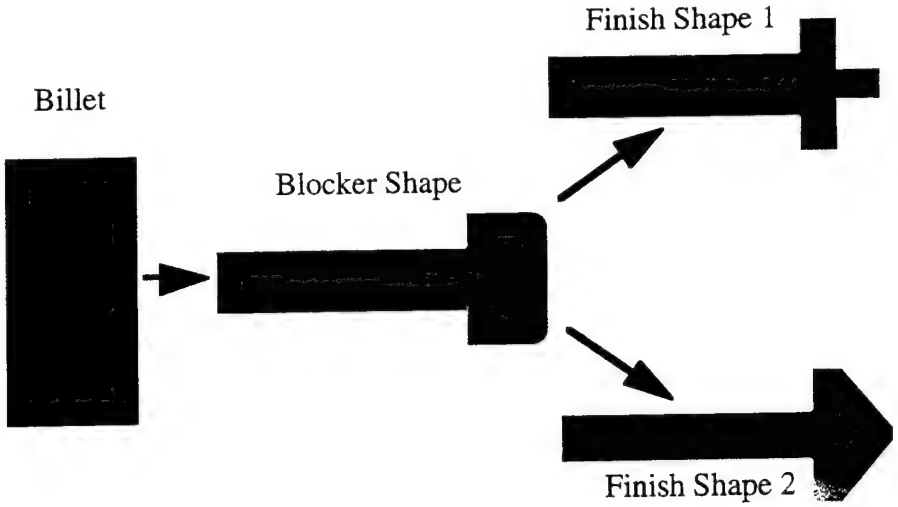

Figure 12. Radial cross-sections of billet, intermediate and finish disk forging shapes

Computer Simulation of Metalforming Equipment

A new, simulation-based, adaptive control law for the press will also be developed as a replacement for the current, operator assisted, 'iterative' control law. The computer simulation for the 1000 ton Erie forge press located in the High Bay, Bldg. 655 will be adapted for regular use by the press operator for determining press 'computer-control' settings prior to actual forging operations. This should reduce considerably the number of trial forgings necessary to "tune" the press for particular forging loads.

Microstructural Modeling Validation

Variable strain rate tests will be performed to validate microstructural evolution models for Ti-49Al-2V and 1030 steel materials. Mathematical models for temporal evolution of percent spheriodization and grain size during deformation processing of Ti-49Al-2V and 1030 steel will be inputs into the microstructural evolution optimization software.

New Investigations

Material Characterization

Characterization of material flow stress behavior and microstructural evolution of a nickel-base superalloy IN-718 as well as a stainless-steel alloy 304L.

Shape Optimization Algorithm

Research with respect to the computational aspects of the shape optimization problem will be continued. Emphasis will be placed upon the inclusion of more physical constraints, as well as methods for reducing the number of floating point operations. The application to shape optimization of new types of basis functions currently being developed by approximation theorists will be investegated. The application of shape optimization principles to extrusion processes will be investigated.

Incorporation of Method for Optimization of Microstructural Development During Post Hot Deformation

Microstructure evolution models describing post deformation behavior will be researched. Then existing microstructure evolution optimization algorithms and software will be modified to take into account post deformation behavior. In effect, this research should identify optimal deformation processing conditions to achieve desired final microstructures *taking into account post deformation conditions*.

Connected Simulations and Optimization

This research effort consists of the development of an environment (hardware/software) for the simulation, design, and optimization of multi-stage metal forming processes. The idea is to simulate each stage of a metal forming process by a computer process and then connect these virtual manufacturing stages together to form the simulation of the whole manufacturing process, as seen in Figure 13. The connected simulation framework will allow the user to obtain information about effects that the changes in any stage of the manufacturing process will have on any other stage. Visualization tools will allow the user to observe these changes as they occur. The addition of optimization algorithms that can vary the sequence of processing stages used and the parameters of the different processing stages according to appropriately designed optimality criteria will allow the designer to conveniently evaluate alternative processes and sequences to obtain designs that are optimized for quality, performance and cost.

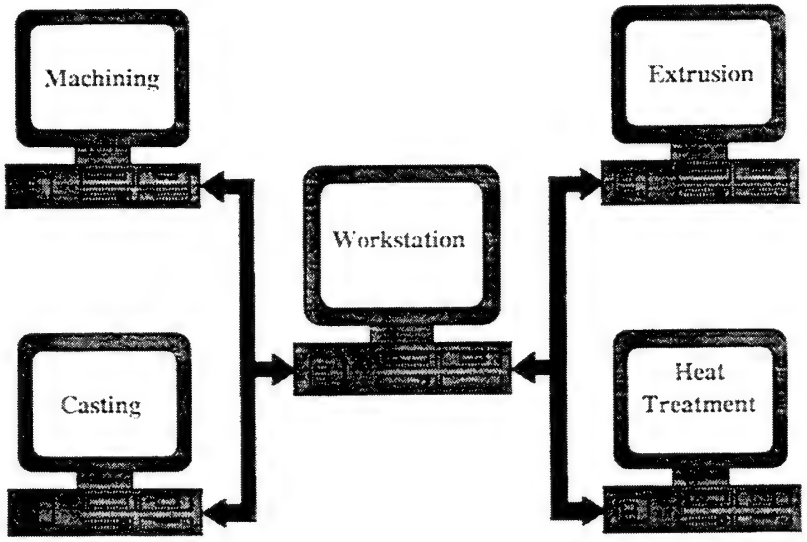

Figure 13. Connected simulation platform concept

Finally, technology transition efforts will continue to build upon the steps taken in FY95 and prior years. Specifically, the optimal design and physical trial for subscale BLING forging

Technology Transfer

Optimal design and validation of isothermally forged automobile valve

Validation trials for the gamma TiAl engine valve forging are planned to be performed at a Pratt and Whitney isothermal press facility. The die design involves FY96 techniques of multivariate optimization to overcome the following three difficulties (also shown in Figure 14):

- limit the tensile stress in gamma TiAl to prevent fracture,
- regulate the strain-rate in gamma TiAl to the desired value, and
- limit the TZM die stresses to prevent fracture.

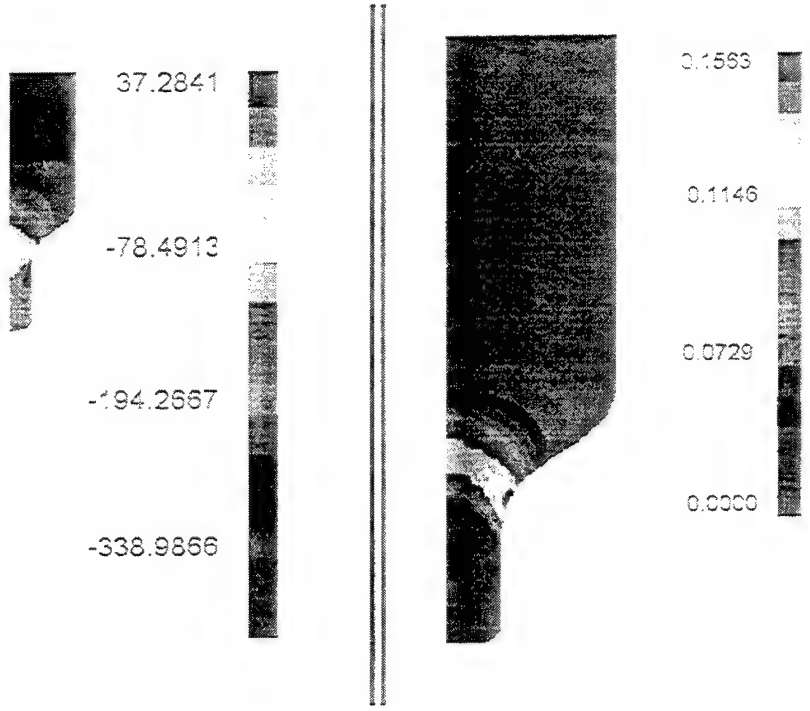

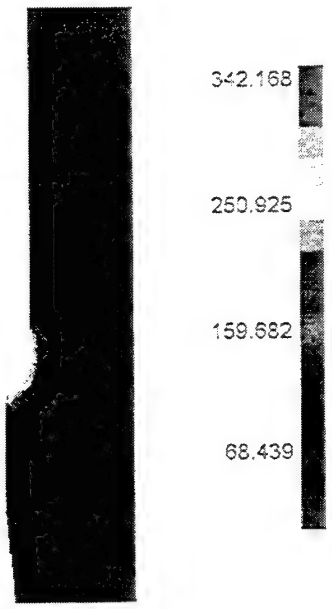

(c)

Figure 14. TZM tooling stresses

An additional constraint is due to the ceiling on the operating temperature of the metalforming equipment. Using the geometry information from the design, TZM tooling will be developed and a total of ten (10) valve forgings will be performed. Metallographic studies will be performed on the valves to determine if the forging was successful in obtaining a component without occurrence of fracture. It is anticipated that the locations just past the valve throat position will be most critical from the integrity perspective.

Rockwell Spindle Forging

Geometric mapping will be developed for a spindle forging of a part currently manufactured by Rockwell International. This part is manufactured in multiple stages and it is deemed that design improvements are feasible in one or more intermediate shapes to provide a graduated rate of shape evolution. This will be facilitated by developing a geometric mapping which will transform the final shape to the initial cylindrical preform geometry. This evolution sequence will provide candidate intermediate shapes for this forging and will also be utilized as a starting condition for the trajectory optimization. The optimization procedure will perturb these initial trajectories and construct an optimal shape evolution pattern.

Metalforming Equipment

Using principles of dynamical systems modeling and current forge press simulation software, software modules, suitable for integration with existing process simulation software (notably finite element methods), will be developed that will facilitate the simultaneous simulation of metal deformation and equipment response.

Papers and Presentations

In Preparation

W.G. Frazier, J.C. Malas, E.A. Medina, and W.M. Mullins, **Modeling and Control of Metal Forming Equipment**, submitted to *IEEE Transactions on Control Systems Technology* , 1996

W.G. Frazier, J.C. Malas, E.A. Medina, S. Venugopal, S. Medeiros, W.M. Mullins, A. Chaudhary, and R.D. Irwin, **Application of Control Theory Principles to the Optimization of Grain Size During Hot Extrusion**, submitted to *Materials Science and Technology* , 1996

W.M. Mullins, R.D. Irwin, J.C. Malas, and S. Venugopal, **Examination on the Use of Acoustic Emission for Monitoring Metal Forging Process: A study Using Simulation Technique**, submitted to *Scripta Materialia*, Pergamon Press, 1996

S. Venugopal, E.A. Medina, J.C. Malas, S. Medeiros, W.G. Frazier, W.M. Mullins, and R. Srinivasan, **Optimization of Microstructure During Deformation Processing Using Control Theory Principles**, submitted to *Scripta Materialia*, Pergamon Press, 1996

J.C. Malas, W.G. Frazier, S. Venugopal, E.A. Medina, S. Medeiros, R. Srinivasan, R. D. Irwin, W.M. Mullins, and A. Chaudhary **Optimization of Microstructure Development During Hot Working Using Control Theory**, submitted to *Metallurgical and Materials Transactions*, 1996

Y.V.R.K. Prasad, S. Sasidhara, H.L. Gegel, and J. C. Malas, A Compendium of Processing Maps for Hot Working of Metals and Alloys, to be published by ASM International, Materials Park, OH, 1997.

J. C. Malas, Y.V.R.K. Prasad, H. L. Gegel, J.S. Gunasekera, and S. Venugopal, Theory and Use of Material Behavior Models for Process Design, to be published by ASM International, Materials Park, OH, 1997.

J. C. Malas and J. S. Gunasekera, S. Venugopal, and W. G. Frazier, Modeling, Design and Control of Material Processes, to be submitted to Oxford University Press, New York, for Oxford Series on Advanced Manufacturing, 1998.

Published

J.C. Malas, A.B.Chaudhary, W.M. Mullins, E.A. Medina, S. Venugopal, S. Medeiros and R. Srinivasan, **Optimization of Microstructure Development: Application to Hot Metal Extrusion**, *Engineering System Design and Analysis Conference Proceedings*, Montpellier, France July 1-4, 1996

E.A. Medina, S. Venugopal, W.G. Frazier, S. Medeiros, W.M. Mullins, A.B. Chaudhary, R.D. Irwin, R. Srinivasan, and J.C. Malas, **Optimization of Microstructure Development: Application to Hot Metal Extrusion**, *Journal of Materials Engineering and Performance*, Vol 5, No.6, ASM International, 1996

W.M. Mullins, R.D. Irwin, S. Venugopal, and J.C. Malas, **The Simulation of Acoustic Emission for Metal Forging**, *JOM*, Vol. 48, No. 9, pp. 15, September 1996

J. C. Malas and S. Venugopal, **Emerging Sensors for the Intelligent Processing of Materials**, *JOM*, Vol. 48, No. 9, September 1996

S. Venugopal, S.L. Mannan and Y.V.R.K. Prasad, **Optimization of Cold and Warm Workability in 304 Stainless Steel Using Instability Maps**, *Metallurgical and Materials Transactions*, Vol. 27A, 1996

Z. Jia, J.S. Gunasekera, and J.C. Malas, **Application of Upper Bound Element Technique (UBET) for Aluminum Extrusion**, ET '96 Proceedings, 1996. (presented at 6th International Extrusion Technology Seminar & Exposition, Chicago, IL, May 1996).

J.S. Gunasekera, C. Fischer, J.C. Malas, W.M. Mullins, & M.Yang, **The Development of Process Models for Use with Global Optimization of a Manufacturing System,** Proceedings of ASME International Mechanical Engineering Congress, Atlanta, GA, 17-22 Nov. 1996.

C. Fischer, J. S. Gunasekera, and J. C. Malas, **Process Model Development for Optimization of Forged Disk Manufacturing Processes**," Proceedings of Second ASTM Symposium on Steel Forgings, New Orleans, Louisiana , Nov 96.

W.G. Frazier, R.D. Irwin, E.A. Medina, and J.C. Malas, **Modeling and Simulation of Metalforming Equipment**, accepted for publication by *Journal of Materials Engineering and Performance* , ASM International, 1996.

J. Gunasekera and S. Venugopal, **Computer-Integration Manufacturing,** Book Chapter in McGraw Hill 1998 Yearbook of Science and Technology (in press)

W.M. Mullins, R.D. Irwin and E.A. Medina, **Stability Analysis of Microstructure Evolution Processes**, Proceedings of Applications of Sensors to Materials Processing, The Metallurgical Society of AIME, Warrendale, PA. (in press)

W.M. Mullins, R.D. Irwin, J. C. Malas, and S. Venugopal, **Examination of the Use of Acoustic Emission for Monitoring the Metal Forging Process: A Study Using Simulation Techniques**, Proceedings of Applications of Sensors to Materials Processing, The Metallurgical Society of AIME, Warrendale, PA. (in press)

S. Viswanathan, R.G. Reddy and J.C Malas, Editors of Applications of Sensors and Models to Materials Processing, The Metallurgical Society of AIME, Warrendale, PA. (in press)

Patent

J.C. Malas, W.G. Frazier, E. Medina, V. Seetharaman, S. Venugopal, R.D. Irwin, W.M. Mullins, S.C. Medeiros, A. Chaudhary and R. Srinivasan, **Optimization and Control of Microstructure Development during Hot Metal Working**, AF Invention #21510, submitted August 1996

International Conferences Attended

3rd International Conference on Engineering System Design and Analysis, sponsored by The American Society of Mechanical Engineers, Montpellier, France July 1-4, 1996

46th CIRP General Assembly: International Institution for Production Engineering Research, invited participant, Como, Italy, 26-30 August 1996.

Research Leader: Dr James C. Malas, **Team**: Dr Anil Chaudhary (V/S), Dr Garth Frazier (V/S), Dr William Mullins (V/S), Mr Steven Medeiros (V/S), Mr Enrique Medina (V/S), and Dr Venugopal Srinivasan (NRC)

Molecular Beam Epitaxy of Advanced Semiconductor Films

Process design and control research applied to molecular beam epitaxy of advanced (compound) semiconductor films is driven by the need for improved yield and 'nanoscale' quality of materials for ultra-high speed digital processing, analog MIMIC circuitry, infrared detection capability, optical processing, and fiber optic control systems.

Research OBJECTIVES are

- to improve research productivity for growing III-IV-V compound semiconductor thin-films,
- to improve quality of films via self-directed control using in situ ellipsometry, and
- to extend processing research to enable virtual materials research capability for MBE.

Research FOCUS is

- developing new control algorithms and methods for prototyping of new sensors
- developing search and optimization methods to affect event-based control
- investigating new sensors and controllers for improved reliability and performance

Background

Several years of effort in the development of an array of software modules within, a now commercialized, high resolution data acquisition and retrieval system called InfoScribe™ to enable automated setup of the MBE process, i.e., a menu-driven ability to automate the warm-up of the MBE machine in terms of effusion cell temperatures and PID settings to commence an epitaxial growth. In addition, a second set of algorithms have been developed to automate bringing a new sensor on-line for data collection either on the MBE machine or on one of the *ex situ* test/characterization stations.

The InfoScribe process design and control system provides the ability to interface directly to each sensor on the MBE machine and future sensors. This ability to connect to a variety of sensors is based on the modular design of the system. The main or root module of InfoScribe provides a graphical user interface and data manipulation features. Each of the sensors associated with the MBE machine have separate programs written to interface them to the control system. These programs/modules are responsible for communicating and verifying the data collected from the sensors.

One of the 'in-house' MBE machines located at the Wright Laboratory, Materials Directorate has three separate programs written to interface the sensors. They are PID, Shutter and Ion Gauge modules. Each of these programs specialize in knowing specifically about the sensor they are connected to. To utilize these modules, the process control module (which may be an external application) has the ability to connect via the Inter-Application-Communication(IAC) interface wherein data is sent directly to the control module and InfoScribe graphical display simultaneously. This allows the operator to view the data while the control program affects real-time control of the growth process. All instrumentation interfaced with the MBE control computer communicates time-stamped data to a full-time data archive. Within the computer control and data collection environment, Knudsen cell temperature, flux, and shutter control are systematically coupled through inter-dependent program modules. Each module provides an independent interface to the respective instrumentation to facilitate parameter entry for device control. These modules share a common language information and command linkage with other intelligent coordination and supervisory modules called Inter-Application Communication utilizing Apple Events.

InfoScribe utilizes IAC to communicate to independent computer software modules. There are two types of modules, the input/output(I/O) module and the control module. The I/O module provides an interface for a selected hardware component of the MBE system which has been designed to automate communication between MBE hardware/software components and allow the operator to control the component from the computer. The module will also provide an interface for any other computer software modules that would need to access the MBE component. Examples of I/O modules are: Ion Gauge module, PID module and Shutter module.
A control module will utilize these I/O modules to communicate with MBE components to provide control of the MBE process during a growth, e.g., process identification or thermal stability. The control module does not know how to communicate directly to the MBE component, but instead knows how to communicate to the I/O module responsible for the communication to the MBE component. This type of system configuration can allow the same control module to be used on several different MBE systems without modification of the software. The InfoScribe architecture is shown in Figure 1 below.

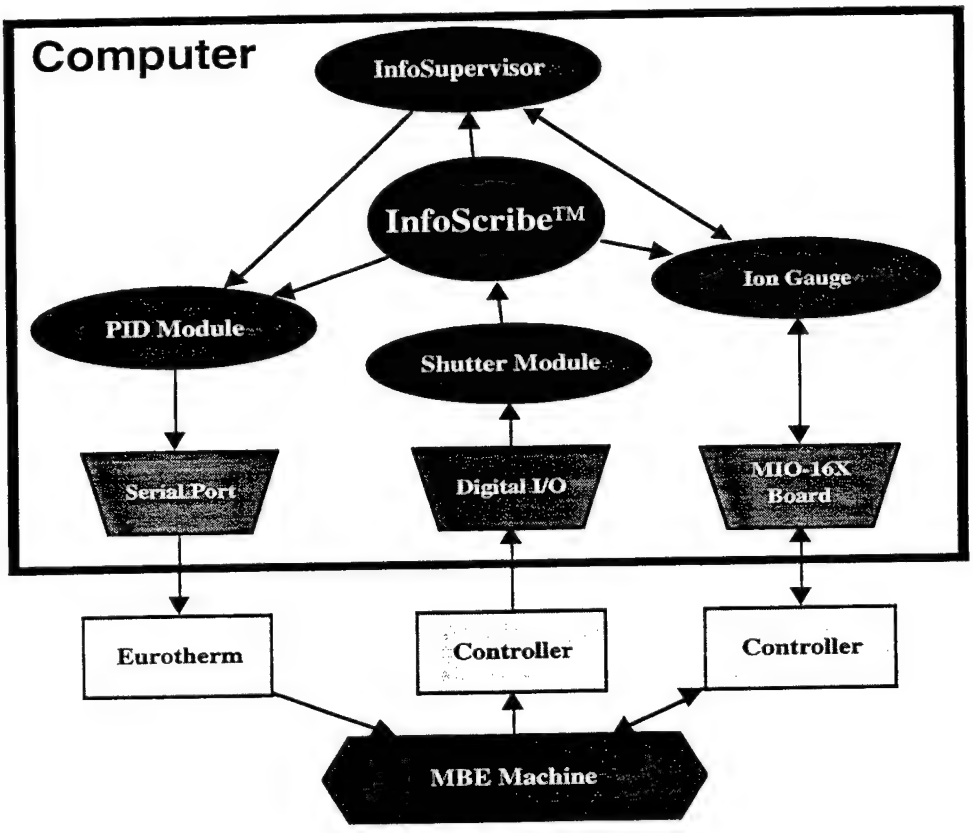

Figure 1. InfoScribe Architecture

The InfoScribe software has two main functions. The first is the collection and presentation of data. This task is completed in real-time during the operation of the MBE process. Figure 2 depicts the data collection screen.

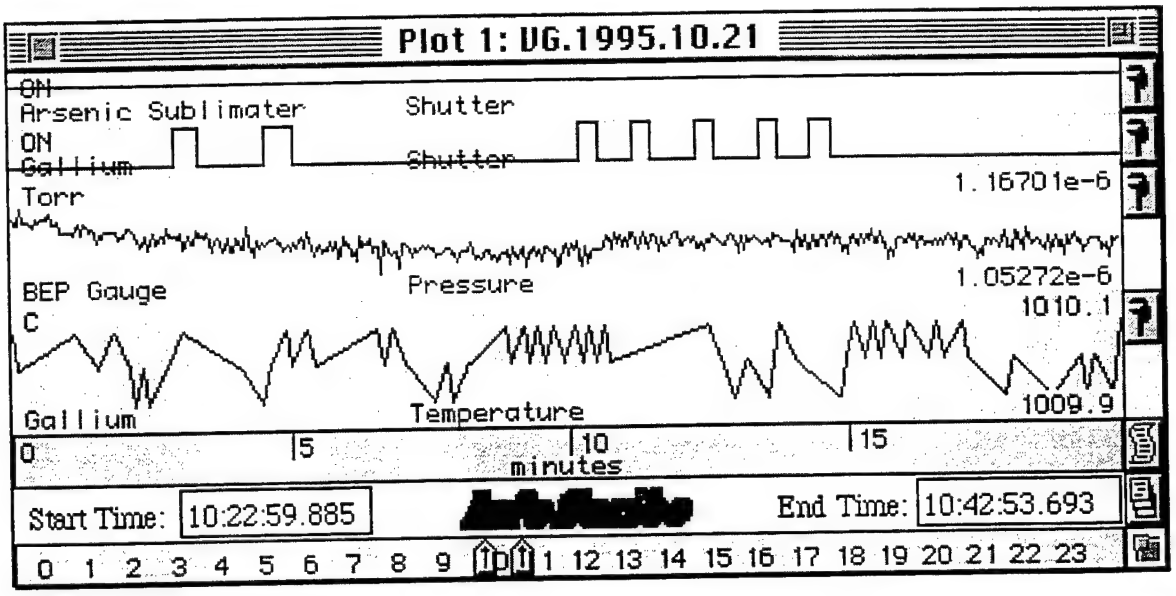

Figure 2. InfoScribe Data Collection Visual Display

InfoScribe is capable of storing and displaying boolean, integers, real, text and pictures (images), etc. dynamically to allow the modules that communicate with InfoScribe to request various data, e.g., a push button, edit field or display based on the data type required. For a boolean input (i.e.. switch) a push button will be displayed on the left hand column of the screen. In the case of a real number, Chamber Setpoint, the Chamber module requests a text edit field to allow the operator to type in the desired value for the setpoint. This value is then sent to the Chamber module which will send the correct codes to the MBE component to change the setpoint.

The design platform for InfoScribe uses the MacOS and operates on both Motorola 680x0 processors and on IBM/Motorola PowerPC processors. The former processor is a complex instruction set computer (CISC) design and its clock speed is limited to less than 100MHz. The later processor is a reduced instruction set computer (RISC) design and its clock speed is currently available at 225MHz with future projections to 500MHz. The significance of these processors is that they are the core of low-cost desktop and mini-tower personal computers and they provide the inter-application communication latency time shown in Figure 3 below.

The condensed latency time in Table 3 shows a mean message transmission time of 34 milliseconds. With the standard deviation of 28 milliseconds, the worst case transmission time is only 62 milliseconds. The best case transmission time is a mere 6 milliseconds. These message transmission times are the basis of the inter-application communication efficiency built into the InfoScribe system. Equally important is that the network based communication architecture is inherently local area network (LAN) capable. This gives the InfoScribe data acquisition and control system the ability to reallocate a compute intensive operation such as material process

modeling on a separate computer for unimpeded processing while data acquisition and process control are handled by the main materials processing computer. This network capability has also been utilized for remote monitoring of a materials process via LAN in the researcher's office separated from the materials processing lab. The network capability also includes Internet access via TCP/IP protocol for long distance monitoring of processes located in physically separated facilities.

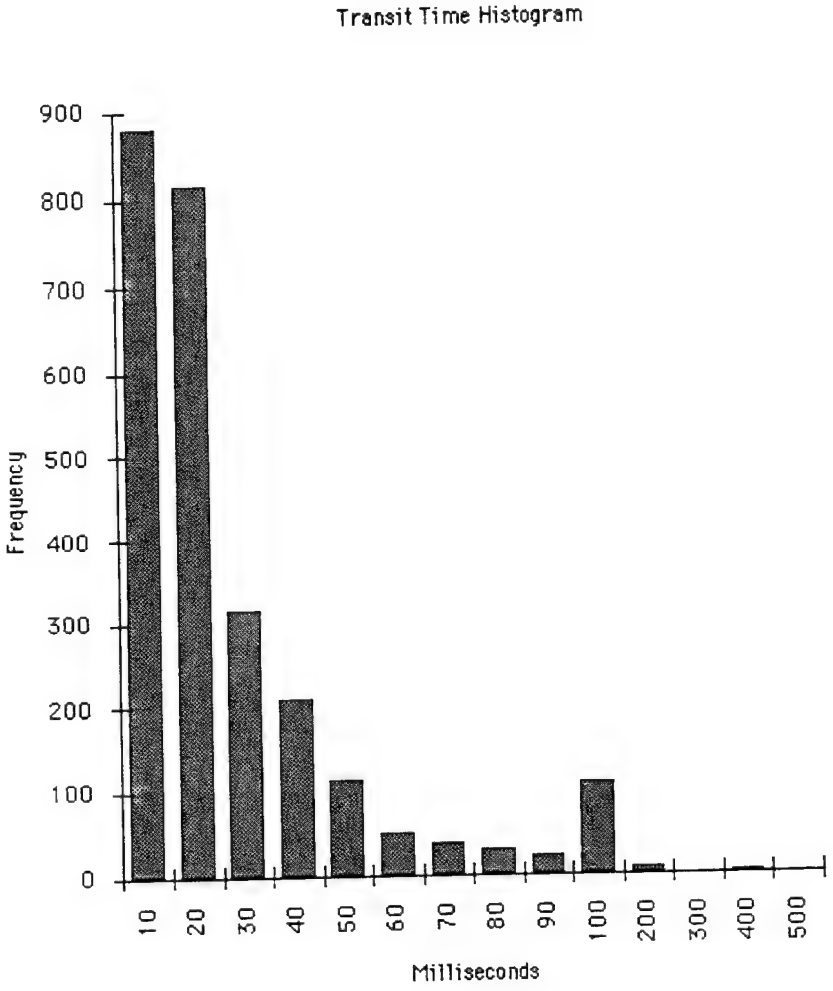

Figure 3. InfoScribe Message Transmission Time

Table 1.

Mean	34 milliseconds
Standard Deviation	28 milliseconds

Research/Technical Achievements - 1996

Several new InfoScribe modules have been developed as follows. The first, the Graphical Growth module, is recipe driven via the design environment to allow a researcher the ability to design a recipe for the module to control the MBE process during growth. This module requires the operator to input information on the substrate and growth parameters. These parameters are then sent to InfoScribe at the beginning of the growth to be stored into a data file. The Graphical Growth module was updated to allow the researcher the ability to design superlattice structures using a sub growth entry. A sub growth is a layer or layers that can be repeated *n* times. Instead of typing in 200 layers for a superlattice, the researcher can setup a loop of 10 layers to repeat 20 times.

Progress has also been made in obtaining *in situ* optical parameters using Dynamic Data Exchange (DDE), a standard inter-application communication scheme in Microsoft Windows platform. There are two DDE communication gateways in the Variable Wavelength Ellipsometry System (WVASE). One is used for command, and the other for data transfer. Both DDE gateways have been tested, and verified. Utilization of DDE enables measured optical parameters from WVASE to be transferred to other application modules such as InfoScribe. A Graphical User Interface (GUI) module has been implemented so that data can be displayed dynamically (both textually and graphically) in real-time for the operator to view the actual film growth. Figure 3 depicts an instance of a display of the GUI module. The graph is a plot of the inputs from WVASE which need to be transformed into parameters which enable the derivation of film thickness and composition. It should be noted that graphical display of the growth of a thin-film is updated in real-time with new data points via DDE.

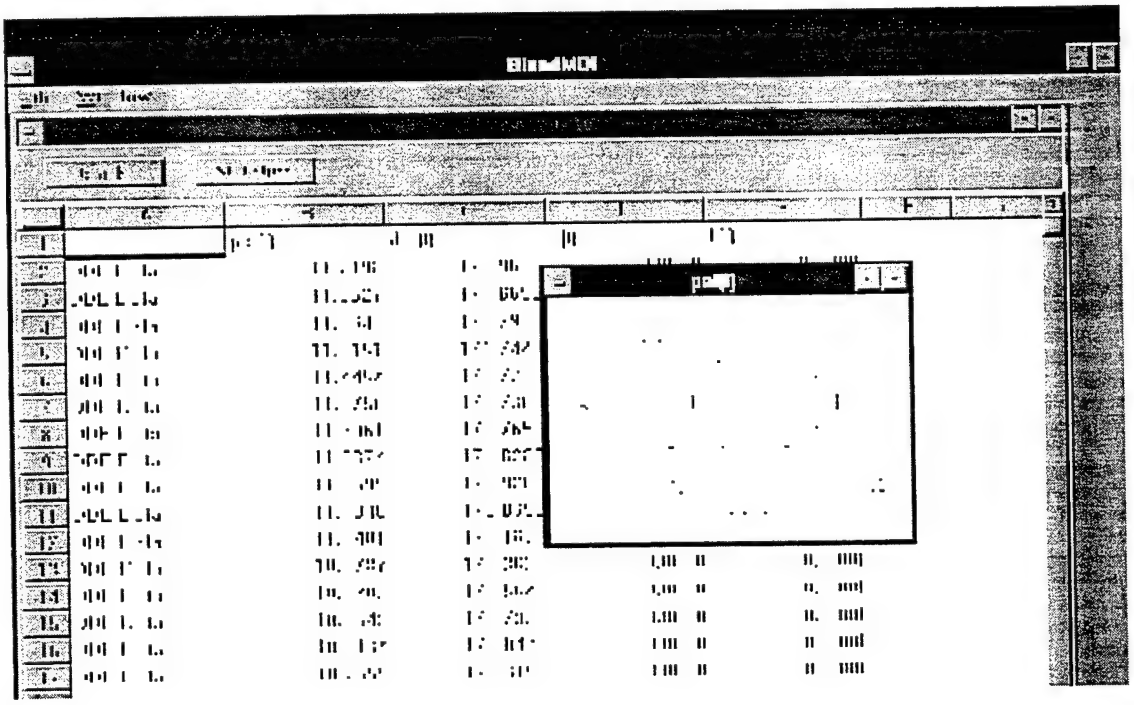

Figure 4. Graphical User Interface (GUI) Display

The Process Advisor™, another module that is capable of on-line process monitoring and optimization, has been enhanced with new features. One of the new features is the real-time on-line consulting and optimization capability using DDE. With the DDE facility, data can be measured via sensors, and transferred to the Process Advisor for interpretation.

The first connection from the PC to the Macintosh via local-area-network (LAN) has been completed. Ellipsometric data has been successfully transferred using DDE and the LAN data communication protocol (TCP/IP) to InfoScribe on the Macintosh platform. To reduce communication overhead and balance the load of the computers, the Process Advisor was ported to the Macintosh Power PC. The Process Advisor will need to control several actuators and access sensor data which can be accomplished faster on the Macintosh Power PC. In addition, the InfoScribe System was updated on both of the in-house MBE machines. A new Macintosh Power PC was installed and the software was updated to operate in the native Power PC language (instruction set).

At the request of the operators an Insitu Messenger module was designed. This module allows the operator to pre-record text messages that can be sent to InfoScribe with a click of the mouse. The main purpose is to annotate the data file with information about the process that is not collected from the sensors. A common usage is for a manual valve setting or preparation information of the process. This module can store up to 20 messages that are sent to the Insitu Notebook parameter.

Another module that has been added is the Ex situ Notebook which is used when the data file is analyzed and the researcher needs to put a note into the data file. A note can be 256 character long and placed anywhere in the data file. There is not a limit to the number of notes a researcher can add to the file. Using this notebook capability, future researchers will have access to both the raw data and the initial and intermediate researcher's notes. Scheduler++, a recipe design interface program was started to replace the Graphical Growth module.

The Graphical Growth module was initially limited to 14 sensors and/or actuators and could only process a time-based recipe. The Scheduler++ module was designed to allow the user to specify events such as temperature of a cell, thickness of a layer, composition of a layer, and etc. to determine when a layer was complete. This module was also designed to work with any process that is using the InfoScribe System.

Future Work - 1997

To date the development of InfoScribe system has provided a generic capability for collecting information from any type of process and storing that information in a uniform data base. InfoScribe has become a generic software platform for expandability - affording materials researchers a set of tools to instrument new processes with new sensors and to automate the collection, visualization, storage, retrieval and archiving of process data.

Development will continue in many areas - the Scheduler++ is to be completed, while replacement of the Graphical Growth module will be accomplished to satisfy new requirements. Next, the event based handler will be completed allowing the operators to establish a specific event (e.g., thickness of the layer is 1 nm) to determine when to open and/or close effusion cell shutters. Further development of the intelligent processing modules will include additional instrumentation interfaces for Reflection High Energy Electron Defraction and Mass Desorption Spectroscopy. Coordination modules for the additional instruments will be explored, while existing coordination modules for thermal and flux calibration will be refined. Development of a supervisory growth control module and system safety/health monitoring. All of these intelligent modules will utilize Direct Dispatch to facilitate an information highway among the modules and processes they control.

The information highway concept will be further developed by linking the MBE process-data archive to a materials and process design database. This database will enable both neural network and conventional material/process modeling, evaluation and analyses. The success of network-based inter-application communication (IAC) in the InfoScribe system evolved from the robust

object-oriented inter-application communication structure provided at the operating system level of InfoScribe's design platform.

Three-dimensional process model visualization will be explored as an ancillary user interface to real-time data acquisition. Although parameterization rules may be required to support effective three-dimensional process model visualization, the need for flexible InfoScribe data viewing capability has been identified. These multiple viewing capabilities will include the current time based data plots along with two-dimensional and three-dimensional graphical views as well as textual user notes. The capability to support multiple and varied data viewer formats will be enabled through an expansion of InfoScribe's data handling bandwidth, fully automated communication addressing, and pre-emptive task scheduling based on module functionality defined priority level.

The above new features will be implemented via the development of an InfoScribe micro-kernel. The micro-kernel will support all of the existing features that the present InfoScribe system provides through its network based inter-application communication. The InfoScribe kernel will maintain Internet connectivity through its existing TCPLink module and LAN support will be maintained through a similar companion module. Figure 5 below shows the new architecture and modules. Note the cross-hatched area depicts the boundaries of the InfoScribe System, and wherein the internet and local area net modules transcend this boundary.

The remaining communications for modules located directly on the processing computer with the InfoScribe kernel will be supported through direct dispatch messaging. All communication is routed directly through the kernel just as the network based inter-application communication was routed through the computer operating system.

With the micro-kernel design, the InfoScribe viewer will not need to be located on the host process control computer, and could be located on a remote computer or both or multiple computers located throughout a laboratory facility. Similarly process modeling could be located on one or more remote computers dedicated to compute intensive modeling activity in a parallel processing paradigm.

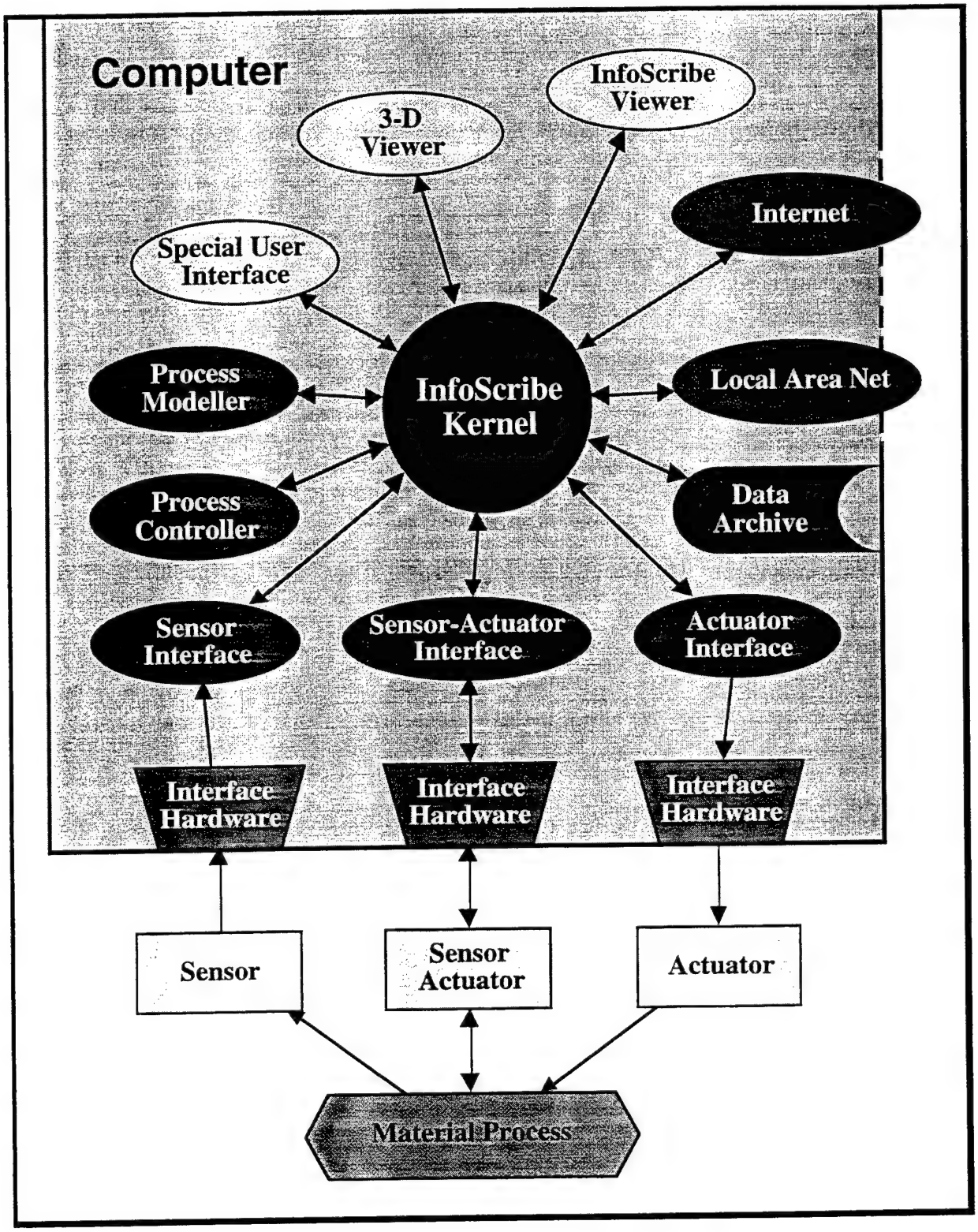

Figure 5. Future InfoScribe Architecture

The direct dispatch communication latency is represented in Figure 6 below to show the improved message transmission time available by using the micro-kernel design. The table below Figure 6 establishes that direct dispatch communication which has a mean latency of only 91 microseconds. Also, since the micro-kernel communication is isolated from operating system dependencies, the direct dispatch communication time will decrease directly as computer processor speeds increase to allow continual system performance enhancement as computer hardware is upgraded. The direct dispatch communication bridge to network communication will be handled through a module specific to TCP/IP Internet protocol and another specific to LAN protocol. While the TCPLink module already exists to support the Internet protocol, a new module will be developed from the network based communication system to support LAN protocol.

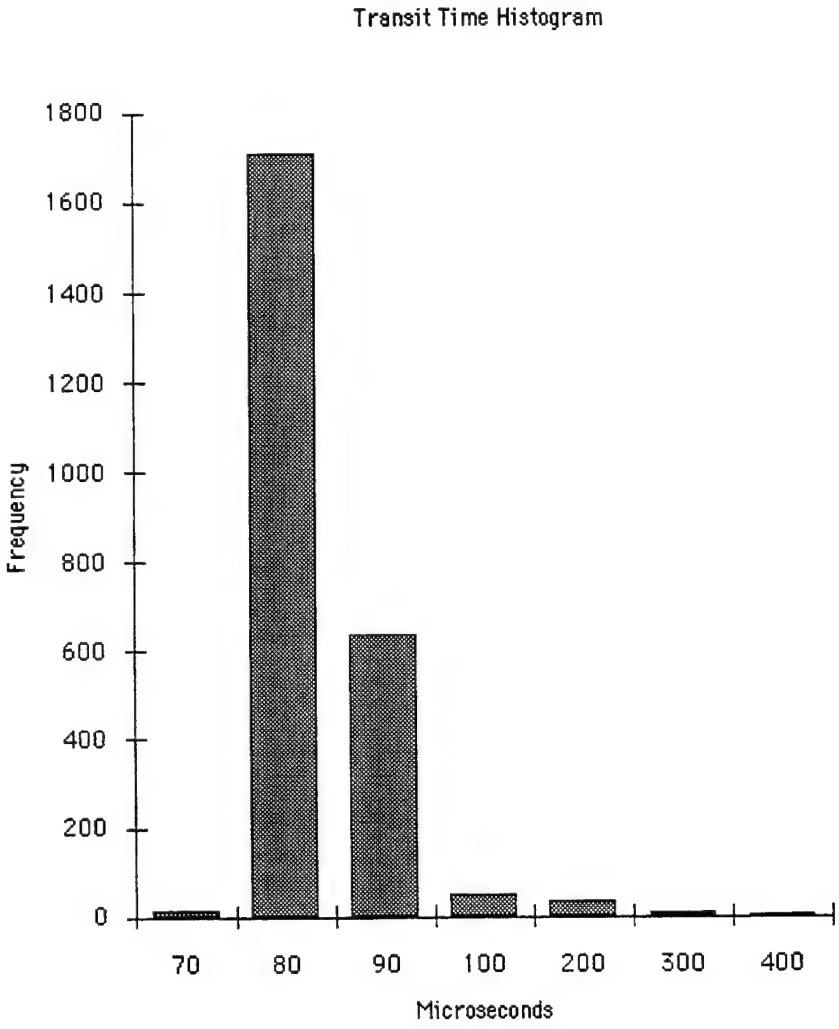

Figure 6. Future InfoScribe Message Transmission Time

Table 2.

Mean	91 microseconds
Standard Deviation	30 microseconds

Further *in situ* graphical monitoring facilities will be added as well. Data measured from sensors will be processed, interpreted, and results will be plotted in real-time. Interpretation of the ellipsometry data will be tested *in situ*. A model relating cell temperatures and properties of the film being deposited will be learned. The model will be used for the closed-loop intelligent control. Temperature set-points, and PID controller settings will be generated from the Process Advisor once the desired properties of the film is specified.

Finally, in conjunction with the above development, a coorporative effort between three (3) research groups from MLPJ, MLSS, MLIM has commenced to grow a rugate filter to be used in an infra-red vein viewing system. A filter is needed to be used with the night vision goggles for viewing viens in a battle field situation. The ideal viewing region for the NVGs is 0.88 to 0.90 microns as depicted in Figure 7.

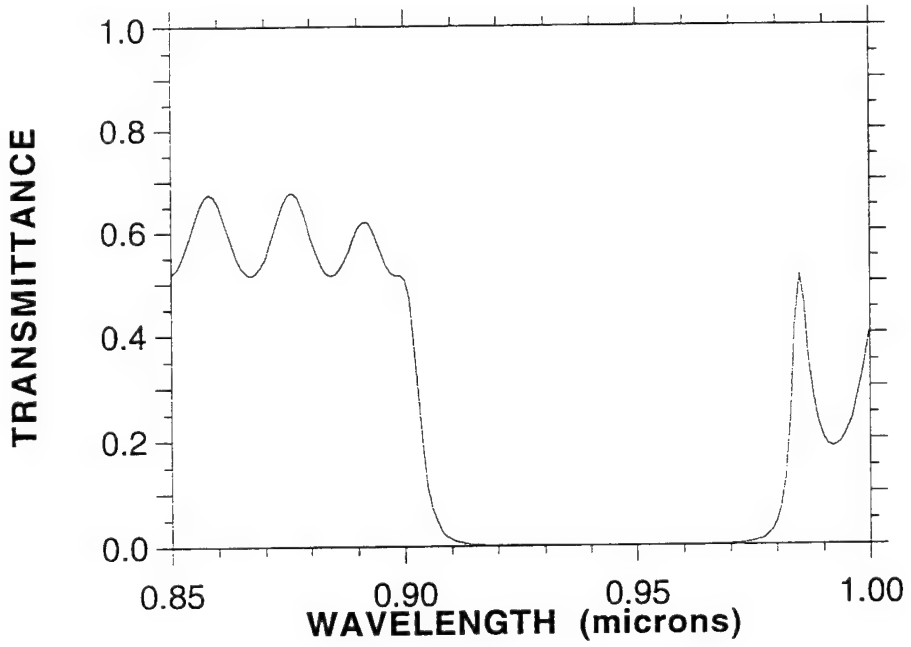

Figure 7. Ideal Viewing Region

An optical filter is needed that will block as much incident light as possible outside of this region, which is depicted in Figure 8 as the inverse of plot in Figure 7 with a desired optical density (rejection strength of filter).

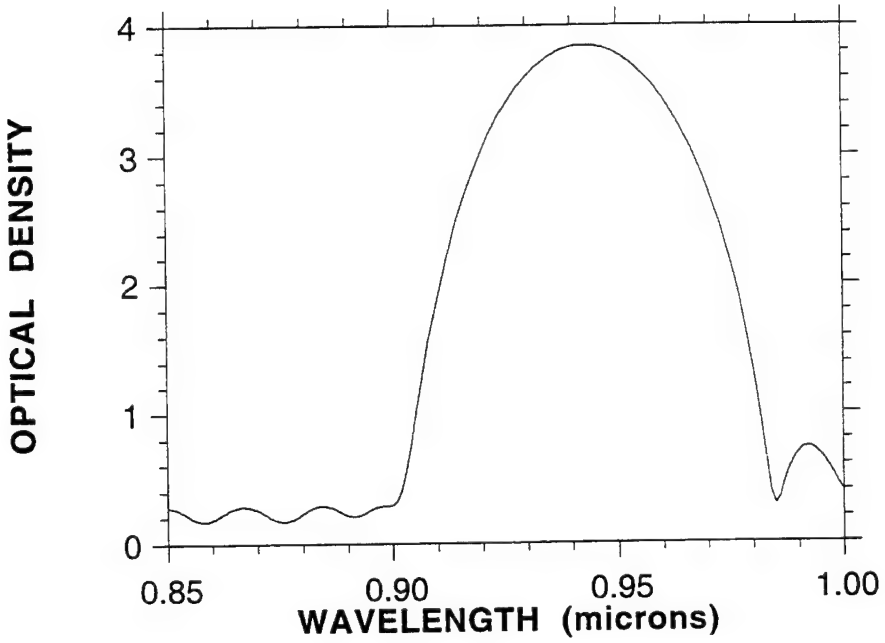

Figure 8. Desired Rejection Region and Strength

The MBE recipe for growing a film to effect the above desired rejection region and strength has been modeled in terms of the necessary refractive index profile of the film as depicted below in Figure 9. InfoScribe and the Process Advisor will be used to control the corresponding variation in film stoichiometry to affect the necessary change in refractive index.

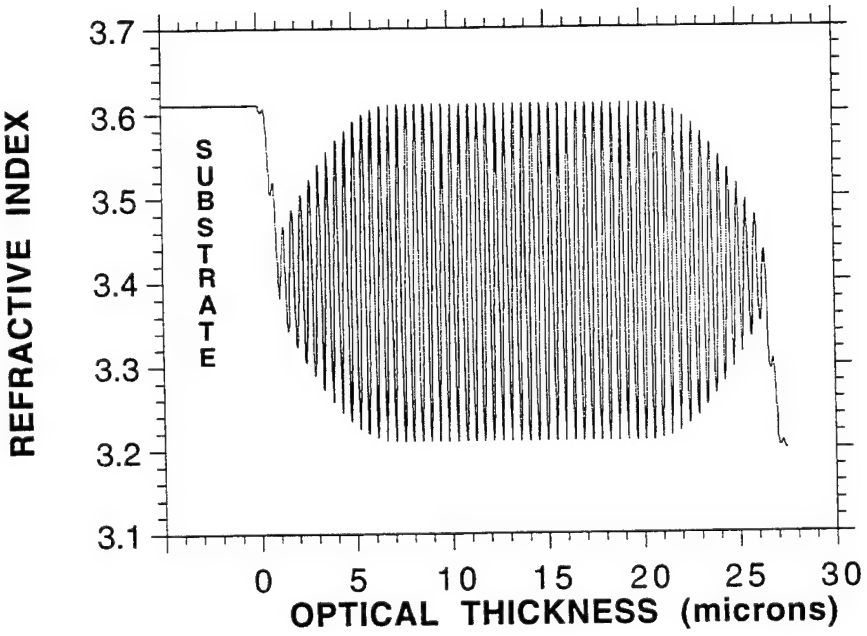

Figure 9. Required Refractive Index Variation of Film

Papers and Presentations

In Preparation

S.J. Adams, K.G. Eyink and T.W. Haas, **Improved Knudsen Cell Thermal Control using Optical Fiber Thermometry,** Monitoring and Control Techniques for Intelligent Epitaxy II, April 6-10, 1997

Published

K.G. Eyink, J.K. Patterson, S.J. Adams, T.W. Haas and W.V. Lampert, **Use of Optical Fiber Thermometry in Molecular Beam Epitaxy**, Journal of Crystal Growth, Spring 1997

Park, G.H., Pao, Y.H., Eyink, K., Igelnik, B., & LeClair, S., **Neural-Net Computing for Interpretation of Semiconductor Film Optical Ellipsometry**, IEEE Transactions on Neural Networks, Institute of Electrical and Electronic Engineers, New York, N.Y., Vol. 7, No. 4, pp. 816-829.Patterson, O.D., Eyink, K.G., & Cong, S, **Real Time, Heuristic-Based Control of Molecular Beam Epitaxy,** Journal of Materials Engineering and Performance, Vol 2, Issue 5, ASM International, October 1993, pp 715-720.

Garrett, P. H., Heyob, J. J., Hunt, V. J., LeClair, S. R., & Patterson, O. D., **Decoupled Flux Control for Molecular Beam Epitaxy**, IEEE Transactions on Semiconductor Manufacturing, Vol. 6, No. 4, November 1993, pp 348-356.

Patents

Heyob, J.J., Patterson, O.D., LeClair, S.R., Haas, T.W., Currie, K., Adams, S., Moore, D., **A Hierarchical Control System for Molecular Beam Epitaxy**, Patent Applied For. 08/131,536, 30 May 95.

Research Team: Mr. J. Heyob, Mr. S. Adams, Mr. S. Fairchild, Dr Y.H. Pao, Dr B. Igelnik, P Yip, C Yang, Dr K. Eyink.

Pulsed Laser Deposition of Thin-Film Tribological Materials

Near and long term requirements for tribological thin-films are extremely hard (80 GPa) and very low friction (ms < 0.05) coatings for high temperature (>500°C) environments, vacuum (<10^{-6} Torr) space environments, and low maintenance (10^7 cycles) aircraft propulsion and space mechanism (solid lubricant) applications.

Research OBJECTIVES are

- investigate *in-situ* sensing methods that determine density and molecular structure
- develop 'intelligent' process design and control methods based upon *in situ* spectroscopy and neurocomputing to enable novel thin film materials

Research FOCUS is

- design and implement process discovery and automation system for DLC/TiC/Ti multilayer tribological thin film pulsed laser deposition (PLD) process
- combine multiple processes, such as PLD and magnetron sputtering deposition, to produce novel multilayer thin-films
- transfer Ti/TiN/DLC multilayer tribological coatings technology using combined PLD and magnetron sputtering methods.

Background

Current research efforts are focused on the processing of and accurately controlling multilayer depositions of diamond like carbon (DLC) films. Of prerequisite importance is the ability to reliably produce DLC films that exhibit desired hardnesses and uniformity, thus requiring deposition at low (<200°C) part temperatures. It is also necessary to control film stress so that DLC can be "graded" into TiC or Ti parts without high stress boundaries. Magnetron sputtered Ti and TiC is currently a well established deposition technique, and can generate films of desired hardnesses in a repeatable fashion. Thus, it is not necessary to further develop magnetron process control technology, but integrate magnetron sputtering with other available methods.

Uniform DLC films containing high sp^3/sp^2 ratios are known to exhibit superior hardness but are difficult to deposit reliably at low temperatures and thicknesses exceeding 300 angstroms. High hardness alone is not enough to meet DLC tribological applications. Bulk film stress must also be contained within reasonable bounds to obtain desired film adhesion, and to prevent catastrophic film disintegration.

One method of controlling film hardness is by introducing interstitial layers of TiC between DLC layers by magnetron sputtering. High interface stress is also present at the substrate/film interface as well. A TiC layer can also be used to relieve stress of a DLC film on a Ti substrate. Thus, a multilayer film can be made of alternating layers of TiC and DLC on Ti substrates. The transition between TiC to DLC and back can be done in a "graded" fashion, by varying stoichiometric amounts of Ti and C. In this fashion, film stresses can be bounded, thus providing a superior film.

In order to control film stoichiometry and microstructure, process parameters that affect DLC hardness and composition must first be identified. A survey of several papers on DLC show a relationship between laser wavelength and energy density required to produce a hard DLC film.

Pulsed Laser Deposition (PLD) has been shown to be an excellent technique to deposit adherent, crystalline thin films of complex chemistry and morphology. Its primary strength is stoichiometric transfer of material. PLD is a complex, highly photo-energetic process, the physics of which are not completely understood. Several methods are available to improve the understanding of the PLD process. One method is to improve the observation technique of the process in real time through improved data acquisition tailored for process modeling applications. Another is to reduce process uncertainty, through the application of feedback control.

One method of simplifying the PLD process is to decompose it into these subprocesses that are the three energy transfer regions that occur. In the first subprocess, energy from the laser is transferred into material in motion. The material is motivated by the laser impinging the target surface. The energies transferred in the material in motion within the plume constitutes the next subprocess. Material chemistry may occur within this second subprocess. The third subprocess is where target material comes to rest on the substrate surface, transferring the plume energy and creating a thin film.

To gain control of the PLD process, suitable sensors must be identified and developed for *in situ* measurements of essential state variables of the deposition process. Sensor information will generate further understanding of basic film growth characteristics. The primary goal of self-directed control of PLD is to significantly improve the consistency and quality of the films, while simultaneously increasing process knowledge. Effective control of PLD also requires the identification of actuation parameters. The high energy laser is the main source of ablation energy, and a suitable choice for the actuator. Since cavity voltage of the laser can be varied per pulse, real-time actuation of energy density can be directly changed during a deposition. Similarly, the pulse frequency can be varied in real time to affect the instantaneous energy on the target. The excimer lasers used for PLD are typically constrained to fixed pulse lengths during operation, so varying the pulse length is not currently possible.

Initial observation of actuator and sensor data indicated that PLD exhibits a nonlinear 'dynamical' behavior. Therefore, a nonlinear dynamical process model representation was used to describe the PLD process. Material deposition relationships were empirically found by varying the laser energy density and the pulse repetition rate and recording sensor data. Derivative information was measured over designed experimental epochs. Molybdenum disulfide (MoS2) was the target material selected for the initial empirical model development. The use of dynamical feedback control of PLD has permitted growth of deposited film crystal structures that were previously unattainable using open-loop control techniques.

Research/Technical Achievements - 1996

The following discussion will be subdivided into two (2) projects. The first is the continued 'in-house' collaborative effort in PLD of tribological materials. The second is the technology transfer of the 'in-house' work via a Cooperative Research and Development Agreement with Hohman Plating Company of Dayton, Ohio.

Pulsed Laser Deposition - *In situ* Process Modeling and Feedback Control

Problem Statement

This research of pulsed laser deposition (PLD) is focused on identifying and relating observed plume characteristics to resulting material chemistry and structure with the goal of controlling

material characteristics for multilayer films. Laser induced florescence spectroscopy and a quartz crystal microbalance are used for *in situ* plume analysis. Studies of PLD diamond-like carbon (DLC) thin films (<100 nm) have already revealed a dependence of laser fluence and target material to the deposited thin film sp^3/sp^2 ratio. In this work process control is extended to produce metal-carbide-DLC gradient materials and incorporate them into multilayer coatings. Empirical process models in the form of recipes are found that manipulate the PLD process to generate multilayer films of desired composition and structure. This creates a potential for producing a new class of materials.

Total deposited thicknesses of smooth diamond-like carbon (DLC) films of high sp3 bonding fraction and uniform structure have been traditionally limited to 0.5-1 mm final thickness. This is due to the inherent increase in the film stress vector sum, which results in inevitable film delamination [7,8,9]. Even when an appropriate sample preparation technique is used, delamination from the substrate occurs, due to residual stresses, hardness, and modulus differences of DLC and substrates of comparatively softer materials such as metals or steel alloys. Practical use of DLC films of relatively high thicknesses requires interposition of hard DLC layers with stress releasing elastic interlayers, such as metals. Thus, a motivation exists for depositing DLC with interlayers. In order to reduce strain at the multilayer boundaries, a stoichiometric gradient would also be useful [10]. In summary, a gradient stoichiometry multilayer film would be capable of reducing total film stresses, while still permitting relatively thick films (>1 mm.) to be deposited.

The generation of gradient stoichiometric films require a method of process control, such that film stoichiometry can be accomplished repetitively and consistently. Furthermore, simultaneously utilizing more than one deposition process method, combined with the execution of multiple steps, increases the operator load to beyond human capabilities. In order to generate multiple layer films with tens or hundreds of layers utilizing multiple deposition techniques, process control and automation becomes imperative. The below describes an apparatus and a method capable of generating multilayer films with graded interfaces utilizing ultraviolet 248 nm PLD of graphite targets combined with direct current magnetron sputtering of titanium [13].

Experimental Design

Computer instrumentation is used to affect process automation of the PLD laser pulse energy and repetition rate. Magnetron power and background gas partial pressures are also controlled, allowing more capable monitoring of film deposition process parameters. Several single loop feedback controllers are used to stabilize process boundary conditions, combined with *in situ* sensor data to assess process behavior. Partial pressure regulation of Ar gas is implemented by utilizing a combination of mass-flow control and pressure sensing by Baratron gage, allowing for gas regulation to 1 mT. Both mass flow and chamber pressure are used to actuate the throttle valve position and gas feed solenoids. Partial pressure setpoint control is then commanded from a "recipe" of process setpoints, enabling gas pressures from 200 mT to UHV to be obtained.

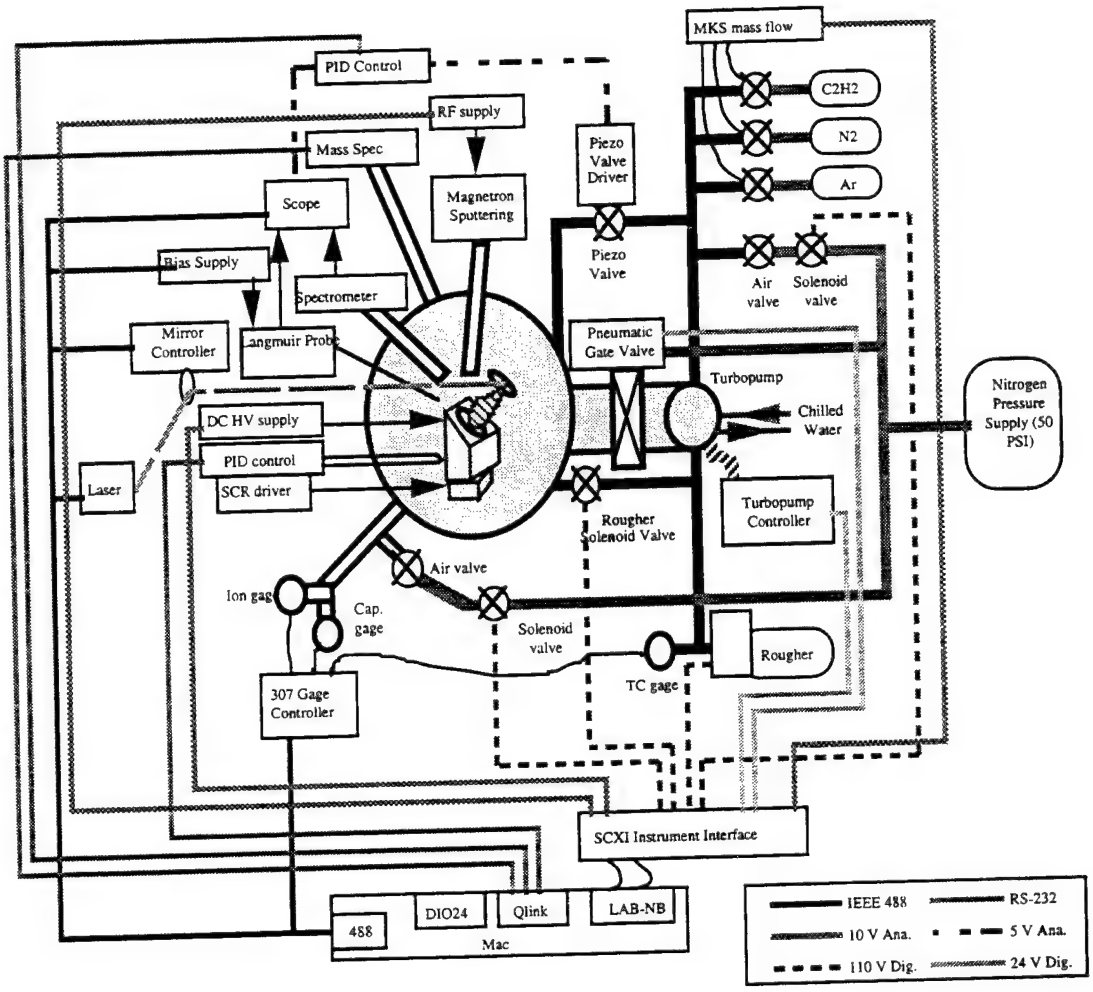

Figure 1. Multilayer apparatus system diagram and instrumentation.

Titanium DC magnetron sputtering operation utilizes power regulation combined with pressure regulation described above. Spectral plasma emission and quartz crystal (QCM) deposition rate are monitored *in situ* to sense the sputtering deposition condition. Setpoint control is commanded from a "recipe" of process setpoints, allowing automatic control of Ti-C ratios by simultaneous operation of PLD deposition and magnetron sputtering. Excimer laser pulse repetition rate and energy density are actuated to deposit carbon from a rotating graphite target, allowing for film generation ranging from Ti, to stoichiometric TiC, to DLC. Laser energy stabilization is via PIN junction UV optical detector combined with laser induced florescence spectroscopy. Laser operating parameters are also controlled via the process "recipe" setpoints.

Apparatus

A diagram of the apparatus suited to create graded multilayer film is shown above. The apparatus utilizes computer automation and control to operate gas valves, magnetrons, mass flow rates, substrate temperature, and laser parameters. QCM and LIF spectroscopy sensors are used to provide *in situ* assessment to the process control algorithms. The apparatus and algorithms also allow for automatic setup of the chamber, and then execution of the "recipe" to generate the film.

Software that operates and controls the apparatus executes commands that control digital and analog signals that control instruments. Substrate temperature, chamber total gas pressure, and magnetron sputtering plasma emission spectroscopy are process boundary condition parameters that are controlled by independent feedback loops. These independent boundary condition control loops only require setpoint data to effect process changes.

Results and Discussion - Experiment Method

Recipe film growth has been used in other deposition processes, e.g. molecular beam epitaxy [11]. Initial investigation into combined dynamics of the PLD and magnetron deposition system indicated that internal process dynamics are greater than one second, primarily due to the PLD of carbon. These slow dynamics permit the generation of a desired film gradient by stepwise setpoint change. Slow process dynamics, combined with computer control at millisecond resolution, eliminate the need for a multi-dimension process dynamical controller.

Gas residency calculations require the computer to update setpoint values in less than 1.3 seconds for the chamber setup used. Ti-DLC and TiC-DLC thickness transitions of 5 nm were originally desired, so setpoint step-approximation permitted deposition of smooth transitions. These transitions were then used to generate the desired material stoichiometric gradients. Control techniques similar to this are referred to as "Gain-Scheduling" [12]. A plot of magnetron voltage, pressure, and spectral output, for laser cavity voltage and pulse rate are shown in the previous film transition figure for four step approximated gradients, labeled "a", "b", "c", and "d". Each recipe step is limited by the process transient time of approximately 2 seconds. Magnetron deposition rate is approximately 0.3 nm/sec, indicating an achievable minimum of 0.6 nm per film transition.

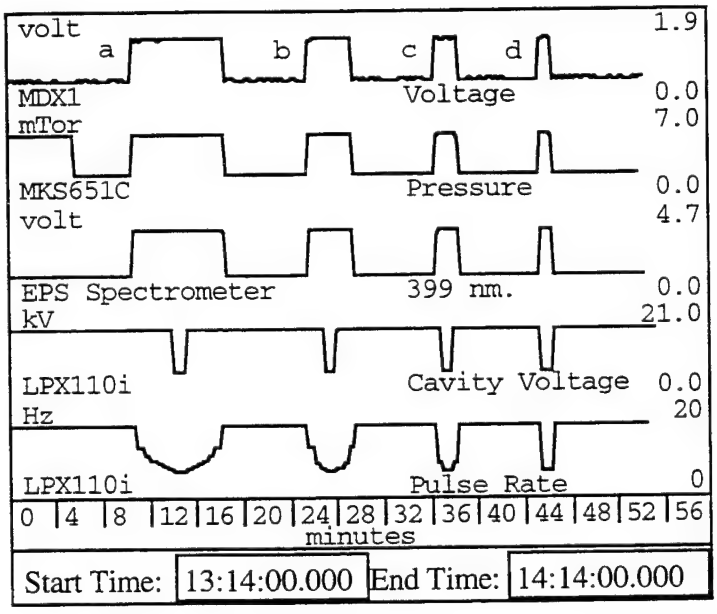

Figure 2. Film transitions for four (4) different gradient layers

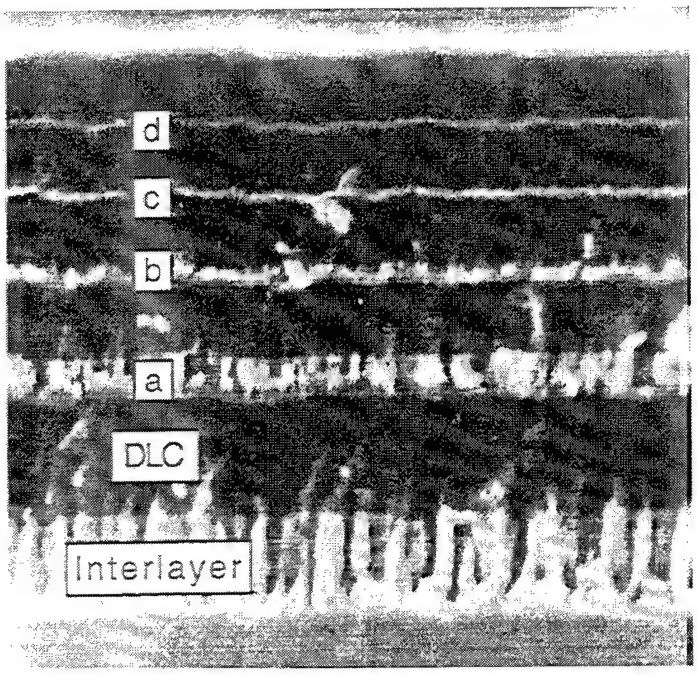

Figure 3. SEM depicting four graded multilayers generated under recipe process control

A high resolution SEM image of the resulting film generated by step approximation is shown above. The transitions labeled "a", "b", "c", and "d" correspond to those shown in Figure 20, with "d" being the 0.6 nm gradient. As can be seen [13] large gradients are possible that contain composition ranging from pure DLC to pure Ti. These gradients are created by a reduction of laser pulse rate over time. A decrease in laser energy density, magnetron power, argon pressure, or their combination can also be used. If recipe control is added, then films with numbers of layers and gradients over a wide range of desired thicknesses and composition are possible. Thicker, more gradual gradients can be generated by stepwise approximation to a continuous slope variable.

Each "recipe" was used to deposit a pre-designed film structure that has desired material characteristics. By combining the time-based setpoint changes over the entire deposition, generation of complex multilayers is possible, including boundary, interface, and multilayers. Since the multilayer film repeats, a looping structure was included so that an arbitrary number of multilayers could be selected from a single recipe edit field. In the case of Ti-DLC and TiC-DLC, graded films of 1-100 nm per layer are possible using this method [10]. The recipe method of control is capable of generating rate changes necessary for graded films without complex multiple dimension control algorithms. Recipe film growth assumes no internal process dynamics are occurring or are compensated for by each process boundary condition control loop. Individual boundary conditions are inherently band limited and stabilized by single loop controllers, so the process is globally stable. Consequentially, recipe methods are able to generate similar films each time, even though the process may vary.

Unmodeled Dynamic Effects

Although PLD of carbon is relatively stable when compared to PLD of dichalcogenides, [14,15] PLD dynamics of carbon become apparent over long periods of time when depositing large numbers of multilayers. [16] The dynamics are due to target ablation damage and temperature

effects as well as window coating. Due to the increased process complexity, instrument faults also become more likely, altering the final film.

Interlayer recipe executed once:

HOUR	MIN.	SEC.	E (mJ)	P (Hz)	PR (mT)	B (V)	M (W)	G (U)	Result
0	15	0	0	0	100	-600	0	Ar	Etch (Si)
0	30	0	0	0	0	0	0	0	Pause
0	35	0	0	0	2	0	100	Ar	Ti 100
0	40	0	200	1	2	-60	100	Ar	Ti 90/C 10
0	41	0	200	2	2	-60	100	Ar	
0	42	0	200	3	2	-60	100	Ar	Ti 50/C 50
0	45	0	200	4	2	-60	100	Ar	
1	10	0	200	6	2	-60	100	Ar	
1	19	0	200	12	2	-60	100	Ar	Ti 25/C 75
1	20	0	200	20	0	-60	0	Ar	C 100 soft
1	25	0	0	0	2	0	100	Ar	Ti 100
1	26	0	0	0	0	0	0	0	Pause

Multilayer recipe section for Ti-TiC-DLC-[Ti-DLC]20: (ML5)

HOUR	MIN.	SEC.	E (mJ)	P (Hz)	PR (mT)	B (V)	M (W)	G (U)	Result
0	1	0	200	20	0	0	0	0	C 100 DLC
0	4	0	0	0	20	0	0	Ar	
0	5	0	0	0	2	-60	100	Ar	Ti 100

Multilayer recipe section for Ti-TiC-DLC-[TiC-DLC]20: (ML7)

HOUR	MIN.	SEC.	E (mJ)	P (Hz)	PR (mT)	B (V)	M (W)	G (U)	Result
0	1	0	200	20	0	0	0	0	C 100 DLC
0	4	0	0	0	20	0	0	Ar	
0	5	0	200	4	2	-60	100	Ar	Ti 50/C 50

Figure 4. Interlayer film recipe combined with multilayer recipes used in both Ti-TiC-DLC-20x[Ti-DLC] (ML5) andTi-TiC-DLC-20x[TiC-DLC] (ML7) films

To illustrate the effects of process dynamics on resultant films, two multilayer films were produced using a similar recipe. This similar recipe resulted in two films of different final thicknesses. The recipes are shown in the table above. The parameters listed for each recipe command line are setpoint execution time, laser energy density and pulse rate, magnetron power, substrate bias voltage, background gas type and pressure. Desired results are also entered in a description field for operator reference. The process recipe shown in the table above contains the interlayer as well as multilayer sections shown for two films, Ti-TiC-DLC-20x[Ti-DLC], referred to as ML5, and Ti-TiC-DLC-20x[TiC-DLC] as ML7.

Multilayer Generation

The interlayer film provides a Ti base that is deposited on the substrate prior to multilayer film deposition. The interlayer recipe also includes substrate pre-treatment by Ar etch and outgas heating. In the case of silicon substrate samples necessary for microscopy, argon etch time is reduced to 15 minutes, as compared to 28 minutes required for 440C steel test samples to avoid substrate damage.

The TiC multilayer recipe shown in table 1 differs for ML7 only in that TiC is deposited by operating the excimer laser at 2 Hz during simultaneous magnetron operation. [13] The Ti multilayer recipe is shown in table 1 for ML5. Simultaneous laser and magnetron sputtering deposition is not performed in the ML5 recipe, so that only Ti interlayers will be deposited.

Recipes were then used to generate multilayer films. Three hours and 5 minutes are required to deposit Ti-TiC-DLC-20x[Ti-DLC] (ML5) and Ti-TiC-DLC-20x[TiC-DLC] (ML7) coatings. Computer timing is to within 1 millisecond, so no appreciable variations in schedule execution occur. During each recipe execution, 35 process parameters are displayed recorded in time so that a complete process log is available for future analysis and reference.

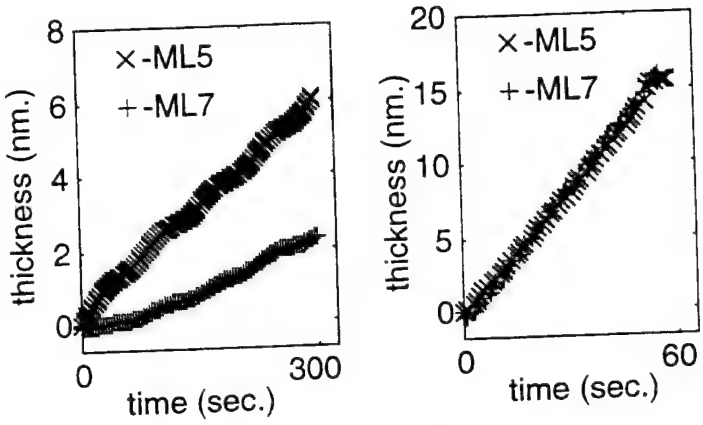

Figure 5. Measured PLD DLC and magnetron interlayer QCM data from Ti-TiC-DLC-20x[Ti-DLC] (ML5) and Ti-TiC-DLC-20x[TiC-DLC] (ML7) recipes

A comparison of ML5 and ML7 quartz crystal microbalance (QCM) thickness and thickness rate data is shown above, both for magnetron and PLD diamond-like carbon deposition. The recipe steps are identical for diamond-like carbon, yet a reduction in deposition rate is noted for ML7 as compared to ML5. Direct comparison shows approximately a factor of 1.8 between deposition final values. Measured PLD DLC rates of 0.01 to 0.05 nm/sec for ML5, and 0.001 to 0.01 nm/sec for ML7 were calculated. A sinusoidal pattern is also present due to a combination of QCM off-axis location and target rastering effects. Measured QCM deposition rates are much less than actual deposition rates at the sample location. This measurement error is due to the characteristic PLD DLC directional plume combined with QCM off-axis location.

Likewise, QCM data collected during the magnetron step in the multilayer recipe shows no appreciable reduction of deposition rate for either ML5 or ML7, even though ML7 includes PLD operation, while ML5 does not. QCM data is overlapping, indicating no appreciable difference in magnetron deposition rate for either run. A measured Ti magnetron deposition rate of 0.3 nm/sec for both runs is an order of magnitude greater than PLD DLC off-axis measurements. No periodic variations were found in the magnetron QCM data.

A DLC deposition rate reduction is apparent in the ML7 film, resulting in less thickness for each PLD diamond-like carbon layer. No appreciable change is present in the magnetron sputtering recipe step execution for either ML5 or ML7. Observed 324 nm LIF spectral emission during the PLD phase of recipe generation also show a reduction in spectral line emission and a subsequent reduction in carbon deposition in ML7 as compared to ML5.

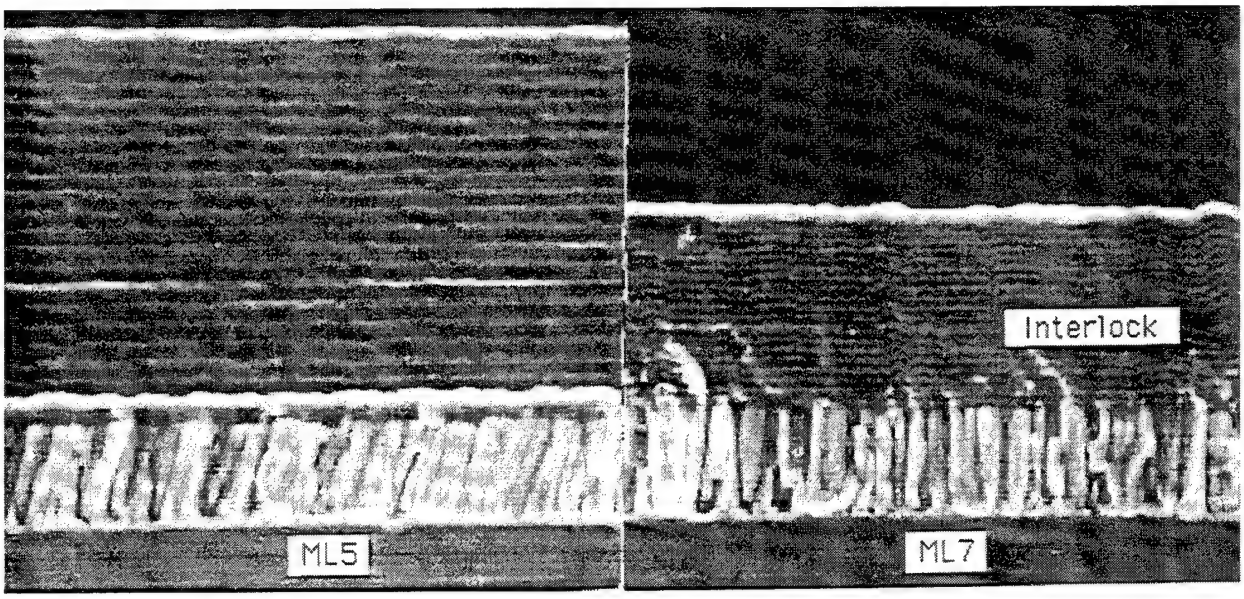

Figure 6. Scanning electron micrograph comparison of Ti-TiC-DLC-20x[Ti-DLC] (ML5) and Ti-TiC-DLC-20x[TiC-DLC] (ML7) recipe generated gradient multilayer films showing thickness disparity due to laser deposition window coating

Also indicated is laser interlock.

Similarly, representative LIF waveforms are digitized during PLD DLC in vacuum, and PLD DLC with an argon back pressure [16]. A reduction in ion velocity is indicated with an increase in Ar back pressure. Less spectral line intensity was also apparent in ML7 as compared to ML5, indicating a reduction in PLD DLC laser ablation. Integrated PIN diode laser energy density data shows no reduction in chamber laser entrance energy density for ML7 PLD DLC recipe, indicating laser entrance window coating, and reduction of carbon deposition.

A comparison of two films deposited show that for a reduced thickness value and reduced spectroscopic intensity, a marked reduction in final multilayer thickness is apparent. Edge SEM images of deposition on silicon wafer for two films are shown above.

Based on QCM and LIF data combined with laser energy data, the change in final thickness is due to window coating and subsequent decrease in PLD deposition rate. Close examination of the previous scanning micrographs indicates a missing or reduced DLC multilayer at number 8 from the interlayer in ML7. Post-film deposition examination of process parameters indicate a laser heat interlock occurred, causing a reduction of PLD DLC deposition for this multilayer. The interlock process data is shown in the following figure.

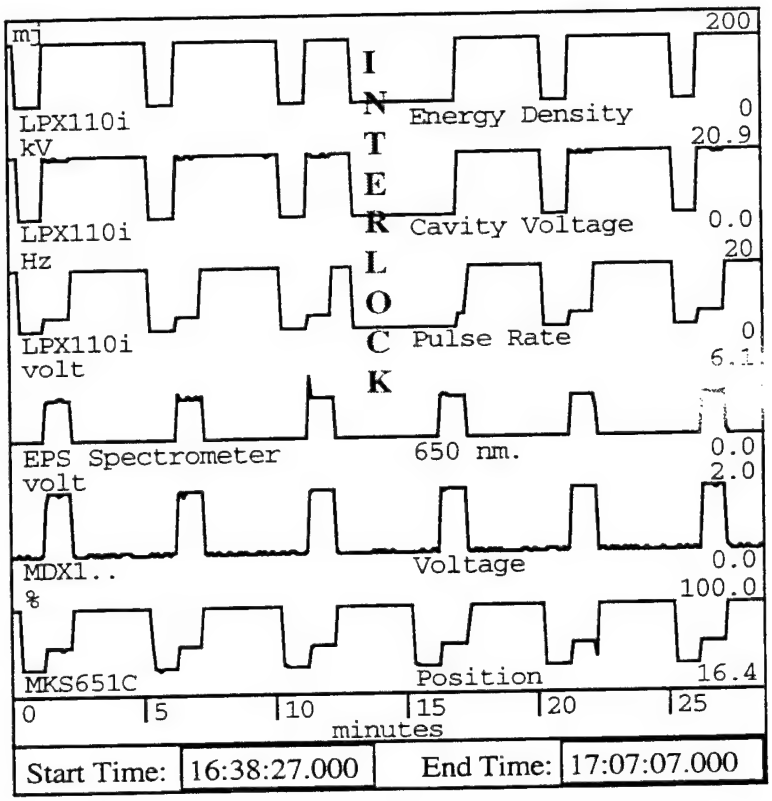

Figure 7. Laser thermal interlock and shutdown, causing partial loss of diamond-like multilayer

Conclusions

The process control system presented here is capable of producing metal-carbide-DLC gradient materials, and is also capable of incorporating them into multilayer coatings, consisting of multilayer stacks of nanolayer composites. Empirical process models in the form of recipes are found that manipulate the PLD process to generate multilayer films of desired composition and structure creating a potential for producing a new class of materials. Recipe process control and automation make combinations of several complex thin film processes tractable. This, combined with characteristic high ion species velocities previously measured for DLC PLD (100 nm/psec) permit direct atomic combination of PLD DLC with slower deposition processes. Investigation of new material gradients and multilayer heterostructures [17] become possible that may not otherwise be feasible.

In situ Process Control: Cathodic Arc of Titanium Nitride

Problem Statement

Electric arc is a thin film deposition process used to deposit titanium nitride thin films on aircraft engine (F-16) and space (shuttle main turbo pump) components. The process was capable of making thin films of high quality over large areas and on large components, but the film consistency varied. Also, occasionally the arc sources would inexplicably extinguish, causing a

defective coating, which results in scrapping the run. Increases in thin film coating process quality standard requirements, such as national aerospace defense contractors accreditation program (NADCAP) and ISO 9000 have forced improvements in existing deposition process technology as well as process run information. Increases in process traceability and records, thus indicating performance, are required to provide customer information and diagnostic capabilities.

In situ process control of cathodic arc provides a method of consistent film deposition by unmasking internal process dynamics that are otherwise not observed by sensors at the process boundaries. Increased film quality and yield have been demonstrated using emission florescence spectroscopy for *in situ* feedback control. In the present studies, feedback control has demonstrated stabilized process performance superior to that of pressure regulation, enabling the compositional changes required for multilayer films.

Further improvement in cathodic arc deposition systems require sensors that indicate more closely what is occurring during a film deposition. Even this information is not useful if it is not applied directly to the process in some way to improve the deposited material. The cathodic arc deposition process is a popular method of depositing thin films (1-10 mm.) of tribological materials for a wide range of applications, ranging form space to automotive needs. Although processes that are capable of depositing films of good quality are commercially available, current processes unfortunately rely on boundary conditions such as pressure regulation, arc currents, and voltages to stabilize the coating composition, while still leaving internal process parameters such as plasma condition uncontrolled. For deposition of multilayer films, additional *in situ* sensors must be combined with a process control recipe in order to determine and stabilize the stoichiometric growth in real time.

Feedback control of *in situ* sensor data is one method of stabilizing a process internally. [1] The objective of this study is to identify an *in situ* parameter that would be suitable for regulation and control of material quality, and then design a system to verify *in situ* feedback of this chosen parameter. Using this method, it is possible to reliably deposit multilayer films with varying composition by adjusting control setpoints in real time.

Experimental Approach

A number of parameters of the cathodic arc affect the final film outcome and morphology. These include arc currents and voltages, deposition gas pressure, substrate temperature, substrate bias voltage, and substrate preparation. During operation of the arc, a plasma is generated, and is sustained by a gas pressure. The particular gas type affects the final film composition. In the case of titanium nitride deposition, nitrogen gas is used to sustain the arc. Spectroscopic emission from this plasma can be used as an *in situ* analytic method of determining film deposition characteristics. A system which uses arc emission to vary inlet gas flow is depicted in Figure 8.

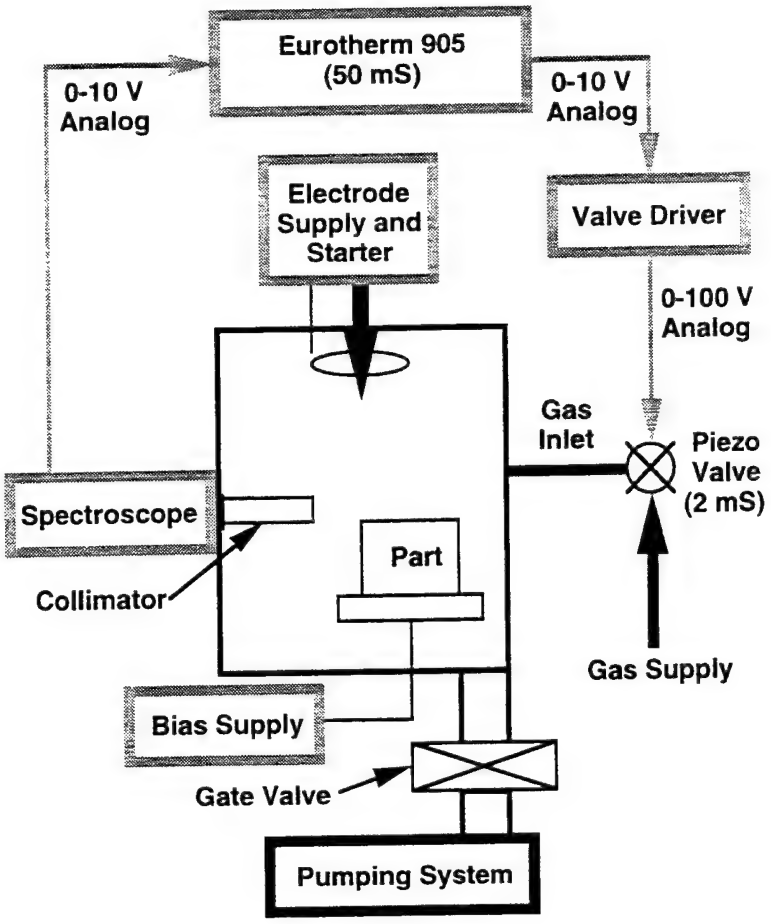

Figure 8. Cathodic arc process control using in situ process control by plasma emission spectroscopy

An optical emission spectroscope is used to monitor the Ti* (Ti I) ion plasma emission at 650 nm wavelength. Other spectral lines were tried, but this line had sufficient intensity to be detected reliably, and was unique. Utilizing this spectral line intensity to actuate a high speed piezoelectric valve to change chamber partial pressure was found to directly sense deposited film composition. In order to determine spectral line control, the arc current and voltage are regulated in these experiments, while gas pressure is varied. Films produced by *in situ* closed loop control were then analyzed by *exsitu* tests to determine variations in stoichiometry, as well as actual tribological properties.

Estimated gas residency times were calculated from pumping rates and mass flows. From these calculations, PID tuning was performed using a Ziegler-Nichols method [2] at setpoint maximum and minimum. The tuning parameters were then modified based on process performance. Acceptable values of proportional band and integral reset used were 600% and 15 sec. respectively. These values proved adequate to stabilize the process involving processing intervals of 4 hours.

Unlike spectral emission regulation used in magnetron deposition or CVD, the spectroscopic signal from the cathodic arc process is noisy, and is of varying probability density, due to the erratic behavior of the arc on the electrode. Furthermore, the spectroscope probability density is a

function of gas pressure, with less noise apparent at lower pressures. Spectroscopic intensity is also affected by cathode temperature and amount of cathode poisoning. Thus, pre-filtering of the spectroscopic signal is necessary for stable control performance.

A preliminary solution is to use a 3-pole Butterworth [3] low pass filter, combining filter properties of having the least amplitude and phase distortion for a given stop band attenuation. A more sophisticated method involving arc plasma intensity signature identification could be used. A mapping, perhaps a functional-link [18] neural net, could be used to identify plasma species intensity and correlate the emission to deposited film characteristics. The additional functionality would require an increased effort, and was not supported under the Cooperative Research and Development Agreement (CRDA).

Using the preliminary design, the piezo valve mechanical response time is limited to 2 ms, so the maximum actuator bandwidth is limited to 500 Hz. Spectroscopic sensor temporal data analysis showed a limited information response time of approximately 100 ms, indicating that a cutoff frequency of 10 Hz was required for this particular chamber and pumping system. The estimated power-spectral density taken over several process runs showed that a process integration time of 25 seconds is sufficient to remove variation due to arc motion. Thus, a slower response time valve could be used.

Stabilization of the process arc was ineffective when variation reductions with a time interval of less than 100 ms were attempted, indicating estimated information bandwidths to be accurate. An increase in compensator gain only destabilized the arc and generated excessive piezo-valve actuation. A reduction of the spectroscopic pre-filter cutoff frequency below 10 Hz reduced the overall controller response.

Two process run data sets collected with 'in-house' developed data acquisition software, referred to as InfoScribe, coupled to Labview are shown in the following graphic, showing closed loop control of the electric arc in comparison with open loop arc spectral line intensity. Spectroscopic data combined with actuator effort are shown in comparison with pressure regulation for intensity setpoints of 10% (b) and 90% (d) respectively. As can be seen in both b and d, pressure regulation indicates a variation of up to 20 % for spectroscopic line intensity occurs due to random arc motion. Because of *in situ* process control, spectroscopic line intensity shows less than 5% variation across several runs.

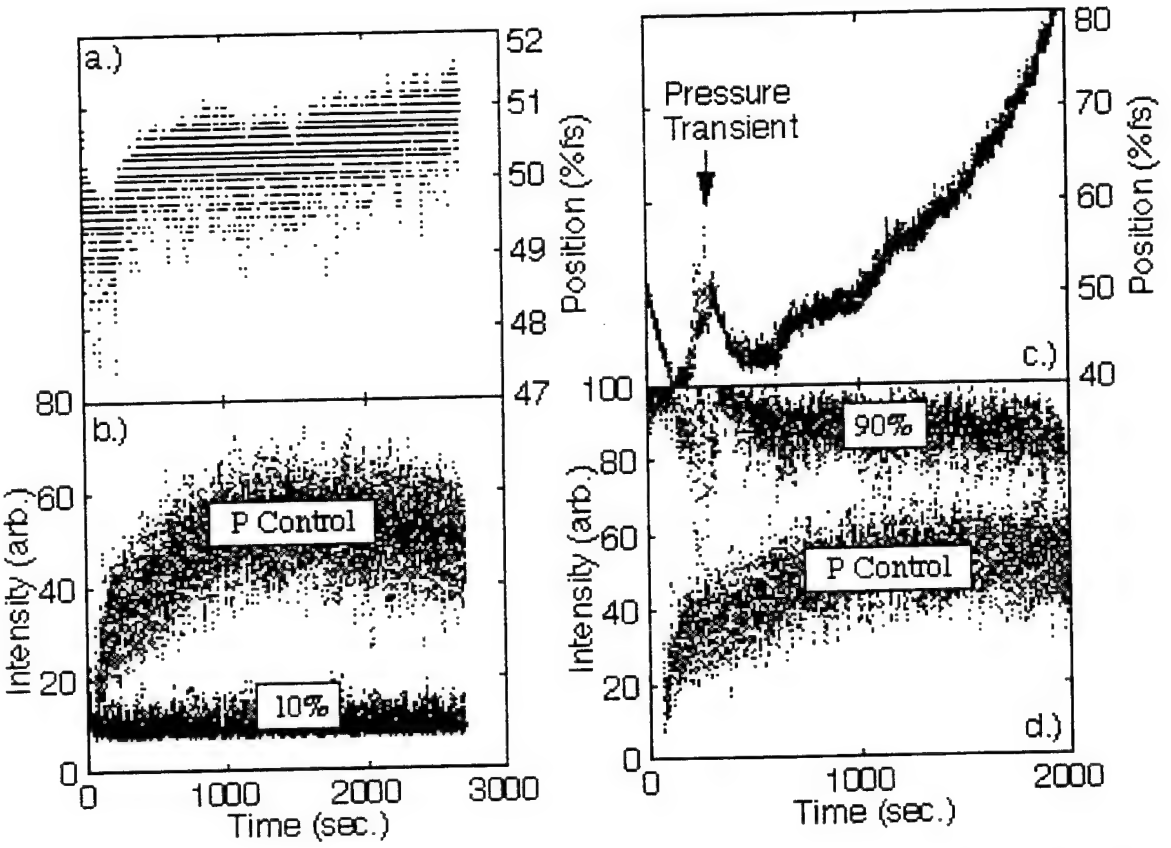

Figure 9. Comparison of spectroscopic signals from in situ process control and pressure control
a.) actuator position at 10% intensity setpoint,
b.) in situ control performance at 10% intensity setpoint,
c.) actuator position at 90% intensity setpoint,
d.) in situ control performance at 90% intensity setpoint.

Actuator effort for both runs is also shown for setpoint regulation of 10% (a) and 90% (c) respectively. Typical actuator effort starts at a low value and steadily increases during the run, indicating a higher pressure is necessary to maintain spectral line intensity. A pressure transient, shown in c, was later found to be due to an instability in the nitrogen pressure gas manifold that feeds several production chambers. This transient was found to occur whenever another deposition process that shared the same manifold was initialized. This problem has since been corrected, but was unknown prior to installation of the *in situ* process control sensor.

Results and Discussion

Once the *in situ* spectral line process control system was performing correctly, experiments were performed to compare films produced by *in situ* process control with films produced by pressure regulation. Pressure regulation used standard values and practices developed by Hohman. Spectral line emission controller setpoint boundaries were defined as 0% intensity equating to the nitrogen gas pressure that extinguishes the arc, and 100% intensity as the nitrogen gas pressure that causes electrode poisoning. Calibration between each run was also checked by utilizing a calibrated white light of fixed intensity that is placed within the dark, sealed chamber. The spectroscope was then checked for drifts and inaccuracies prior to each process run. Samples

using both pressure regulation and *in situ* process control were produced to compare the coatings:

1. Coatings were produced using a standard TiN deposition procedure used by Hohman with mass-flow and Baratron gage pressure regulation. This method of pressure control uses mass flow control in a proportional plus integral scheme. Spectral line intensity was also recorded during these coating runs. This method was used to produced samples designated as "TiN reg".

2. Coatings were produced using a standard TiN deposition procedure used by Hohman, but with control of gas using closed-loop *in situ* plasma emission process control feedback instead of gas pressure regulation. In these runs, nitrogen gas pressure is allowed to vary while spectral line intensity is regulated. Titanium spectroscopic line intensity is then used to generate coatings at three setpoints, with two process runs performed at each setpoint. The spectral line intensity samples are produced as follows:

Coatings produced at 10% relative intensity of control signal, designated as "TiN 10%".
Coatings produced at 50% relative intensity of control signal, designated as "TiN 50%".
Coatings produced at 90% relative intensity of control signal, designated as "TiN 90%".

In total, four different TiN coatings were prepared in 8 runs, to provide duplicate samples of each type. Several test runs were also performed prior to these sample comparison experiments to verify proper controller tuning and performance for both pressure regulation and *in situ* plasma emission process control. Coating chemical composition was then evaluated using X-Ray photoelectron spectroscopy with an M-Probe instrument at 0.2 eV resolution. Samples were sputtered with a 1 keV Ar gun for 10 min. to remove surface contamination.

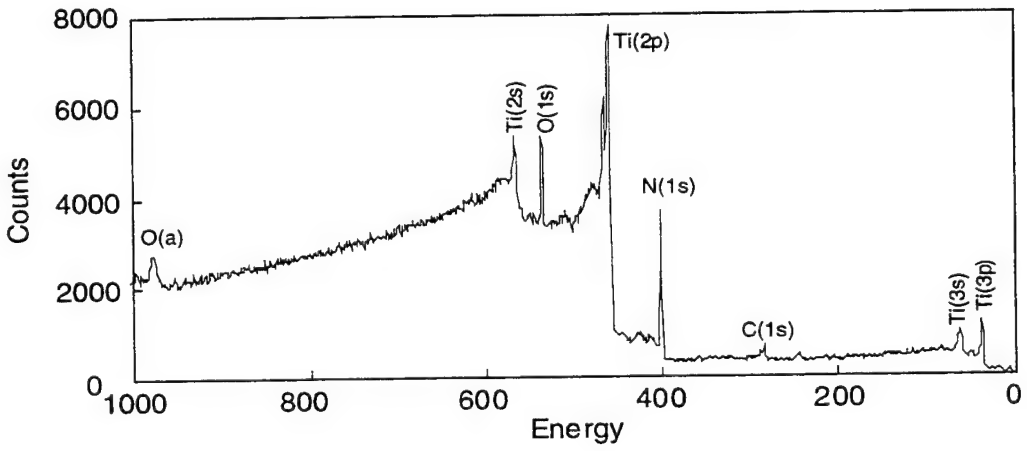

Figure 10. Typical XPS spectrum of film produced by in situ process control

Typical spectrum of the coating elemental bonding energies is shown in the previous graph. The spectrum shows the presence of Ti, N and O with traces of Ar and C. The indicated argon presence is due to the XPS surface etch procedure. Traces of carbon are typical for deposition systems with diffusion pumps. Possible origins of the indicated oxygen contamination are due to oxidation of nonreacted Ti in the coatings with oxygen from the atmosphere. Another possible source of film oxygen is from residual water pressure in the chamber. Residual water is more likely, given the large physical size of the deposition chamber used.

Sample ID	Ti at.%	N at.%	O at.%	Ti/N ratio
TiN reg	49.10	38.73	12.80	1.27
TiN 10%	51.60	40.85	7.55	1.26

TiN 50%	48.19	42.65	9.16	1.13
TiN 90%	46.50	43.54	9.50	1.06

Figure 11. Composition analysis of films produced under pressure control ("TiN reg") and in situ process control (TiN 10%, TiN 50%, TiN 90%)

A summary of film chemical composition for the main elements Ti, N and O of several films is shown for comparison in the previous table. A ratio of Ti/N was also calculated and is included. It can be seen that a coating produced by pressure regulation is slightly over stoichiometric in respect to titanium. However, the excess of nonreacted Ti is small (no metallic Ti was registered with XPS). Possibly some of the excess Ti atoms are dissolved into the TiN phase, while others formed oxides, present after each deposition, that typically precipitate out as a powder.

Coatings deposited with plasma emission control at 10% and 50% signals were found to be slightly over stoichiometric as well. Coatings produced with 90% signal were found to be close to stoichiometric in chemical composition. It was also noted that less precipitated powder was present after each deposition run, and less oxygen contamination was present for coatings produced with plasma emission control.

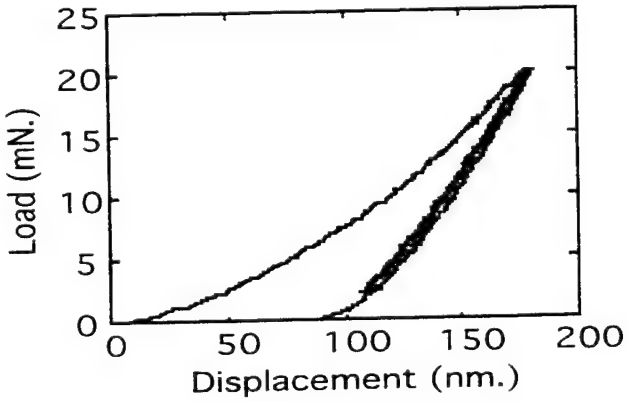

Figure 12. Typical nano-indentation curve measured on films produced by in situ process control and pressure control.

Hardness and elastic modulus of the produced TiN coating were estimated. For this purpose a Nanoindentor II instrument with a Berkovich indentor was used. In these tests, an indentor was loaded with a force of 20 mN and load-displacement curves were recorded. Typical procedure is shown in the previous graph. The curve is generated by increasing load to the maximum, unloading to 10% load, 50 sec holding for a thermal drift correction, loading to maximum load again and final unloading. The hardness data were taken for maximum load at a penetration depth of approximately 180-200 nm. Young's modulus is then estimated from the final unloading curve slope.

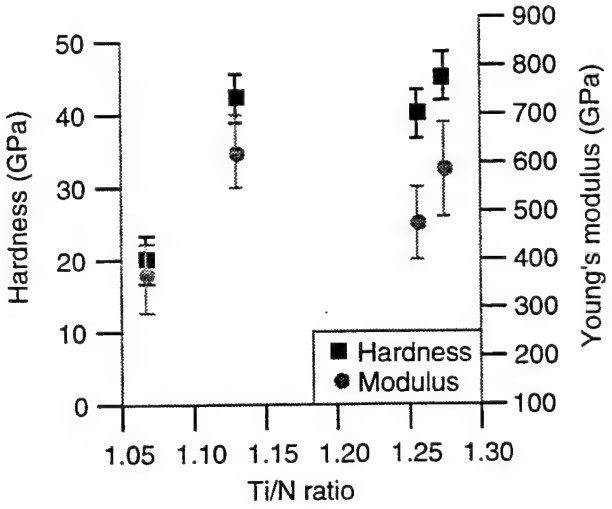

Figure 13. Mechanical test results of films produced by *in situ* process control and pressure control

Results of the films produced are accumulated in the previous figure for hardness and elastic modulus as a function of Ti/N ratio. These data suggest that all coatings with slightly over stoichiometric Ti content have approximately the same hardness of around 40 GPa and a modulus of around 550 GPa. This includes TiN produced under pressure control, and TiN produced under spectroscopic regulation of 10% and 50% intensity, as indicated at the top of the figure.

The stoichiometric TiN hardness produced under 90% spectroscopic regulation is reduced to about 25 GPa, which is a typical value for TiN deposited by Cathodic arc. [4] These results suggest that a slightly over-stoichiometric composition is favorable for achieving optimum mechanical properties. This agrees with results of previous investigations [5,6], which show that for TiN coatings with insufficient N content, the structure is more dense, and consists of fine grains and a developed dislocation network. Coatings of this composition are also known to have higher levels of compressive stresses, which also affect measured hardness values.

Conclusions

Consistent coating that can be produced over long time periods is a practical advantage of ***in situ*** spectroscopic intensity process control. ***In situ*** sensing increases process stability by sensing internal process parameters where the deposition is actually occurring, and not at boundary conditions, such as pressure. These issues are important when coating large parts of high cost. In some cases, the process is required to generate a uniform coating over a part of complex shape and large size, as well as high cost. Risking stabilization of a deposition process by pressure alone opens up the chance of scrapping the part, and ultimately eliminating the customer base.

In situ process control of cathodic arc allows for more consistent film deposition by unmasking internal process dynamics that are otherwise not observed by sensors at the process boundaries. Consequent film quality and yields are increased, as well as increased process attribute records and run data. This additional process information increases the operator's knowledge of overall process condition as well as providing additional data to satisfy new standards, such as national aerospace defense contractors accreditation program (NADCAP) and ISO 9000.

In situ spectroscopic intensity process control provides an additional advantage by better informing the operator of the true process condition, as well as attempting to compensate for any unforeseen variability not apparent at the process boundaries. Comparison of films show a reduction of oxygen in all cases of films produced under *in situ* process control as evidenced by a reduction in powder generation, while maintaining desired mechanical properties. When high process repeatability is demanded over long time periods across several runs, these advantages demonstrate *in situ* spectroscopic intensity process control is superior to pressure regulation on Cathodic arc production systems.

As a consequence of information generated by this work, several process interactions were discovered that ultimately saved untold dollars by improving the process for more repeatable operation. This ultimately provided the desired coatings that have a greater wear life for the F-16 fighter engines, as this process is used to coat engine parts for Pratt and Whitney as well as the space shuttle. The work done under example one was done under Cooperative Research and Development Agreement, CRDA # 95-335-WL-01 (7/95 - 7/98) The direct government payback is $20,196, with Hohman Plating & Mfg. Inc. as the project partner. The project timetable for completion is 2 years.

References

1. A.A.Voevodin and S.J.P.Laube, "In-situ plasma monitoring of pulsed laser deposition of diamond-like carbon films", Surfaces and Coatings Technology 76-77 (1995) 670-674.

2. J. G. Ziegler, N. B. Nichols, "*Optimum Settings for Automatic Controllers*", Trans. A. S. M. E., Nov. (1942) 759-768

3. P. H. Garrett "*Analog I/O Design*" Ch. 4, Reston Publishing Co. Reston Va. 1981

4. H. Randhawa, P.C.Johnson and R. Cunningham, "Hardness of TiC" J. Vac. Sci. Technol., A 6(3), 1988, 2136-2139.

5. J.E. Sundgren, B.E.Jacobson and M.K.Hibbs, Z. Metallk, "Microstructure of nitride and carbide coatings prepared by physical vapor deposition methods", 75, 1984, 855-861

6. A.J.Perry, "On the existance of point defects in physical vapor deposited films of TiN, ZrN, and HfN", J. Vac. Sci. Technol., A 6(3), 1988, 2140-2148.

7. M. K. Pucheert, P. Y. Timbrell, R. N. Lamb, D. R. McKenzie, "Thickness-dependent stress in sputtered carbon films", Journ. Vac. Sci. Technol. A 12(3) May/Jun 1994 P. 727-732

8. Kwang-Ryeal Lee, Yong-Joon Baik, Kwang-Yong Eun, "Stress relief behavior of diamond-like carbon films on glasses", Diamond Related Materials, 2 (1993) 218-224

9. Suman B. Iyer, K.S. Harshavardhan, Vikram Kumar, "Buckling patterns in diamond-like carbon films", Thin Solid Films, 256(1995) 94-100

10. A. A. Voevodin, M. A. Capano, S. J. P. Laube, M. S. Donley, J. S. Zabinski, "Design of a Ti/TIC/DLC Functionally Gradient Coating Based on Studies fo Structural Transitions in Ti-C Thin Films", Solid Thin Films, in press

11. O. Patterson, J.J. Heyob, S.J. Adams, V. Hunt, P.H. Garrett, K.R. Currie, K.G. Eyink, T.W. Haas, S.R. LeClair, "Progress toward a comprehensive control system for molecular beam epitaxy " WL-TR-92-4091, Materials Directorate, Wright-Patterson AFB, Ohio, December 1992, ASD 92-2624.

12. Karl J. Åström, " Control Perspective" Proc. of the IEEE, Vol. 75, No. 2, Feb 1987

13. A. A. Voevodin, M. A. Capano, A. J. Safreit, M. S. Donley, J. S. Zabinski, "Combined magnetron sputtering and pulsed laser deposition of carbides and diamond-like carbon films", App. Phys. Lett, Submitted

14. E. F. Stark and S. J. P. Laube," Self-directed control of pulsed laser deposition", JMEPEG (1993) 2:721-726

15. S. J. P. Laube and E. F. Stark, "Artificial Intellegence in Process Control of Pulsed Laser Deposition", Proceedings of International Federation of Automatic Control Symposium on Artificial Intelligence in Real Time Control, Valencia, Spain, 3-5 Oct. ,1994, p.159, Elsiver Science, Ltd., The Boulevard, Langford Lane, Oxford OX51GB UK.

16. A. A. Voevodin and S.J.P. Laube, S.D Walck, J.S. Solomon, M.S. Donley, J.S. Zabinski, " Pulsed laser deposition of diamond-like amorphous carbon films from graphite and polycarbon targets" , Journal of Applied Physics 78 (6), 15 September 1995

17. A. A. Voevodin, M. S. Donley, J. S. Zabinski, *"Pulsed Laser Deposition of Diamond-like Carbon Wear Protective Coaitngs: A review"*, Surface and Coatings Technology, in press.

18. Pao, Y.H. & Takefuji, Y., *Functional-Link Net Computing Theory, System Architecture and Functionalities*, Chapter in Readings in Computer Architectures for Intelligent Systems, edited by J. Herath, Computer Society Press, 1992.

Future Work - 1997

Specifics of general materials processes that are candidates are needed to bear additional testimony to the methods developed here. Future research in virtual materials research relies on verification of this concept over several processes and material types. A list of candidate process tasks within ML follow, that will be developed to implement virtual materials research.

FY97 WL/MLBT Tasks

PLD and DC magnetron hybrid deposition system: Hardware/software (HW/SW) design, implementation, and re-build for multilayer magnetron/PLD recipe control, including incorporation of magnetrons and mass flow instruments.

Time of flight PLD analysis - HW/SW interface for TOF mass spectrometer to explore plume phenomena, requiring the specification and design of interface hardware and data storage.

High speed tribotester control - HW/SW improvements and functional enhancements as well as code debug/maintenance for experimental data result storage and retrieval.

Vacuum Tribotester control - Vacuum Tribotester HW/SW design, build, and code for experimental data result storage and retrieval.

PLD and E-beam hybrid deposition - Ion beam HW/SW, add/rewrite existing PLD recipe control code to accommodate and fully utilize process changes, requiring a complete process redesign.

FY97 WL/MLPJ Tasks

PLD of HTSC on large area systems - Design and specify instrumentation and write code to control large area system.

FY97 WL/MLPO Tasks

MOCVD - Design and specify control system to perform rapid thermal anneal of SiC substrates. Implement HW/SW and test system.

FY97 WL/MLBM Tasks

MBE of semiconductors - Design and specify instrumentation and write code to control MBE film growth, utilizing ellipsometry and multiple layer recipe control.

These are processes that can benefit from virtual materials research. The success of each process will depend greatly upon the amount of cooperation offered by the indicated deposition process groups. The capability to create a synergistic relationship will ultimately determine the amount of success.

Papers and Presentations

In Preparation

Laube, S.J.P., **Extremely Tough Multi-layer Gradient Thin Films**, Proceedings of Australasia-Pacific Forum on Intelligent Processing and Manufacturing of Materials, July 14-17, 1997, Gold Coast, Australia.

Laube, S.J.P., & Voevodin, A.A., **Pulsed Laser Deposition *In situ* Process Modeling and Feedback Control for Multi-layer Deposition**, Journal of Surfaces and Coatings Technology, Elsevier Science B.V., Amsterdam, Netherlands.

Laube, S.J.P., Voevodin, A.A., & Korenyi-Both, A., **Cathodic Arc Titanium Nitride *In situ* Process Feedback Control for Multi-layer Deposition**, Journal of Surfaces and Coatings Technology, Elsevier Science B.V., Amsterdam, Netherlands.

Published

Voevodin, A.A. and Laube, S.J.P., ***In Situ* plasma monitoring of pulsed laser deposition of diamond-like carbon films**, Journal of Surfaces and Coatings Technology, Elsevier Science B.V., Amsterdam, Netherlands, Vol 76-77, 1995, pp. 670-674.

Voevodin, A. A, Laube, S.J.P., Walck, S. D, Solomon, J. S, Donley, M. S, Zabinski, J. S, **Pulsed Laser Deposition of Diamond-Like Amorphous Carbon Films From Graphite and Polycarbonate Targets,** Journal of Applied Physics, American Institute of Physics, Woodbury, N.Y., Vol. 78, No. 6, 15 September 1995.

Stark, E.F. & Laube, S.J.P., **Self-Directed Control of Pulsed Laser Deposition Process,** Journal of Materials Engineering and Performance, Vol 2, Issue 5, ASM International, October 1993, pp 721-726.

Patents

Laube, S.J.P., Voevodin, A.A., Zabinski, J.S., & LeClair, S.R., **Process Control and Apparatus for Gradient Multilayer Thin Film Growth**, Invention AFD #00142, 28 Mar 96.

Laube, S.J.P., Stark, E.M., **Automation of Pulsed Laser Deposition**, Pat. Pending #08/386,240, 09 Feb 95.

Laube, S.J.P., Stark, E.M., **Hierarchical Feedback Control of Pulsed Laser Deposition**, AF Invention #21467, 16 Dec 94, Patent # 5,535,128, 9 Jul 96.

International Conferences

Stark, E.F., & Laube, S.J.P., **Artificial Intelligence in Process Control of Pulsed Laser Deposition**, Proceedings of 1994 International Symposium on Artificial Intelligence in Real-Time Control, Valencia, Spain, 5 Oct 94.

Research Leader: S. J. P. Laube, **Team**: Dr A. Voevodin, Dr J. Zabinski, K. Keener (SOCHE)

Pulsed Laser Deposition of Superconducting Films

Processing of superconducting films is driven by the need for large scale passive microwave array components, notch filters for both defense and private sector (cellular) telecommunication technology, and low loss conductors for air and spacecraft power generator components (stator/armature wire). In addition, longer term large scale high quality superconducting film/device applications include conformal antennas and/or patch antennas, transmission lines, and resonators for ECM, EC^2M, and ESM applications.

Research Objectives are:

- to design and implement process discovery system for YBCO thin film pulsed laser deposition (PLD) process,
- to investigate inexpensive *in situ* sensing methods to identify film properties *in situ*,
- to improve stabilization and enable variable (spatial and temporal) laser energy density,
- to generate large area YBCO films (4" wafer) and evaluate PLD plume steering for MEMS applications/devices.

Research Focus is:

- to design and implement *in situ* process monitoring of composition and thickness of YBCO thin film via pulsed laser deposition (PLD) using Raman spectroscopy,
- to evaluate post processing or cooldown of substrate to assess optimum rate and oxygen pressure to maximize YBCO T_c and J_c,
- to implement *in situ* process remodeling via functional link net (FLN) control of PLD process to increase material uniformity, yield and quality.

Background

In reference to the first objective, due to process uncertainties and a lack of total process understanding for YBCO PLD, high temperature superconductor film yields are low, and usually require several weeks of trial and error to produce a single good film. Furthermore, these films are generally small in terms of physical dimensions, with films occupying areas of less than one square centimeter. Self-directed control means that the material behavior during processing determines the control of the process, thus removing process uncertainties by direct evaluation of the material as it is produced. Implementation of self-directed control requires *in situ* sensing as well as stabilizing process dynamics. Implementation of *in situ* sensing has already shown that the process is capable of producing material of consistent, superior quality with deposited areas in excess of ten square centimeters. Self-directed control of process dynamics via *in situ* sensing provide a new way for producing YBCO with high yield over large areas. Large areas, high yield, and superior quality, are paramount for production of large YBCO passive microwave components.

As with most material processes, a systematic approach to self-directed control begins with stabilization of boundary conditions. Stabilization of: 1) process substrate temperature, 2) laser energy density, and 3) O_2 background pressure have resulted in a substantial reduction in process boundary variability, and has established feasibility for self-directed control of the YBCO PLD process.

Subsequently, source parameters for each boundary condition must be identified, e.g., the main actuator of PLD is the high energy excimer laser. The laser emits a 25 nsec pulse of ultraviolet light, and the energy density is adjustable by changing laser cavity voltage. This high energy pulse is used to ablate target material, creating a plume of highly energetic species necessary to generate YBCO of desired stoichiometry. Thus, stabilization of the laser energy is critical to producing films that are consistent and of superior quality.

Research/Technical Achievements - 1996

Previously, laser energy density has been stabilized by utilizing a PID controller, combined with a CMAC learning table, to adjust laser cavity voltage. This stabilization implementation is capable of compensating for gas aging and thyratron switching variations, based on a bolometric energy sensor. However, even with the laser energy stabilization, the process still exhibited high variablility. To attempt to produce high quality films consistently, improved observation and control through the use of *in situ* sensors were studied for feasability and partially implemented. The first *in situ* sensor to be examined is optical emmission spectroscopy using laser induced fluorescence. The laser used for this particular PLD process is a krypton fluoride device which delivers 250 mJ of energy in a 25 ns pulse, which equates to an average power of 10 MW. When the high energy laser beam impacts the target, some of the target material is ablated. As the ablated material travels away from the target in the form of a plume, the constitutive elements begin to lose energy in the form of fluoresence, which is termed laser induced flourescence (LIF) . Optical emission spectroscopy can be used to detect the LIF spectrally. A high speed spectroscope monitoring an emission line over time can be used indicate several film parameters. Waveform rise time and delay after the laser pulse indicates relative velocities of the species and the area under the curve also indicates relative species density. Additionally, it also provides a measure of the plume's kinetic energy by observation of its time of flight. Examining the shape of the curve is and indication of the temporal distribution of the plume. It had been found previously even though the PID-CMAC stabilized laser is indicating a constant energy density, a large variation in the plume spectroscope sensor occurred when different laser cavity voltages were required to achieve that energy. Due to gas aging and other phenomena, the excimer laser utilizes different laser cavity voltages to generate the same optical energy density. Although a constant energy density is indicated, spatial and temporal changes occur on the laser pulse and beam modes, grossly affecting film quality. An example of the optical emission over time and the corresponding plume are shown in Figure 1, clearly demonstrating the variations in the plume intensity and shape for a constant laser energy density.

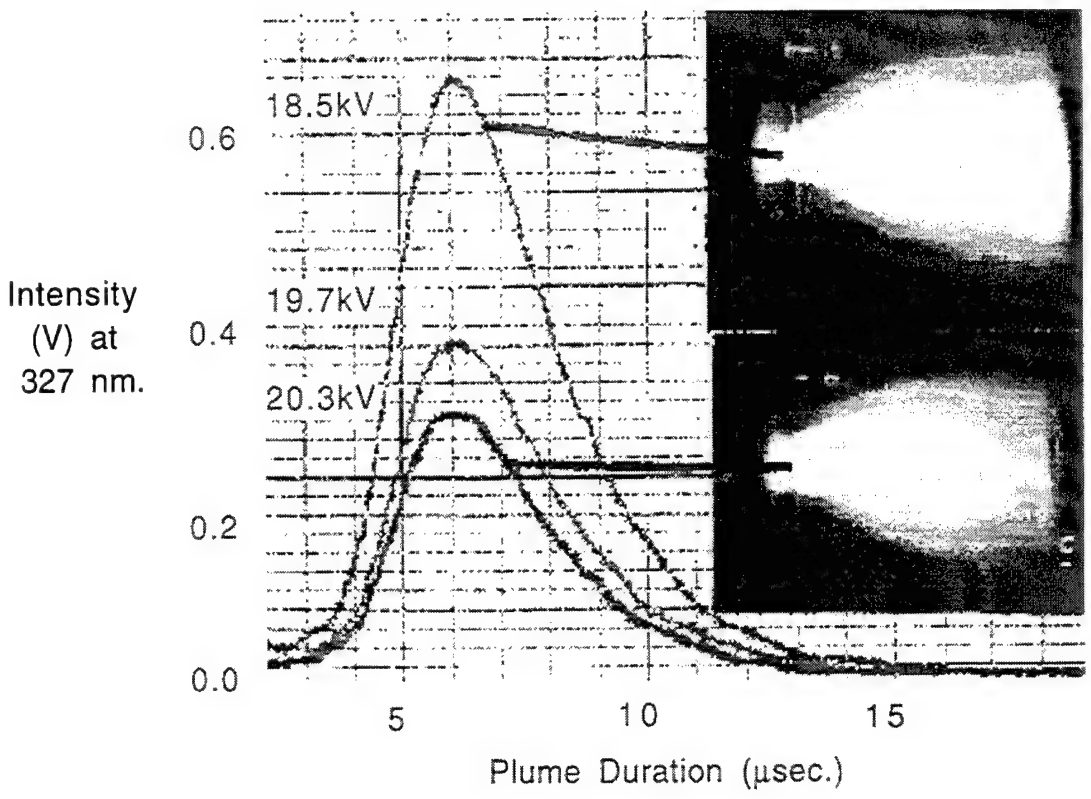

Figure 1. Laser Plume Variations for 200 mj/cm^2 Pulse Energy Density at Different Laser Cavity Voltages.

Given these changes in the plume, it was necessary to implement an *in situ* control loop to reduce process variation. Of the sensed boundary parameters mentioned above, constituent velocity was considered the most promising for use as an *in situ* control variable. Figure 2 indicates that the relationship between constituent velocity and laser energy is very close to linear, simplifying the steps necessary to effect close loop control.

Additionally, the constitutent velocity is indicative of the energy of the ionized species. It has been found that the energy of the species has a significant effect on the quality of the films, further emphasizing the need to control based on constituent velocity. An SISO PID control scheme was utilized to implement closed loop control based on velocity. The PID control has many unique characteristics. A reference voltage is input by the operator to define a starting voltage for the laser. This value is used to start the process while the oscilloscope is gathering enough data to produce an accurate average. This value is also used if a data acquisition error occurs so the process remains stable and does not have to shut down. Since this term approximates the excitation voltage needed to maintain the desired velocity the effect of the proportional term of the control is minimized. Thus the integration and derivative terms tend to dominate.

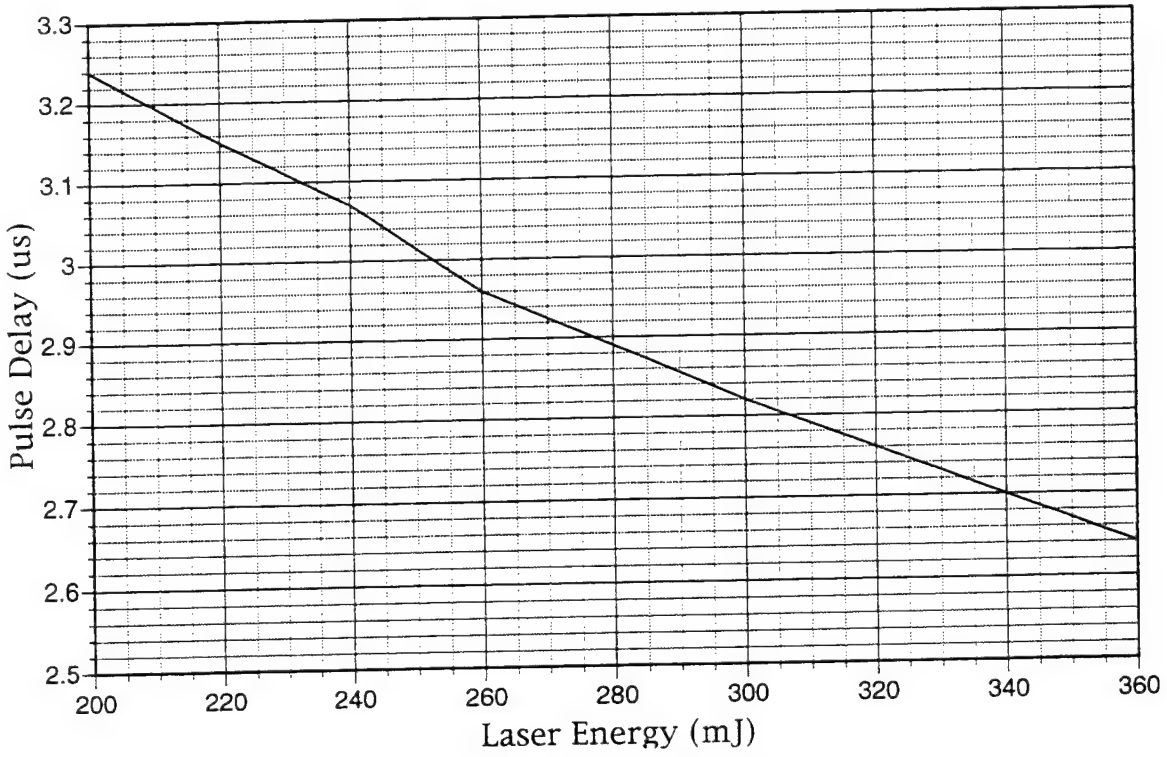

Figure 2. Velocity or 'Time-of-Flight' of plume constituents vs Laser Energy

Additionally, the constitutent velocity is indicative of the energy of the ionized species. It has been found that the energy of the species has a significant effect on the quality of the films, further emphasizing the need to control based on constituent velocity. A 'single-input-single output' PID control scheme was utilized to implement closed loop control based on velocity. The PID control has many unique characteristics. A reference voltage is input by the operator to define a starting voltage for the laser. This value is used to start the process while the oscilloscope is gathering enough data to produce an accurate average. This value is also used if a data acquisition error occurs so the process remains stable and does not have to shut down. Since this term approximates the excitation voltage needed to maintain the desired velocity the effect of the proportional term of the control is minimized. Thus the integration and derivative terms tend to dominate.

The controller also has some standard features found in many PID controls. Integrator windup protection is provided to maintain stability in case the actuator reaches saturation. Also the derivative term is taken from the velocity measured instead of the error term. This keeps the control from reacting to changes in the velocity setpoint. Figure 3 shows the response of the velocity controller to step changes and illustrates the controller effectively tracking the reference input provided to it.

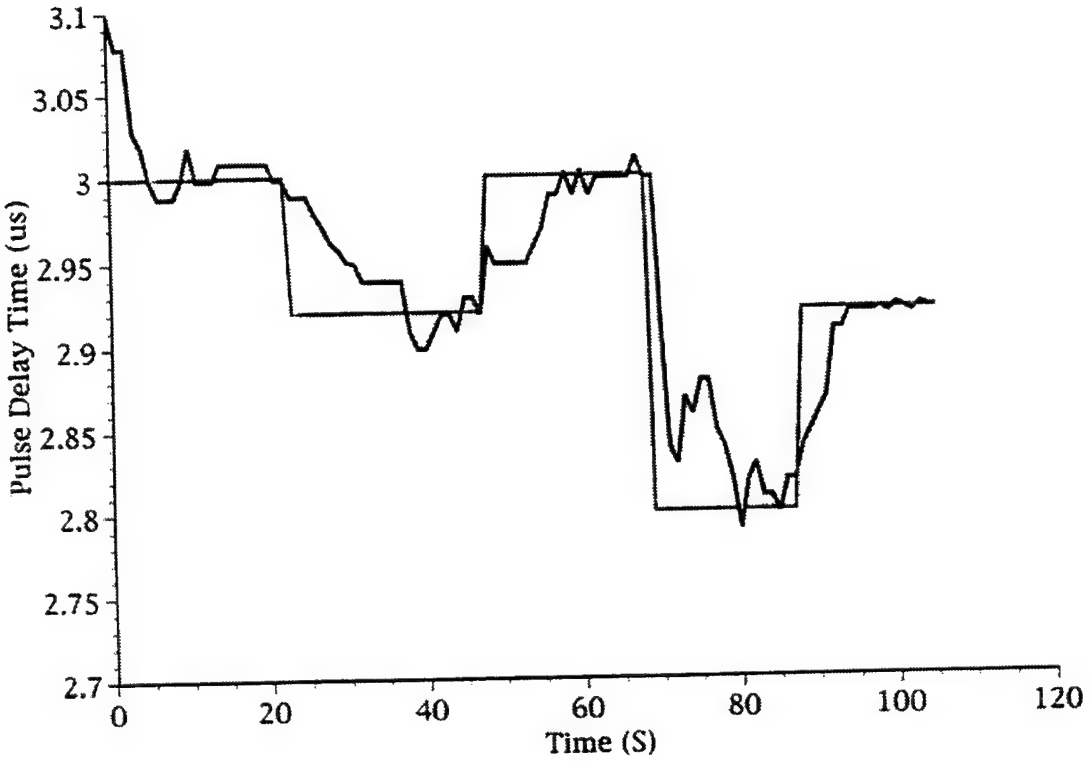

Figure 3. Step Response of Closed Loop Control System

The system is intentionally over-damped for several reasons. The pulse-to-pulse variation of the laser presents a large noise term in the monitored signal even after filtering. This noise could create instability if the system were critically damped especially in the derivative term. Also the FIR filter used to filter the signal creates a delay in the control loop. Therefore the gain must be kept low in order to satisfy stability criteria for the loop. The over damped controller is still quite effective for the PLD process because the perturbations it is designed to minimize are slow by nature. Target damage for example is one of the main process disturbances identified to date. It occurs over a period of several minutes and is easily accommodated by the controller.

The second *in situ* sensing method to be examined was fiber-optic Raman spectroscopy. Raman spectroscopy involves the inelastic scattering of incident light. It is a well established materials characterization technique which provides a unique chemical signature for many different materials. In addition to chemical composition, many other material properties of interest can be measured or inferred, such as crystalline orientation , morphology, temperature, and in this particular case, film thickness. Published literature also demonstrates that some spectral features vary with a films superconducting properties. To adapt this technique for use as an *in situ* sensor is a formidable task. Raman spectroscopy is a weak scattering effect (on the order of 10^{-6} weaker than normal elastic scattering of light), and detecting the effect from a black film requires careful setup and a sensitive probe and detector. Figure 4 depicts spectra from 3 YBCO films of varying quality.

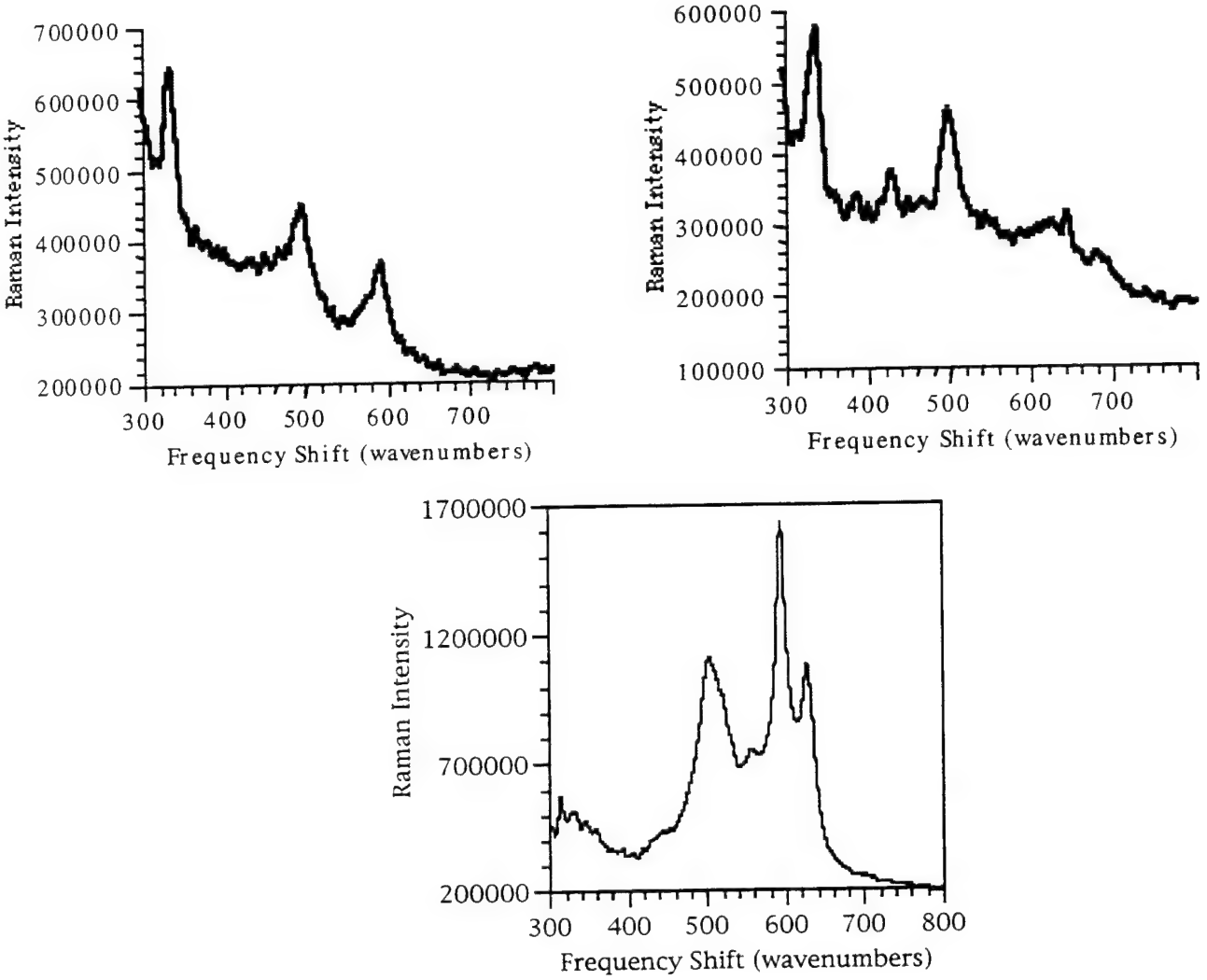

Figure 5. Raman Spectra of YBCO Thin Films with T_c's of a) 91°K, b) 87.2°K, c) 42°K

Peaks at 336,436 and 500 are indicative of the superconducting 123 phase of YBCO while the peak at 600 is indicative of the 123 semiconductive. The peak at 640 is a result of the contamantent barium cuprate, which also not a superconductor. The trends in figure 5 are to be expected from the above. The films with a large peak at 336 have a high T_c while the film that exhibits a large peak at 600, indicating that more of the non superconductive 211 phase is present, has a much lower TC. The film in Figure 5 c) not only has the 211 YBCO phase, but the impurity barium cuprate discussed above. The presence of the impurity would serve to further reduce the desired material qualities. It should be noted at this point that the ratio of peak intensities are not stoichometric in nature, because different materials (or phases) due not scatter at the same intensity. For example, the Raman sensitivity of barium cuprate is an order of magnitude greater than 123 and the 211 phase is two orders of magnitude more sensitive.

In addition to being able to quantitavely being able to detect desired composition, it has been discovered that Raman Spectroscopy can also be an effective film thickness monitor for this material system. However, determining thickness of a YBCO thin film can be challenging because the film, 80 to 4000 angstroms (Å) thick, is deposited on a substrate approximately 0.5 mm thick.

The measurement technique developed involves monitoring the Raman spectrum of the substrate as a function of the YBCO material deposited. Spectra of a bare $LaAlO_3$ .substrate as well as several very thin YBCO films were taken.

The spectrum of a bare $LaAlO_3$ substrate is shown in Figure 6. The peak at 485 cm^{-1} which is characteristic for LaAlO3 is monitored for this study. The graph in Figure 7 shows a plot of the this peak amplitude vs film thickness. The peak heights are normalized to the bare substrate's response since the units are arbitrary. The data shows an exponential decay of the peak height verses film thickness. This result is consistent with optical attenuation properties. The peak amplitude decreases by about half (3 dB) for every 300 Å of material.

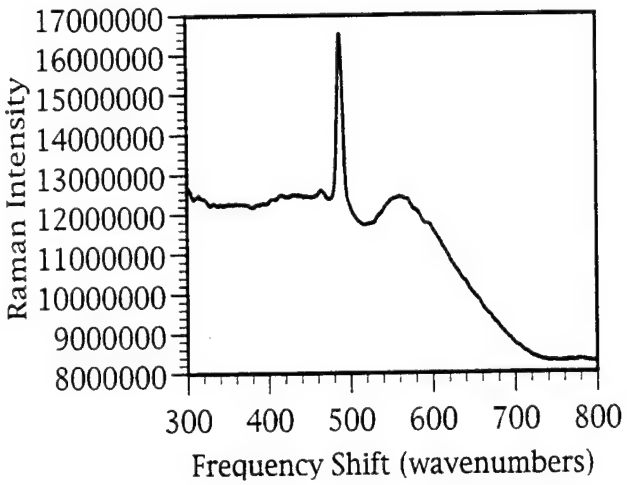

Figure 6. Raman Response of $LaAlO_3$

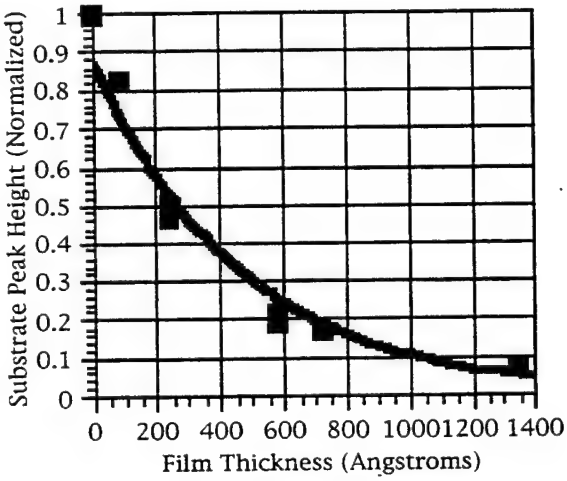

Figure 7. Response vs Film Thickness

To verify these results a 4000 Å film sample made with a cerium oxide buffer layer was analyzed and compared to the spectrum of a cerium oxide target. Cerium oxide (CeO_2) is very Raman active with a large peak at 178 cm^{-1} which was used for this analysis. The film displayed a peak height 40 dB below that of the target (after adjusting for different integration times). Figure 8 shows this data plotted along with the previous $LaAlO_3$ data using a log Y scale. This provides confirmation that a Raman signal passing through thin film YBCO is consistently attenuated at the rate of 10 dB per 1000 Å of material.

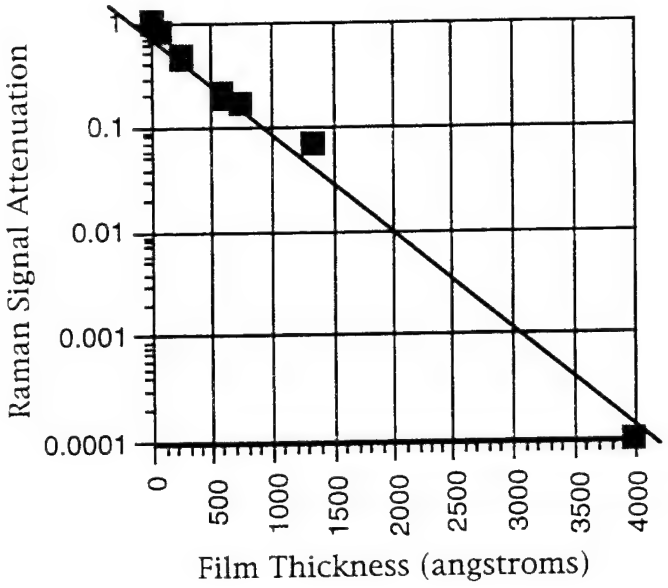

Figure 8. Raman Signal Attenuation of YBCO thin films

A significant implication is that film thickness can be determined by monitoring the Raman spectrum of the substrate material. *In situ* measurements can be used to measure and control film thickness with great accuracy and resolution. *In situ* Raman also provide a tool for researchers to observe the formation of the YBCO biaxial texture critical for high J_c.

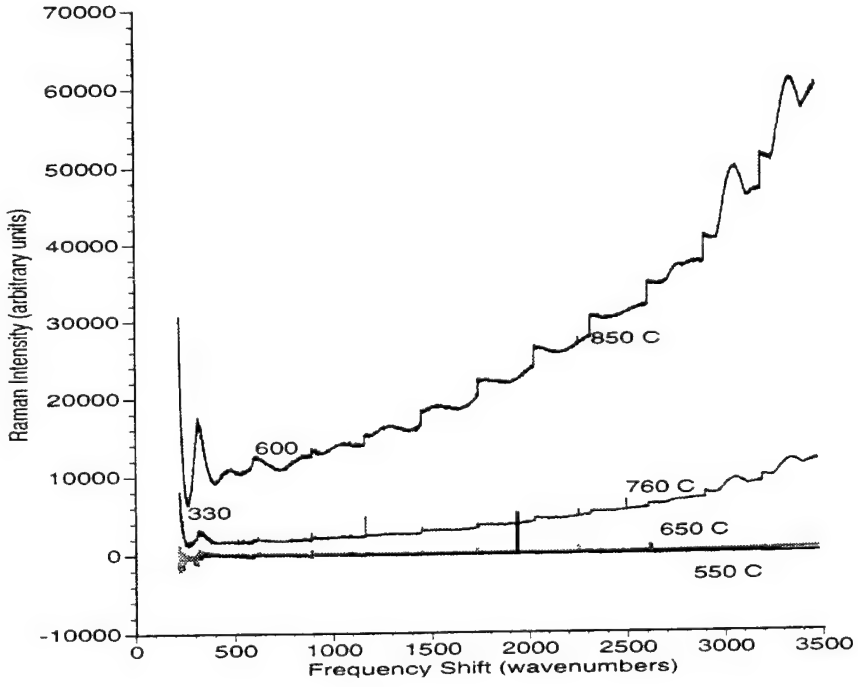

Figure 9. Optical Spectra of BlackBody radiaton at various chamber temperatures.

Several other environmental issues such as probe temperature, black body radiation, and plume noise also must be dealt with before success with this sensor is assured. In order to ascertain whether black body radiation would obscure the Raman spectra, optical spectra was taken at

several temperatures. From the results, as shown in Figure 9 above, it can be seen that at 760°C, the black body radiation is not significant for the area of interest (150-850 wavenumbers). However, as the temperature increases further, black body radiation quickly becomes a problem.

Future Work - 1997

With the progress achieved in FY96 regarding the identification of dominant process boundary conditions and *in situ* parameters that indicate film quality, the basis for self-directed control has been established, and in the case of optical emission spectroscopy, demonstrated with a closed loop PID control of laser energy based on a plume emission line.

Thus, research efforts in FY96 will focus on the implementation of self-directed control schema utilizing Raman spectroscopy to monitor film characteristics such as T_c. The scheme will require the installation of a fiber optic Raman probe *in situ* , which wil require a large sustained effort. Further investigations relating to process boundary conditions and subsequent film quality will also be conducted. One such candidate area of interest is the film morphology (grain size, orientation of grains and uniformity of both) throughout the thickness of the film. It as also become apparant throughout the course of FY96 research that the crystialline orientation of the grains in the film is an important factor in the resulting film properties. Polarized Raman spectroscopy studies can also prove invaluable to determining the overall orientation of grains and could be a process boundary condition for directly controlling film properties. In addition, search algorithms that utilize artificial intelligence (AI) based pattern recognition techniques are currently being developed to automate the mapping of process boundary conditions to film qualities. The research objective is to seek methods which augment the researcher in perusal of the process data discovering relationships which serve to better understand the YBCO PLD process and further enable the growth of superior and reproducible superconducting films.

Finally, in the interest of addressing affordability issues related to superconducting films for military applications, it is desirable to demonstrate large-scale YBCO depositions, i.e., a uniform, high quality films on large wafers, e.g., 5" diameter substrates. The research objective is to demonstrate a substantial material and process cost reduction with improved process yields, combined with superior films, deposited on larger areas. Of specific interest is to enable more affordable production of large superconducting passive microwave components, such as zero-loss bandpass filters and extremely high-Q resonators. Ultimately, superior AirForce threat and detection capability will be realized by a pervasive upgrading of all weapon systems that use passive microwave components.

Papers and Presentations

In Preparation

Dr. Rand R. Biggers, Capt. John D. Busbee, and Mr. David P. Lubbers, **Emission and Raman Spectral-Component Monitoring for Measurement and Control of Pulsed Laser Deposited HTS Thin Films**,Australia-Pacific Forum on Intelligent Processing and Manufacturing of Materials, Gold Coast, Australia, July 1997

Busbee, J. D., Lubbers, D. P., Jackson, A. G., Biggers, R. R., Liptak, D. C., and Iman Maartense, **Raman spectroscopy for determining YBCO thin-film paramters in situ**, TMS Symposium on *Advanced Sensors in Materials Processing*, Orlando, FL, February, 1997.

Published

Jackson, A.G., Laube, S.J.P., and Busbee, J.D., **Sensors, methods and physical properties**, *JOM*, The Minerals, Metals & Materials Society, Warrendale, PA, September 1996.

Patent

Lubbers, D., Busbee, J., Litpak, D., Biggers, R., Maguire, J., & LeClair, S.R., **In situ Raman for Control of YBCO Thin Film Current Density**, Patent Applied for 12 Aug 96.

Research Leader: Capt John Busbee, **Team:** Dr R. Biggers (WL/MLPO), D. P. Lubbers (SOCHE), Mr. D. Liptak (SOCHE), & D. R. Dempsey (UDRI).

Physical Vapor Deposition of Nonlinear Optical Films for Rugate Filters

Narrow bandwidth rugate filters have many applications for laser hardening. However, current monitoring and control techniques for rugate filter fabrication are limiting. Improved algorithms are needed so that narrower bandwidth filters can be manufactured. Neural networks have shown promise for this application.

Research OBJECTIVES are to

- Develop accurate training sets consisting of spectral profiles of the filter as its being deposited and the corresponding optical thicknesses
- Use this data to theoretically demonstrate that neural networks can be used to improve the monitoring and control of rugate filter depositions

Research FOCUS is

- Install neural network software into the PVD deposition system
- Manufacture a rugate filter with new monitoring and control system utilizing the neural network

Background

A rugate filter consists of an optical coating having a sine wave refractive index profile deposited on a substrate (Figure. 1). As shown in the figure, the refractive index variation is continuous and periodic throughout the coating. A sine wave refractive index profile having numerous identical cycles yields one highly reflective band (Figure. 2).

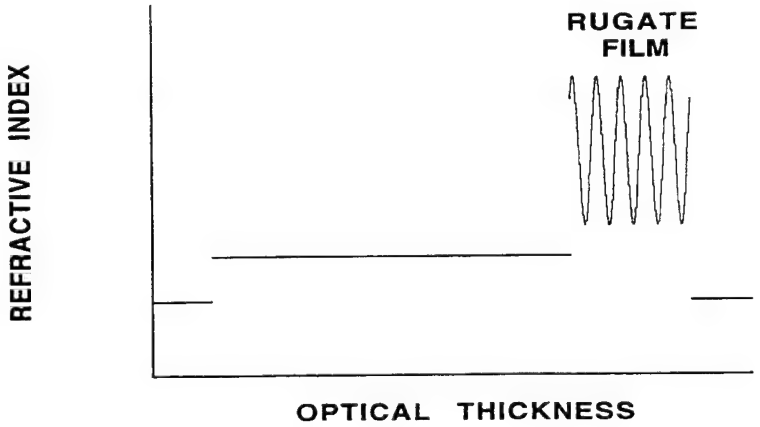

Figure 1. Fundamental rugate filter construct.

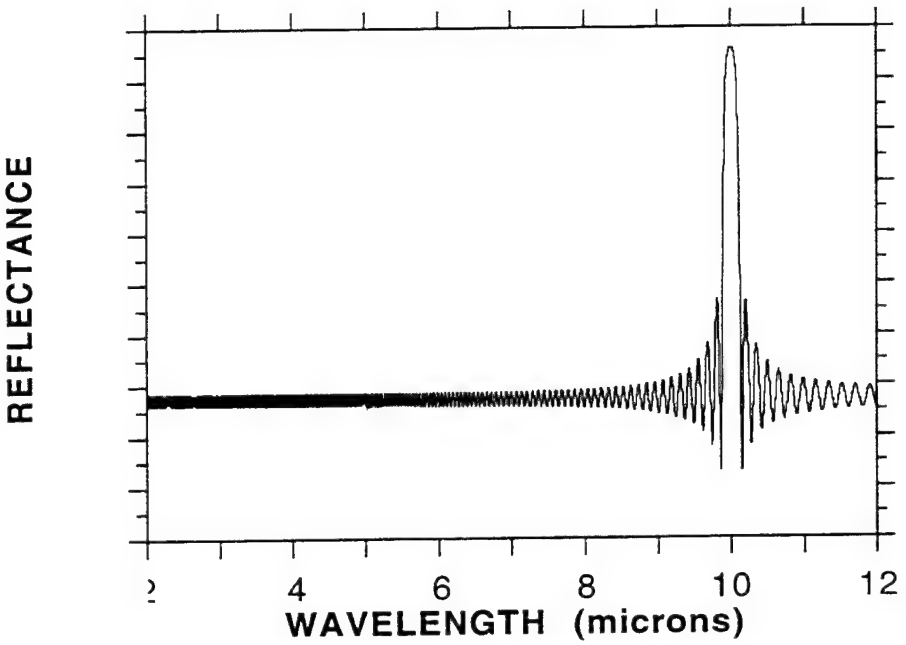

Figure 2. 10 nm-band reflectance spectrum.

There are five independent parameters describing the sine wave refractive index profile (Figure 3). These parameters are:

n_a = average refractive index
n_{pv} = peak-tovalley refractive index excursion
n_aP = period of sine wave in optical thickness
Q = phase at the substrate in radians
N = number of sine wave cycles

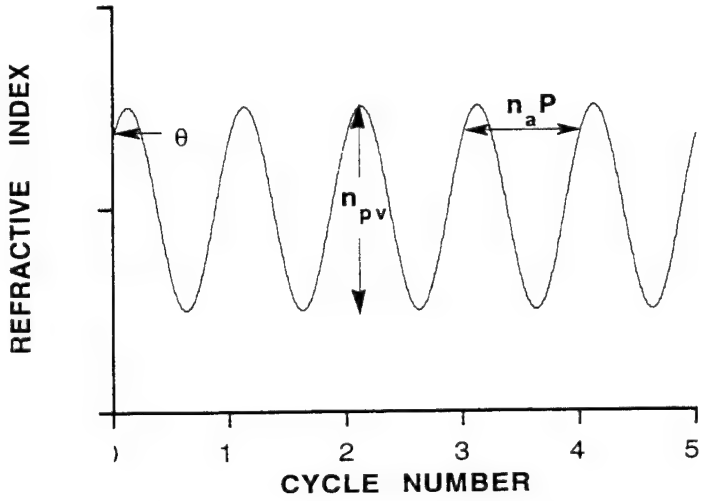

Figure 3. Fundamental rugate filter parameters

The variation throughout the optical thickness of the coating is a sine wave refractive index profile, n(x), which is described by:

$$n(x) = n_a + n_{pv}/2 \sin\{ 2p\ x/n_aP + Q \}$$

The reflection band can be tailored in amplitude, bandwidth and wavelength location, with higher order reflection bands being absent. The wavelength that spectrally locates this reflection band is determined by:

$$1 = 2\, n_a P$$

Rockwell Science Center uses Chemical Vapor Deposition (CVD) sytem to fabricate rugate filters. Making an inhomogeneous optical coating requires the ability to produce refractive index values that nature does not readily provide. CVD allows this to be accomplished by varying the chemical composition of two different materials with different refractive indices. The amplitude excursion of the sine wave is determined by by the difference in refractive index between the two materials. Continuous refractive index values between the maximum and minimum peak values are obtained by precise control of the percent composition of the two materials.

A successful rugate deposition is determined by the system's ability to match the theoretical refractive index profile by continuously varying the percent composition of each material. The materials are deposited by two different sources, thermal and electron beam. In-situ sensors monitor the two deposition rates. The rate of the thermally driven material is held relatively constant, while the rate of the e-beam driven material is varied sinusoidally. The critical parameter that must be monitored for accurate control of the e-beam source is the optical thickness of the filter as it is being depositied. The thickness value and the detected rate from the thermal source are used to determine the required deposition rate from the e-beam source. These values must be correlated to produce the desired refractive index value (Figure 4).

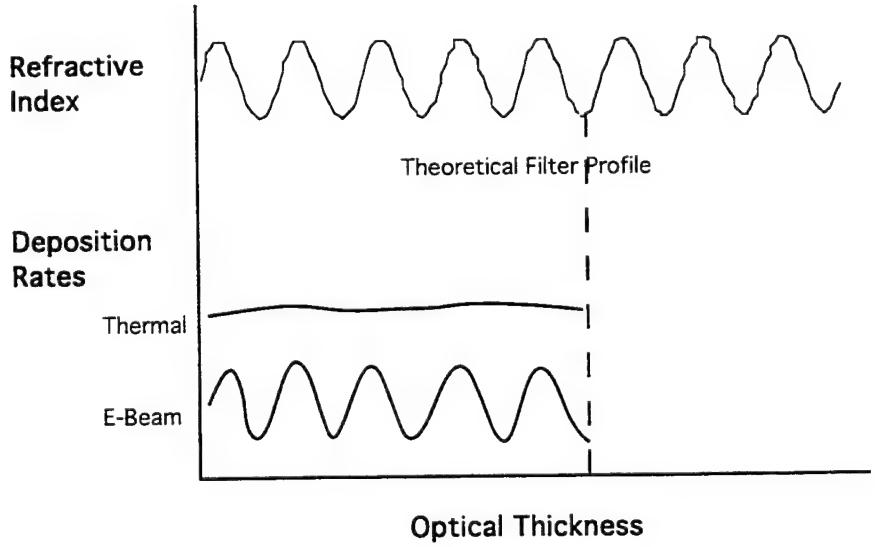

Figure 4. The theoretical refractive index profile of the rugate filter, and the deposition rates of the thermal and electron beam sources.

Monitoring the optical thickness of the filter as it is being deposited is difficult. A broad band spectral monitor is used to generate the real time spectral response of the filter as it is grown (Figure 5). At specific time intervals, a spectral profile of the filter's optical response is obtained. A curve fitting routine is then used to predict the optical thickness from a section of the spectral response curve. However, this prediction technique is not very accurate. The standard deviation in the RMS error in the optical thickness prediction may be as high as 50 angstroms. This monitoring and control method is a limiting factor for producing narrow bandwidth filters.

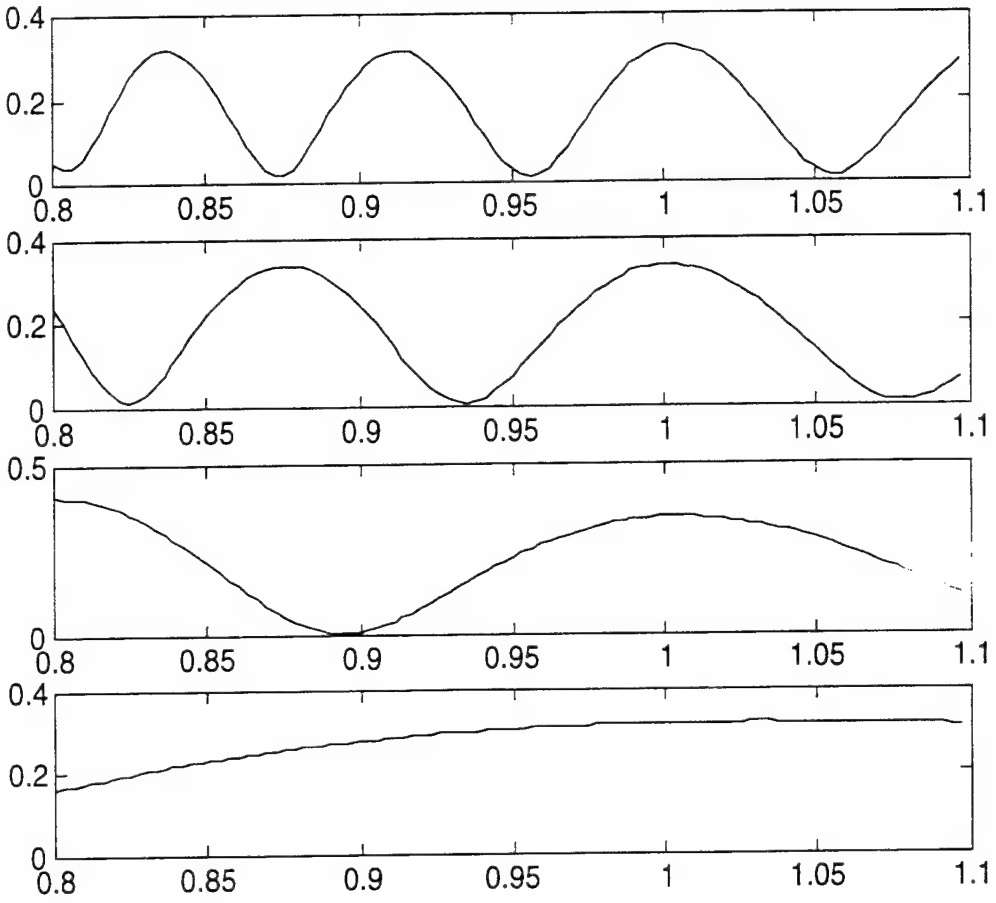

Figure 5. The spectral profile of a rugate filter as it is being deposited. Starting at the bottom, the spectra correlate to optical thicknesses of 0.5, 2.0, 3.5, and 5.0 microns.

Research/Technical Achievements - 1996

A neural network was developed to reduce the variance in the predicted optical thickness. Simulations were performed with a training set composed of theoretical rugate filter deposition data. The neural network is trained on spectral profiles (Figure 5) which correspond to specific optical thicknesses. The neural net learns the functional relationship between the spectral profiles and their corresponding optical thickness values.

A standard deviation of 3 angstroms in the RMS error for optical thickness prediction has been achieved, which is a considerable improvement over the 50 Angstrom value achieved with previous methods. The following plot shows the prediction error for a training set consisting of 678 spectral patterns between 0.05 and 5.25 microns. The testing set consisted of the same patterns combined with 10% noise. The neural network was able to learn the functional relationship between the spectral patterns and the optical thickness, and to make very accurate optical thickness predictions inspite of the noise.

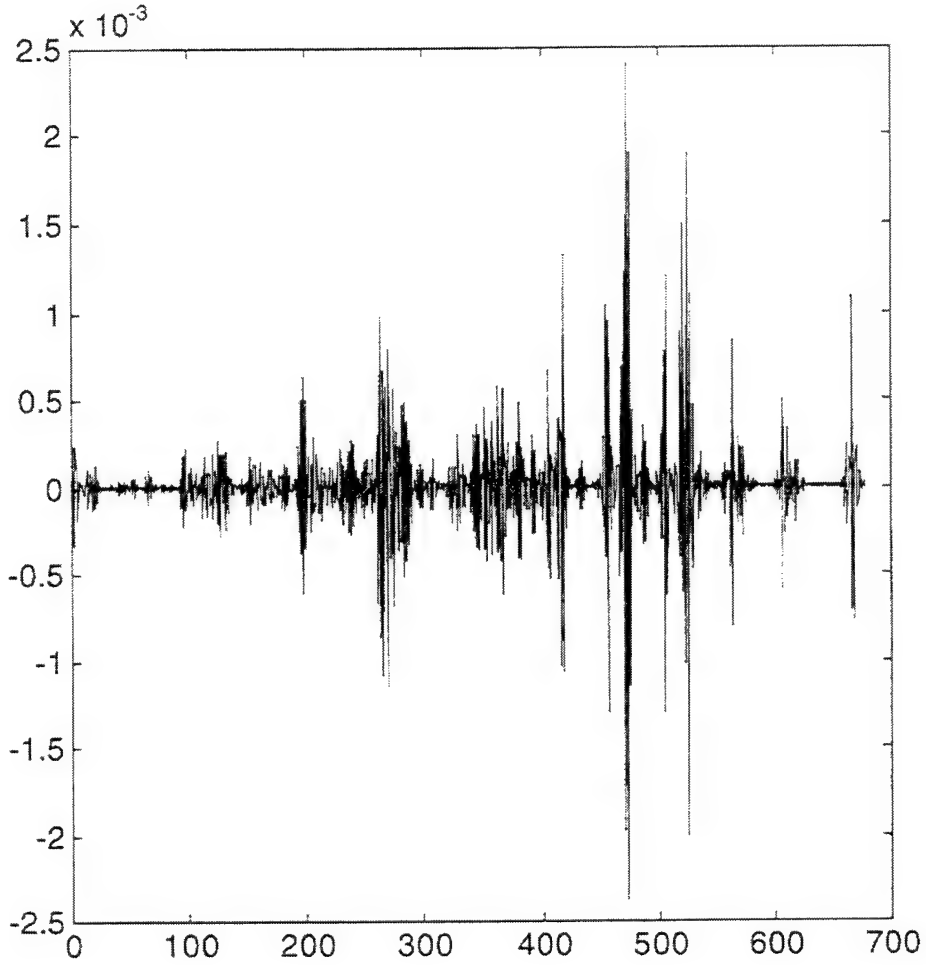

Figure 6. Testing error for the neural network.
The standard deviation in the optical thickness prediction is 3.4 angstroms.

Future Work - 1997

To date, only theoretical data has been used for neural network training. The next step is to obtain spectral data from actual depositions, which will be more representative of the process noise, for neural network predictions of the optical thickness. Good results are expected, since the noise added to the theoretical data was considerably more than would be expected in an actual deposition. A neural network control system will be installed at the contractor's site and compared with the existing system for monitoring and control.

Papers and Presentations

In Preparation

Fairchild, S., Cao, Y., Chen, P., Southwell, W., Leclair, S. *"Control and Monitoring of Rugate Filter Fabrication Using Orthogonal Functional Basis Neural Network"*, submitted to IEEE Journal

Patent

N/A

International Conferences Attended

International .....

Research Leader: Mr. Steve Fairchild, **Team**: Mr. Walt Johnson, Dr. Bill Southwell (Rockwell Science Center), Mr. Yang Cao, Dr. Phillip Chen, Dr. Steve LeClair

Chemical Vapor Deposition of Oxidation Resistant Coatings on Ceramic Fibers

Research OBJECTIVES are

- extend *in-situ* sensing and control methods to encompass process design and enable eventual 'virtual materials' research
- develop 'intelligent' process design and control methods based upon *in situ* spectroscopy and neurocomputing to enable novel thin film materials processing

Research FOCUS is

- investigate, design and develop improved methods for controlling Chemical Vapor Deposition (CVD) process,
- develop *in situ* process control methods to achieve desired composition, morphology and thickness of CVD coatings on fibers and substrates,
- develop *in situ* sensing methods to monitor desired composition, morphology and thickness of CVD coatings on fibers and substrates,
- extend and apply these *in situ* sensing and control methods for use in other processes such as Physical Vapor Deposition (PVD), Chemical Vapor Infiltration (CVI), etc.

Background

In FY95, Advanced Technology Materials, Inc. (ATMI), received a Small Business Innovative Research Program (SBIR) to work collaboratively with the Materials Directorate to develop a liquid delivery system for CVD. The delivery system consists of a well engineered pumping system with a resistively heated vaporization chamber which are both microprocessor controlled. This particular liquid delivery system, a Sparta 450, can mix up to four different liquids in any desired ratio, up to 1 part per thousand, before being pumped into the vaporization chamber. In addition to the system being very flexible, it is computer controlled. A separate flush pump was provided by ATMI which allows the vaporizer system to be cleaned after each use without wasting valuable precursors.

Although ATMI supplies the components for a liquid delivery system, a collaborative team made up of personnel from MLLN and MLIM had to specify the way in which the liquid precursors from each of four different bottles would be routed to the pumps. This customization process was typical since each customer has different requirements relative to the handling and purging of the liquid delivery system. MLIM developed a design for implementation with assistance from MLLN and ATMI which: 1) provided for the ability to deliver each precursor individually to the pump by pressurizing each bottle with 10 PSI of Ar, 2) allows for the delivery of solvent to purge any of the four lines, 3) can flow Ar into each of the lines to push back precursor into the bottles or to dry the lines, and 4) can pull a vacuum on the lines to both remove impurities left and minimize the amount of pump bleeding required to get the air out of a liquid line before starting the pump. The LDS system was implemented by MLLN with the aid of ATMI and integrated into the CVD system by both MLIM and MLLN.

With the installation of the new liquid delivery system, 12 additional solenoids were added to control the routing in the liquid manifold while 7 existing solenoids were used to control the state of operation of the Vaporizer. Computer control of these solenoids was added in a modular fashion using LabVIEW. LabVIEW allows a graphical user interface to create a panel of buttons which show all of the selections of each of the solenoids in an orderly fashion. LabVIEW

software was also developed which would interface to the Sparta 450 pump using RS-232 protocol. The pump software was developed based on PC software and specifications provided by ATMI. ATMI does not integrate the solenoids into the pump controller so software had to be developed in LabVIEW which synchronizes the Sparta 450 pump with the 19 solenoids based on the appropriate mode of operation.

The flush pump which was provided by ATMI was also synchronized in software with the solenoids to provide seamless transfer from CVD operation with precursors being pumped into the reactor to venting solvent using the flush pump. Thus the vaporizer solenoids needed to change when the pumps were started and stopped respectively. In order to interface the flush pump, a custom interface board was developed by MLIM so that pump rate could be directly controlled from the computer.

Heating of the vaporizer is accomplished by four Athena PID controllers which are built into the pump control box. These controllers were interfaced to the Power Macintosh computer through custom software which was developed using LabVIEW and an interface which was purchased to convert the RS-232 protocol into an RS-485 2-wire bus. The 2-wire RS-485 interface allows for up to 32 controllers to be placed on the same 2-wire bus. The software which was developed for the controllers allows for 20 different parameters and 4 different modes of operation to be selected for each controller which is on the bus.

Heating of 4 additional components is accomplished by using a heater control box which was designed and built by MLIM with the aid of MLLN. The heater control box contains four different Athena controllers and supporting solid state relays which were supplied by ATMI to maintain compatibility with the vaporizer heater controllers. The box was developed to be a general purpose heater control system which provided four 120VAC receptacles which are individually fused, four type K thermocouples, and a master power switch. Using this setup the inlet gas to the CVD reactor, the reactor inlet tubing, the fiber inlet, and fiber exhaust ports are all heated using PID control. These four controllers were interfaced onto the same 2-wire bus as the vaporizer controllers allowing all 8 controllers to be accessed from the same modular LabVIEW software which was developed.

In addition to moving the CVD system to a new laboratory room and fume hood, the CVD system was changed from being operational at low pressures, on the order of 100 torr, to an atmospheric CVD system. Making this change currently precludes operation at pressures below atmospheric pressure, but allows the fiber spools to be placed at each end of the system removing the tedious fiber handling process and making the system much more flexible and efficient. This removes the fixed limitations of fiber which can be coated in a single deposition. To accomplish this task, a venturi pump system was purchased and installed which uses compressed air to regulate the pressure of the CVD reactor. The mass spectrometer which had been reallocated to the CVD project during the previous fiscal year needed to be redesigned into the new system. It was desired that 100uM filters be used to filter out particles which could clog the system. Further, heater tape control of the 100 uM capillary tube was added in the event that heating of the exhaust gas would prevent condensation of the gases before the measurements. In addition, routine maintenance revealed electronic problems in the roughing pump system which needed to be repaired. After approximately a month and a half, and changing the oil in the turbo molecular pump, these issues were finally resolved and the system was operating as expected. Using the mass spectrometer, the reactor composition can be measured and thus inert gas can be pumped in until the atmospheric gases are depleted and the seals are at a high enough partial pressure to keep out the atmospheric gases. In addition, an ion gauge which is used to measure the vacuum of the analysis chamber was installed. It can be interfaced to a computer to provide remote pressure measurements to keep track of the integrity of the system. If the vacuum is abnormally high, greater than 10-5 torr, then the system needs to be checked, otherwise its fine. Without the ion gauge, problems are only detected when the system actually fails.

At the exhaust of the system, a "burn box" which is designed to burn off excess hydrogen in the gas stream was repaired and automated. It can now be remotely enabled or disabled using the computer. The control box needed electronic repair while the heating element housing needed physical modification. MLLN added insulation to the housing to force it to operate at a higher temperature to better ensure the decomposition of any unreacted exhaust products. Any unreacted products from an oxygen depleted state of the reactor would burn due to the compressed air being injected. MLIM repaired the control box because one of the internal solid state relays had become "fused" and thus was always on. This was dangerous because given that the box was turned off from the front control panel for installation or removal of components, the operator had no indication that there was actually 120 VAC on the terminal strip on the rear of the box.. Routine maintenance of making sure that the equipment is in good working order will prevent such problems. For instance, if the device is activated and it is immediately hot, then it was obviously active before being turned on and should be taken out of service immediately for repairs.

Hardware was additionally purchased and installed which provided for the feedback of critical liquid delivery system valves. The state of the valve is specified in software, but the position of the valve is also measured so any loss of pneumatic pressure would be detectable. This is also useful for software development since complicated sequences of modular software can be monitored by a completely independent software module to verify that the valves are being properly sequenced.

Two of the expensive Eurotherm temperature controllers which control the temperature of the furnace needed to be repaired. Since the damage occurred after a thunderstorm it is suspected that either water damage or electrical interference may have damaged them. To prevent future problems an in house isolation transformer system was installed which can protect a portion of the electronic equipment in the laboratory from power surges and under/over voltage problems. Maintenance was also performed on the fume hood to prevent condensation on the ceiling vents from occurring.

A LabVIEW™ software module has been has been developed which integrates all of the computer controllable hardware into a single application: 7 mass flow controllers, 1 pressure controller, 24 solenoids and corresponding pneumatic valves, 2 liquid pumps, 11 temperature controllers, fiber velocity, mass spectrometer, laser scanner, 4 analog temperature measurements, and the vaporizer pressure measurement. Further, all of this data which is collected is sent to InfoScribe™, an 'in-house' data recording and display package. This data, some 300 parameters, is recorded in real-time as the process is operating. Additionally, overnight monitoring of the process can also be accomplished. Using overnight monitoring, it was determined that the provided laboratory vacuum varies much more than is acceptable for our purposes - to more than 100 torr.

Research/Technical Achievements - 1996

The enclosed plot, Figure 1, represents data (collected over a period of roughly 90 minutes) which has been recently enabled as a result of the above engineering development of the CVD apparatus. The data displayed are: 1) process exhaust pressure (torr), 2) vaporizer pressure (torr), 3) calculated pressure drop across vaporizer frit (torr), 4) Sparta 450 pump pressure, 5) Sparta 450 pump flow rate (mL/min), 6) fiber velocity controller (On/Off), 7) fiber velocity feed rate specified (cm/min), and 8) the mass flow controller number 3 which is the oxygen injection rate in SCCM.

The purpose of this deposition was to: 1) run at a lower temperature than normal and see if the process operation improves, 2) to vary the amount of oxygen to see the effect on the mass spectrometer data, and 3) to for the first time with this system operate the fiber in a continuous manner.

A number of points about the below data should be noted:

First, the pressure at the exhaust should have remained constant during the deposition - it was being controlled by a pressure controller and a new venturi pumping system operated from the provided laboratory compressed air. This implies either the control valve requires maintenance, or that the provided laboratory air is not as stable as this pressure control system requires.

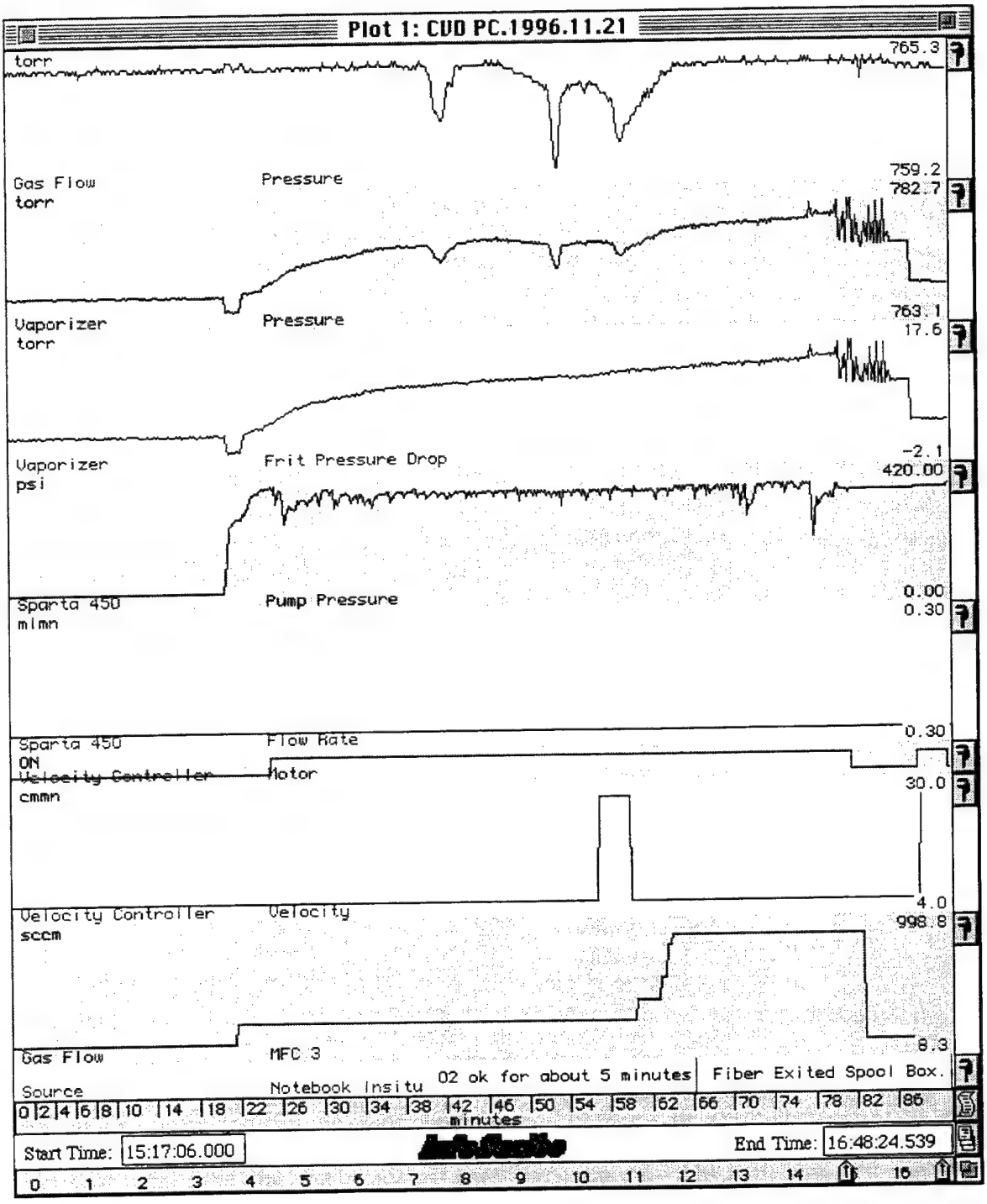

Figure 1. InfoScribe Data From Recent Deposition.

Second, the pressure drop across the frit continues to rise over the 65 minutes or so that the Sparta 450 pump is actually running. Since the frit is being clogged at an unacceptable rate this implies that: 1) the temperature, rather than being too hot as initially thought, is in fact too low, 2) since previous coatings which were being examined didn't seem to contain one of the two components, it must be clogging the frit, 3) if higher temperatures don't solve the problem, a much coarser frit will be required.

Third, the Sparta 450 pump shows a constant pressure, as expected, which further points the pressure spikes to the valve or house air.

Fourth, since the process is continuous, have a plot of the fiber feed rate makes it easier to remember when and exactly what changes were made to the fiber velocity. This makes deciphering which segment of fiber was exposed to particular gas phases and temperatures much easier.

Fifth, the changes in the oxygen flow rate are displayed along with the corresponding mass spectrometer data in the next figure. This data handling methodology makes interpreting the data much easier as well as increasing confidence in conclusions drawn from the results. The mass spectrometer data, extracted from InfoScribe allows seamless display of the different types of data so that confident statements about the process can be made. For example, based on the mass spectrometer data the system was purged out well with argon, but the 28 AMU peak would not completely disappear as well as it has in the past. Upon post deposition examination it was learned that a gasket was missing, which is indicative of the data displayed: a very slight amount of air entering the system, but measurable. Thus the CO peak, 28 AMU, which is labeled contains a bias based on the steady state amount of N_2 being introduced, 28 AMU.

The mass spectrometer data corroborates the observed three pressure spikes. Without the spectrometry correlation with the pressure spikes, the acquired process data would be difficult to explain, i.e., why after 15 minutes of presumed steady state operation would the constituents suddenly change drastically? The mass spectrometer data also shows that initially the CVD system is operated in an oxygen depleted state, more CO than CO_2. As the oxygen is quickly increased, the amount of CO dramatically decreases, as expected. Using the mass spectrometer can be used to both monitor desired gas species and to control the CO to CO_2 ratios using the O_2 mass flow controller. This allows the CVD system to be operated in an oxygen rich environment while saving O_2 gas.

To help save argon gas, a custom circuit was developed which allows the vaporizer to be overpressurized with argon rather than a continuous flow (24 hr/day) at 100 SCCM. The custom circuit was integrated into the control cabinet which houses the solenoids and mass flow controllers. When activated, it opens the mass flow controller gate valve as well as the vaporizer gas valve, sets the mass flow controller flow rate to 25 SCCM, activates the mass flow controller and waits until the vaporizer reaches 850 torr before shutting off. When the pressure reaches 800 torr it automatically reactivates. A hardware solution is much better than software for this application because all software-related perturbations and/or failures do not affect the vaporization system. Over-pressurization also allows the seal of the vaporization system to be verified after maintenance.

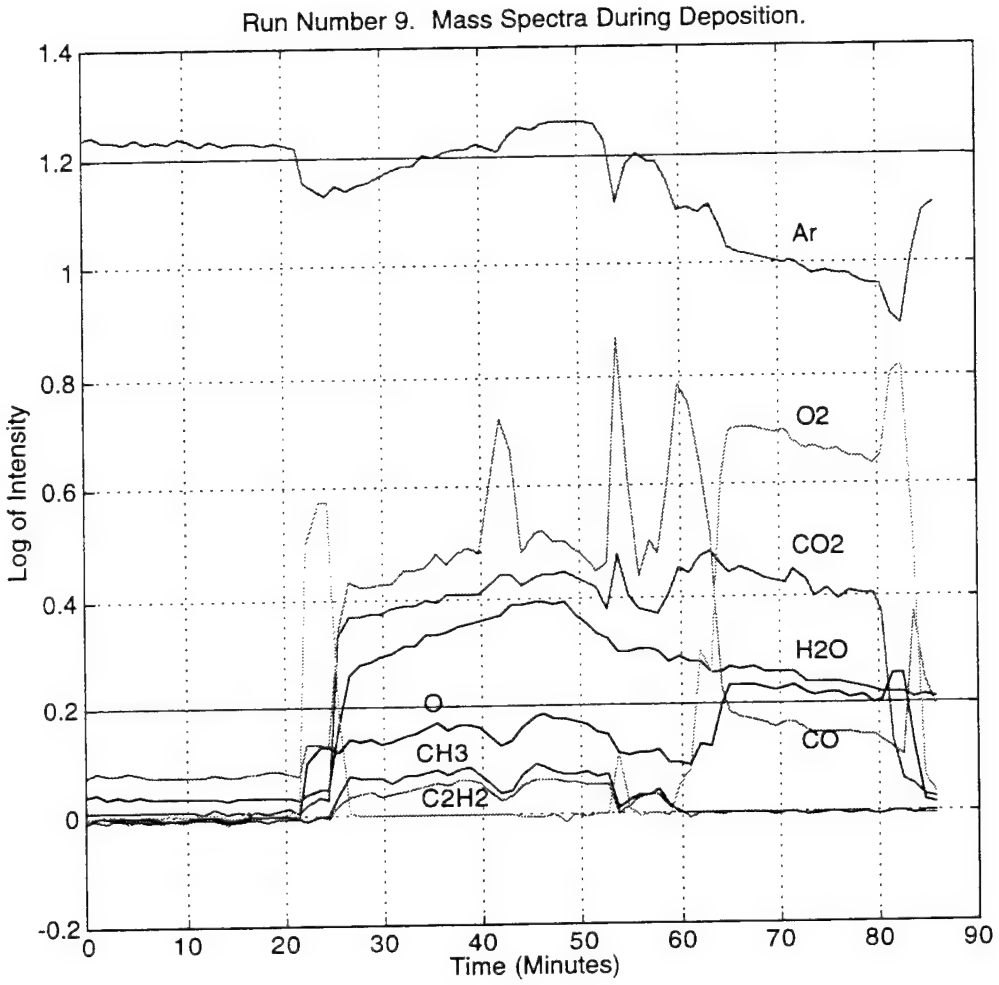

Figure 2. Mass Spectrometer Data From InfoScribe.

Two primary material parameters which must be ascertained *in situ* to enable real time control of this process: coating thickness and composition. A fiber-optic Raman spectrometer was purchased to measure these parameters. Figure 3 shows Raman spectra of the alumina monofilament after having been cleaned with acetone. A number of points can be made with respect to the spectra shown in Figure 3. First there appears to be marked differences between the bare fiber and the fully coated fiber. First, of the four peaks, three are correct while the first peak is merely system noise - fluorescence which got past the optical filters. The three peaks which are shown correspond to the single crystal a_x form of alumina: 645, 418, and 380 cm^{-1}. A puck of lanthanum magnetoplumbite which was analyzed shows the peaks representative of polycrystalline $\alpha - Al_2O_3$ (corundum), as well as other additional peaks. These peaks must be attributable to the lanthanum components or the resulting modes which are indicative of the lanthanum components being present. With these results, certain areas of the Raman spectra will be more relevant for analyzing the coated fibers.

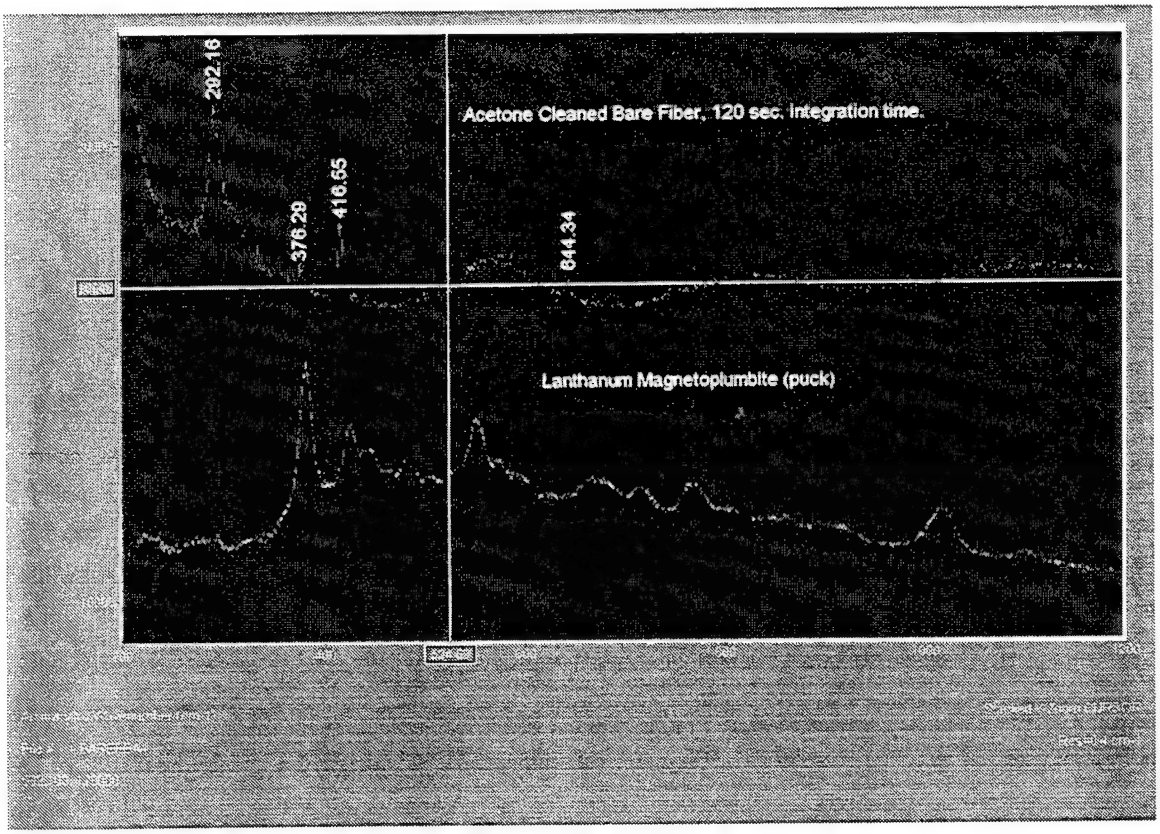

Figure 3. Raman Spectra of Bare Fiber and Lanthanum Magneto-plumbite.

A hierarchical control architecture has been developed which will aid in developing a control system for the process as the nuances of the different types of instruments, data collection, and data processing are realized. The control structure, shown in Figure 4, depicts the CVD control architecture, developed in collaboration with Prof. Pat Garrett (University of Cincinnati), into three different hierarchical levels: Environmental, *in-situ,* and *ex-situ.* Regarding the environmental (energy input/output) level, all of the solenoids, controllers, and heaters are independent variables that can be individually monitored and iteratively adapted to enable real-time control

Because CVD is a dynamical system, processing conditions change (as exemplified by the drift in the previous mass spectrometer data) and hence a single *a priori* feedforward solution is unacceptable. In fact, each time a vaporizer frit is changed, the CVD system exhibits new processing characteristics. Thus, a real-time, adaptive control system is a necessity for repeatability and achievement of desired thickness and composition.

The *in-situ* level of the architecture is responsible for measuring the actual materials processing (changes in materials behavior as a consequent of the above referenced environmental process conditions) parameters. These *in-situ* parameters are necessary for adapting the environmental level to correct for drift in the process. For example, compensating the CO level by adjusting the level of CO_2 using state space techniques would represent *in-situ* level compensation.

The *ex-situ* level represents all of the desired properties of processed material which are typically measured via characterization techniques. The challenge for real-time control is to measure these properties *in-situ*, and therein, couple the *ex-situ - in-situ* levels of the architecture which is to be demonstrated via an *in situ* mapping of the Raman and mass spectrometer spectra.

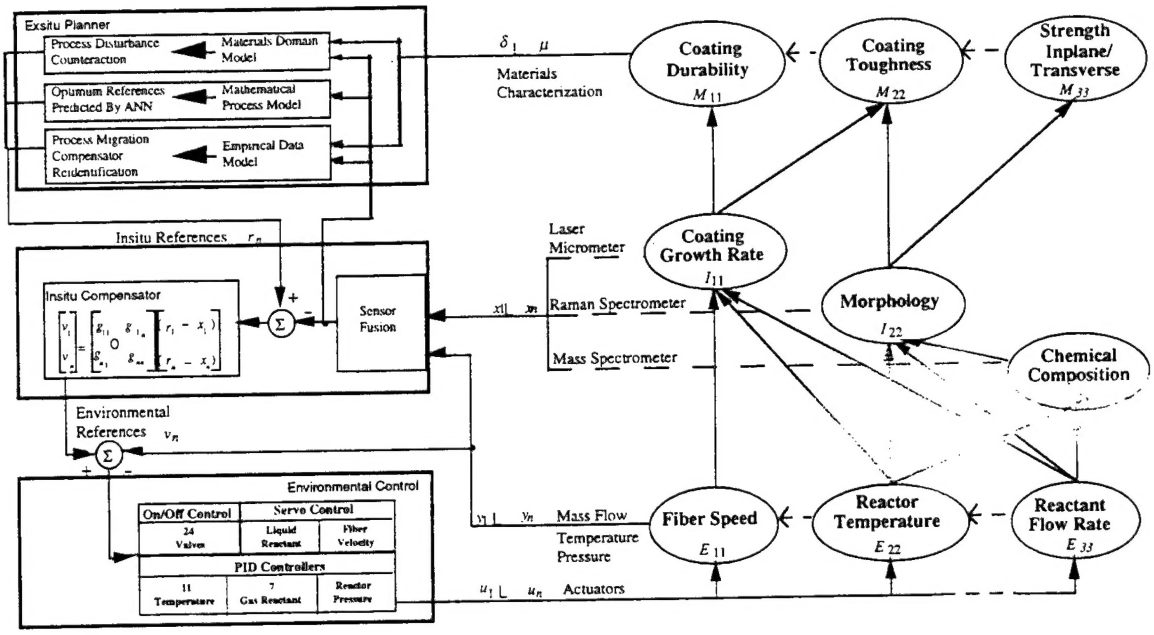

Figure 4. CVD Subprocess Control Influences

Future Work - 1997

To gain a complete understanding of the Raman spectra that has been collected, a modal analysis of the Lanthanum Magneto-plumbite coating is being undertaken. This analysis will identify each Raman band with a specific bond in the coating. By comparing these results with the experimentally obtained spectra, it can be shown conclusively that the spectra of the coating is being obtained.

A second Raman microprobe will be use to simultaneously monitor and generate spectra for the gas phase reaction. This will give a true indicator of the gas phases throughout (end to end) the reactor and provide further opportunities for process model refinement and real-time control. SEM images will be used to correlate material properties of CVD runs with the information taken by all of the *in situ* sensors.

Interface software and a custom mount will be developed to monitor, via fiber optic Raman spectrometry, real time spectra of the fiber coatings. Once the spectrometer can observe the coating composition, the transition of using this information to control the process will begin. The Raman spectra will be related to the mass spectrometer data, temperature, and liquid delivery information to create a hierarchically controlled process with *in situ* compensation and *ex situ* materials characterization.

Further optimization and reconfiguration of the liquid delivery system will be undertaken in an attempt to determine which temperatures and flow rates of carrier gas provide the best coatings. It is anticipated that based on the work done in FY96 that the temperature of the vaporization system will need to be hotter, that the length of time which a frit lasts is unacceptably short, and that some of the tubing will need to be rerouted to remove areas which contain dead volumes of liquid. More temperature controllers will be acquired and will require that another temperature control box, just like that of FY96, be built. The additional controllers are required to heat the exhaust gases before

entering the mass spectrometer. Unless the condensation is prevented, skewed measurements will result. Additionally, the freshly coated fiber will be subjected to water condensation.

The mass spectrometer will also be further automated. A pneumatically controlled valve will be added which will allow the analysis chamber to be opened and closed on command. In addition, the ion gauge can be activated remotely once the software and wiring have been added. This will allow the mass spectrometer to become a truly remote instrument which does not require operator intervention before and after measurements are taken. In addition, the effect of oxygen on the CVD system and the resulting coatings needs to be investigated. Oxygen can be injected at different portions of the reactor, either upstream or downstream of the actual deposition gas. Different injection points provide different coating results. Once these varying results are obtained, the desired coating must be determined, i.e., how much carbon or lack there of is required in the final coating. This will be done in close collaboration with MLLN.

Once the desired composition coating can be made for the monofilament fibers, it is expected that the system will be modified in an attempt to cure the fibers immediately after they are coated - this would save considerable time, effort and cost if successful. This modification is predicated on the fact that the deposition zone is short in length and relatively low in temperature. This means that our expensive three zone furnace can be replaced by a small cheap single element furnace; then the three zone furnace would be placed in line with the single zone furnace. This would allow first coating in the single element furnace and then curing of the fiber in the three zone furnace. If this can be done, then the Raman composition will be much easier to determine because it will be looking at a coating with a crystal structure as opposed to an amorphous coating. The overall quality of the produced fiber would then be much higher.

Technology Transfer

The computer software which was developed during the previous fiscal year will be transferred to ATMI for use on their CVD system in Danbury, CT. The software which will be transferred will allow environmental control of temperatures, pneumatic valves, both a Sparta 450 pump and a flush pump, and mass flow control. These new capabilities, enable ATMI to stay abreast of ML researchers in advancing the science of interfacial coatings for use in high temperature composites. These composites are essential for achieving increases in efficiency of power generation systems and aircraft engines (both civilian and defense) and for next generation space shuttle components, and among other high temperature applications.

Papers and Presentations

Several articles have been published, and more papers and presentations are in preparation.

In Preparation

Jackson, A. G., Laube, S. J. P., and Jones, J. , **Spectroscopic methods for control of thin film growth**, TMS Symposium on *Advanced Sensors in Materials Processing*, Orlando, FL, February, 1997.(ASC-96-2788)

Garrett, P. H., Jones, J. G., and LeClair, S.R., **Insitu Subprocess Control Architecture For Robust Processing Of Materials**.

Jones, J.G., Jero, P.D., and Kent, D.J., **Process Control Of CVD Fiber Coatings,** Ceramic Society Annual Meeting, Cincinnati, OH, May, 1997.

Busbee, J.D., Jones, J.G., **Raman and Mass Spectroscopy For Insitu Control For CVD Of Ceramic Fibers,** Australia-Pacific Forum On Intelligent Processing And Manufacturing Of Materials, Sydney, Australia, July, 1997.

Presented

Jones, J.G., Busbee, J.D., and Maguire, J., **Improved CVD Coating Properties Via Remodeling and Raman Spectroscopy**, Intelligent Processing of Materials Session - Aeromat, June, 1995.

Published

Garrett, P.H., Jones, J.G., Moore, D.C., and Malas, J.C., **Emerging Methods For The Intelligent Processing Of Materials,** ***IOM,*** Engineering and Performance, Vol. 2(5), October, 1993.

Garrett, P.H., Jones, J.G., Palaith, D.L., **Hierarchical Process Control Of C... Vapor Infiltration,** Proceedings of Intelligent Processing of Materials - Aeromat, June, 1995.

International Conferences

Jones, J., Garrett, P., Busbee, J., LeClair, S.R., Brown, P., & Maguire, J, **Optimization Of Fiber CVD Using Raman Insitu Control,** International Conference "Artificial Intelligence In Real-Time Control" Bled, Slovenia, November 29-Dec 1, 1996.

Research Leader: Mr John Jones, **Team:** Capt John Busbee, Dave Liptak, Dr Paul Jero, Lt Dave Kent

DISTRIBUTION LIST

DTIC-OCC (2 copies)
8725 John J Kingman Road
Suite 0944
Fort Belvoir VA 22060-6218

WL/DORT Bldg 22 (2 copies)
2690 C Street Ste 4
WPAFB OH 45433-7411

AUL/LSE Bldg 1405
600 Chennault Circle
Maxwell AFB AL 36112-6424